THE GELATION OF AGAROSE

A thesis submitted for the Degree of
Doctor of Philosophy of the University of London
and the Diploma of Membership of the
Imperial College of Science and Technology

by

Martyn Raymond Letherby B.Sc. (Hons.) (Bristol)

Department of Chemical Engineering and Chemical Technology,
Imperial College of Science and Technology, London S.W.7.

May 1980

Declaration

This thesis gives an account of work carried out in the Department of Chemical Engineering and Chemical Technology, Imperial College of Science and Technology, London, S.W.7, between September 1977 and April 1980 and is original except where specified by reference.

Abstract

The initial aim of this work was to study the gelation process of aqueous solutions of agarose using photon correlation spectroscopy in order to further our understanding of the gelation mechanism.

The outcome of this research has been the proposal of a model for the agarose system which differs markedly from currently accepted ideas. The agarose batch used in this work was found to contain 0.44% by weight of an insoluble ash which has been identified as being a calcium sulphate matrix with numerous ionic impurities. It is here proposed that this ash forms the "hard-core" centre of large agarose-containing units identified by light scattering techniques. These large units are a small fraction of the total solute. Thus the agarose/water system is not simple but may be thought of as being a dispersion of colloidal "hard-core" particles in a homogeneous agarose solution.

A mechanism has been proposed for the gelation process as a result of light scattering studies and microscopy. The initial act of gelation is thought to involve aggregation of the "hard-core" units into linear chains which form a backbone structure for the incipient gel. The model has been shown to be consistent with numerous experimental observations such as intensity light scattering, ion interactions and hydrolysis.

It thus appears that the inorganic ash content of the sample, which is believed to be intrinsic to the system, plays an important role in determining gel-forming properties.

Acknowledgements

I should like to express my gratitude to my supervisor, Dr.D.A.Young, for his constant advice and encouragement. I should also like to thank all members of the academic and technical staff for their co-operation and helpfulness.

In particular I wish to acknowledge the assistance given by Dr.G.Parry in connection with electron microscopy, Dr.R.Osborne for kindly carrying out X-ray diffraction measurements and Dr.E.D.T.Atkins of the University of Bristol Physics Department for providing information concerning his recent X-ray diffraction studies of agarose.

I should like to thank my colleagues; A.Carter, C.L.Chong, Dr.J.Davis, Miss A.Hill and Mrs K.Ma for their good-humour and friendship.

I wish to thank my wife, Gayle, for her patience and help in the production and typing of this thesis.

Finally I wish to acknowledge financial support from the Science Research Council.

Contents

	Page
Declaration	2
Abstract	3
Acknowledgements	4
List of tables	8
List of figures	9
Chapter 1 Introduction	16
Chapter 2 The Agarose/water System	
2.1 Agarose	19
2.2 Properties of the Agarose/ water System	22
2.3 The Agarose Molecule	26
Chapter 3 Photon Correlation Spectroscopy	
3.1 Principles of Light Scattering	31
3.2 Fluctuations and Correlation Functions	35
3.3 Operation of a Digital Correlator	38
3.4 Ideal Polymer Solutions	
3.4a Light Scattering Studies	42
3.4b Polydispersity	46
3.4c Internal Motions	48
3.5 Complex Systems	50
3.6 Gels	54
Chapter 4 Experimental Techniques	
4.1 Photon Correlation Spectroscopy	
4.1a Apparatus	58

	Page
4.1b Index Matching	60
4.1c Operation	63
4.1d Analysis of Results	65
4.2 Optical Rotation Studies	
4.2a Apparatus	68
4.2b Sample Cell	71
4.2c Measurements	73
4.3 Sample Preparation	73
Chapter 5 Results	
5.1 The Hysteresis Cycle	75
5.1a The Gel State	76
5.1b Gelling Solutions	
5.1b(i) Scattered Intensity Data	84
5.1b(ii) Photon Correlation	88
5.1b(iii) Viscosity	91
5.1c Non-gelling Solutions	
5.1c(i) Scattered Intensity Data	97
5.1c(ii) Photon Correlation	102
5.1d Optical Rotation Studies	111
5.1e Aggregation Temperatures	114
5.2 Complementary Experimental Data	
5.2a Batch and Pretreatment Dependence	116
5.2b Hydrolysis and Elemental Analysis	120
5.2c Pyrolysis and Filtration	126

Page

5.2d Microscopy and X-ray Diffraction Studies 127

5.2e Ion Interactions 141

Chapter 6 Discussion and Interpretation

6.1 The Hysteresis Cycle 148

6.1a $(\text{Wavevector})^2$ Dependence 153

6.1b $(\text{Wavevector})^3$ Dependence 157

6.1c Viscosity 158

6.2 The Agarose Unit 159

6.3 Properties of the Agarose Unit 163

6.4 The "Hard-core" 177

References 179

List of Tables

		Page
4.1	Corrected values for scattering angles and wavevector	62
5.1	Observed frequencies and longitudinal sound velocity for agarose gels	81
5.2	Calibration of the Ubbelohde viscometer	93
5.3	Viscosity results for agarose solutions	
5.3a	0.75 wt% agarose solution	94
5.3b	0.50 wt% agarose solution	95
5.3c	0.30 wt% agarose solution	95
5.3d	0.20 wt% agarose solution	96
5.3e	0.10 wt% agarose solution	96
5.4	Concentration dependence of aggregation temperature	114
5.5	Hydrolysis of agarose	123
5.6	Elemental analysis	126
5.7	D-spacing from X-ray powder diffraction	140
5.8	Critical concentration for potassium thiocyanate	143

List of Figures

		Page
2.1	The structure of agarose	20
2.2	Derivatives of agarose	20
2.3	Variation of optical rotation with temperature for a 0.2 wt% agarose gel	24
2.4	Variation of optical absorbance with temperature for a 5.0 wt% agarose gel	24
2.5	Temperature dependence of the longitudinal to transverse relaxation time ratio T_1/T_2 for a 2.0 wt% agarose solution	25
2.6	Variation of optical rotation with temperature for a 0.05 wt% agarose solution	25
2.7	Changes in the degree of polarisation of fluorescence (p) with temperature for a 0.3wt.% agarose solution	27
2.8	The proposed agarose double helix	29
2.9	Proposed gelation mechanism (Rees)	29
3.1	Scattering of an incident light beam by a dielectric medium	32
3.2	A randomly fluctuating intensity signal	36
3.3	Intensity signal and photon counting	36
3.4	Operation of a digital correlator	40
4.1	Photon correlation spectroscopy apparatus	59
4.2	Autocorrelation function obtained from a 0.1 wt% agarose sol at 63 °C	66

		Page
4.3	Autocorrelation function obtained under identical conditions to that shown in Figure 4.2	67
4.4	Autocorrelation function obtained from a 0.75 wt% agarose solution at 52.3 °C	69
4.5	Diagrammatic representation of the polarimeter	70
4.6	Sample holder for polarimetry experiments	72
5.1	Autocorrelation functions obtained from a 0.5wt.% agarose solution near the sol/gel transition	77
5.2	Oscillatory autocorrelation function observed when cooling a 0.75wt.% agarose solution through the sol/gel transition	78
5.3	Temperature dependence of oscillatory autocorrelation functions	79
5.4	Angular dependence of oscillatory autocorrelation functions	80
5.5	Observed and predicted frequency spectrum for agarose samples	82
5.6	t_n (elastic constant) versus t_n (concentration) for agarose gels	83
5.7	Scattered intensity versus temperature for a 2.5wt.% agarose solution	85
5.8	Scattered intensity versus temperature for a 0.1wt.% agarose solution	86

Page

5.9 Intensity fluctuations above the aggregation temperature 86

5.10 First cumulant versus (wavevector)^2 for a 0.1wt.% agarose solution at 92.5 °C 89

5.11 First cumulant versus (wavevector)^2 for a 0.5wt.% agarose solution at 79 °C 89

5.12 First cumulant versus (wavevector)^3 for a 0.1wt.% agarose solution at 92.5 °C 90

5.13 First cumulant versus (wavevector)^3 for a 0.5wt.% agarose solution at 79 °C 90

5.14 Variation of the parameter Φ with temperature for various agarose solutions 92

5.15 Temperature dependence of the solution viscosity for agarose solutions 98

5.16 Temperature dependence of the relative viscosity of agarose solutions 99

5.17 Concentration dependence of the relative viscosity of agarose solutions 100

5.18 Scattered intensity versus temperature for a 0.05wt.% agarose solution 101

5.19 Intensity fluctuations on cooling a sample in the aggregated state 101

Page

5.20First cumulant versus (wavevector)^2 for a 0.05wt.% agarose solution at 92.5 °C 103

5.21First cumulant versus (wavevector)^2 for a 0.05wt.% agarose solution at 59 °C 103

5.22First cumulant versus (wavevector)^2 for a 0.05wt.% agarose solution at 45 °C 104

5.23First cumulant versus (wavevector)^2 for a 0.05wt.% agarose solution at 40 °C 104

5.24First cumulant versus (wavevector)^2 for a 0.05wt.% agarose solution at 33.4 °C 105

5.25First cumulant versus (wavevector)^2 and (wavevector)^3 for a 0.05wt.% agarose solution at 23 °C 106

5.26First cumulant versus (wavevector)^2 for a 0.05wt.% agarose solution in the aggregated state at 50 °C 108

5.27First cumulant versus (wavevector)^3 for a 0.05wt.% agarose solution in the aggregated state at 50 °C 109

5.28Temperature variation of the effective hydrodynamic radius for non-gelling agarose solutions 110

	Page
5.29Behaviour of optical rotation for gelling agarose solutions near the sol/gel transition	112
5.30Temperature variation of optical rotation for a 0.2wt.% agarose solution	113
5.31Temperature variation of optical rotation for a 0.3wt.% agarose solution	113
5.32Concentration dependence of the aggegation temperature,T*	115
5.33Batch dependence	117/118
5.34Pretreatment dependence	121/122
5.35Variation of pH of an agarose solution with time of reflux at 100 °C	124
5.36First cumulant versus $(\text{wavevector})^2$ and $(\text{wavevector})^3$ for a filtered 0.5wt.% agarose solution at 52 °C	128
5.37,38 Optical micrographs of dilute agarose solutions	129/130/132
5.39Optical micrograph of a dehydrated agarose film (0.49wt.%)	132
5.40Optical micrograph of a hydrolysed agarose solution (54.5 hrs.)	133
5.41Optical micrographs of agarose ash	134
5.42Scanning electron micrographs of a dehydrated agarose film	136

Page

5.43Transmission electron micrographs of agarose ash 137/138

5.44X-ray fluorescence studies of agarose ash 139

5.45 First cumulant versus (wavevector)^2 for a 1.04wt.% agarose solution in 2M potassium thiocyanate at 54 °C 144

5.46First cumulant versus (wavevector)^2 for a 1.00wt.% agarose solution in 2M potassium iodide at 54 °C 145

5.47Concentration dependence of the effective diffusion coefficient in ionic solutions at 54 °C 145

5.48Scattered intensity versus temperature for a 0.5wt.% agarose solution in 2M potassium thiocyanate 147

6.1 Schematic representation of the hysteresis cycle 149

6.2 Variation of effective hydrodynamic radius(r) with temperature 151

6.3 Postulated "hard-core" particle 156

6.4 Variation of parameter Φ with temperature for various agarose solutions 156

6.5 Predicted relative viscosity versus volume fraction for moderately concentrated solutions 160

6.6 Volume fraction (from Kynch/Vand) versus concentration (wt.%) of agarose solutions 160

	Page
6.7 Model of a 0.1wt.% agarose solution	164
6.8 Static structure factor and pair correlation function	167
6.9 Relative refractive index versus radial distance for proposed "hard-core" particles	167
6.10 Contribution of each shell of the proposed "hard-core" to the particle scattering factor P(K)	169
6.11 Particle scattering factor P(K) and P(K)/K for the proposed "hard-core" model	170
6.12 Comparison of the scattered intensity with the prediction based on the "hard-core" model	171
6.13 Temperature of aggregation(T*) versus ℓn (concentration/wt.%)	175
6.14 Effect of intramolecular repulsion	175

CHAPTER 1

Introduction

The gel state is important both biologically and commercially. Polysaccharide gels, for example, have biological functions in the walls of plant cells, in animal fluids and connective tissue and in the bacterial capsule. They also have widespread commercial uses particularly in the foodstuffs, cosmetic, paper and textile industries. These gels are also invaluable to the research scientist by whom they are employed in many applications such as gel filtration, gel electrophoresis, exchange chromatography and as culture media.

The macroscopic properties of polysaccharide gels are quite remarkable. For instance, agar gels may contain 99.9% by weight of water and yet still be capable of retaining their shape under stress. Evidently the gel-solvent interaction is immensely strong. In order to understand the properties of such systems the role of the polysaccharide molecules in so drastically modifying the properties of the solvent must first be understood.

Gels may be classified on a structural basis: [1]

a) Well ordered lamellar structures. In this category one may include soap gels, phospholipids and interacting clay particles.

b) Covalent polymeric networks such as vulcanised rubber, resins and paint films.

c) Polymer networks formed through physical aggregation, the networks being predominantly

disordered but with regions of local order. Here one may include gelatin, poly-vinyl alcohol gels and alginate and carrageenan gels.

d) Particulate disordered structures such as flocculent precipitates.

With this notation polysaccharide gels would be included in category "c", for the gel structure of polysaccharides is generally believed to arise from an association of chain segments to form "junction zones" [2]. These "junction zones" are joined into a network by polymer chains which are involved in two or more "zones".

The challenge of these systems lies in the determination of the precise molecular arrangement in these "junction zones" and the nature of the intermolecular interactions.

In this work the gelation of a commercially important polysaccharide, agarose, has been studied using the technique of Photon Correlation Spectroscopy which is particularly well adapted to the study of the Brownian motions of particles in condensed fluid media. Photon Correlation Spectroscopy was developed in the mid 1960's when the advent of digital electronic techniques enabled the correlation function of the scattered light from a polymer solution to be measured. It had been shown [3] that the correlation function contained information about the dynamic properties of the system such as the translational diffusion coefficient, the rotational diffusion coefficient of the solute molecule as a whole and the relaxation times of the internal modes of specially large polymer molecules. Thus Photon

Correlation Spectroscopy (P.C.S.) provides a quick, non-destructive, non-intrusive means of monitoring the dynamic properties of a polymer solution.

CHAPTER 2

The Agarose/water System

2.1 Agarose

Agar has become very familiar as a gel material and has been employed by microbiologists as a culture medium since the 1880's. It is also of great importance in many industrial applications. The source of agar is a family of red seaweeds (Rhodophyceae) of which gracilaria and gelidium are examples of the more commercially important species.

Agar is extracted from the seaweed [4,5,8] with dilute sulphuric acid, filtered, and the solution allowed to gel. The gel is then frozen, when upon subsequent thawing most of the water and organic impurities are removed. The concentrated gel is then dried in a current of air. This crude product is washed for 10-15 days, changing the water daily, to remove further impurities such as free iodine and organic matter.

The structure of agar was investigated by Araki [5,6,7] who separated the fraction of greatest gelling ability and named it agarose. Agarose is a neutral galactose copolymer comprising alternating 3-linked β-D-galactopyranose and 4-linked 3,6-anhydro α-L-galactopyranose residues (figure 2.1).

Other fractions consisting of sulphated polysaccharides were collectively named agaropectin.

Agarose gels have been found superior to agar gels for many applications. For instance, in gel diffusion-filtration

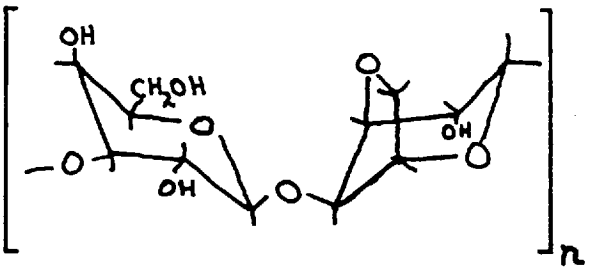
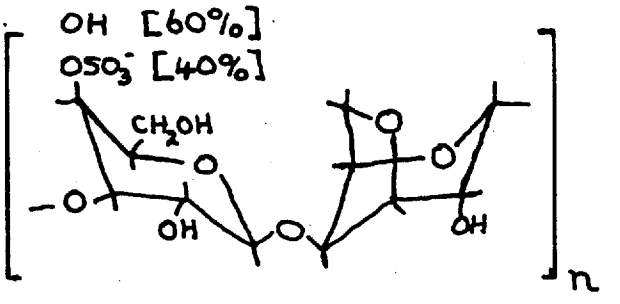
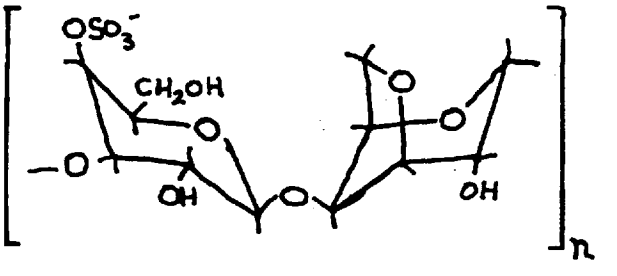


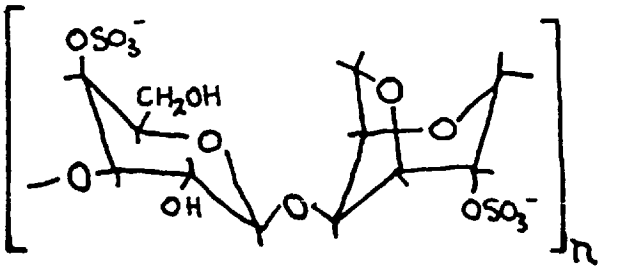
Figure 2.1 The Structure of Agarose



Furcellaran



k-carrageenan



i-carrageenan

Figure 2.2 Derivatives of Agarose

the negatively charged agaropectin can cause complications by interacting with the protein molecules being separated. In addition granulated agarose gels for use in column chromatography are less easily deformed and have a longer storage life than granulated agar gels.

Several techniques have been proposed for the preparation of agarose from agar [26]:

a) Acetylation [8]

b) Cetyl pyridinium chloride method [9]

c) Fractional precipitation with polyethylene glycol [10]

The first two techniques, as well as other proposed preparations, although providing excellent separation are tedious and expensive. Fractional precipitation, however, provides a relatively simple procedure and avoids the use of expensive reagents. The product from this method has been found to be suitable for electrophoresis, gel diffusion-filtration and as an overlay for virus plaque formation [10].

Agarose is actually a member of a family of polysaccharides having the same covalent backbone structure but differing by the conformation of the linkages and the amount of sulphate present (figure 2.2).

Agarose, as the non-sulphated member of this family, exhibits such phenomena as hysteresis in the melting and setting temperatures of the gel to a greater extent than do the polyelectrolyte modifications because chain association is more favoured for agarose.

In practice the separation of agarose from its sulphated derivatives is not complete and commercial agarose samples are graded with respect to their sulphate content, gel strength, gel point and electroendosmosis.

Guiseley [27] has investigated several varieties of agarose obtained from different sources. The sulphate and ash contents of the samples were determined and found typically to span the ranges $[SO_4^{2-}]$ ~0.1-0.8% and ash ~0.3-1.4 wt.%. The effect of the presence of methoxy groups on gelation was also studied, and it was found that a high methoxy content led to an increase in the gelation temperature.

2.2 Properties of the Agarose/ water System

Araki's discovery of the nature of agar meant that previous physico-chemical research on agar was of little relevance to studies on agarose gelation and that the properties of the separate fractions of agar must be studied. Agarose, as a typical gelling polysaccharide, has received much attention although emphasis seems to have been placed more on the macroscopic viscoelastic properties of the gels rather than on an understanding of the molecular phenomena involved in gel formation.

Agarose gels are typically turbid and rigid, and prone to the phenomenon of syneresis; the spontaneous loss of water on standing. A notable feature of the system is the considerable hysteresis displayed in the melting and setting temperatures. A hot aqueous agarose solution

(c~1.0wt.%) when cooled, will set to a rigid, turbid gel at ~40°C. Upon reheating the gel will melt at ~90°C. Recooling will again result in gel formation at ~40°C. This cycle may be repeated indefinitely [11]. This hysteresis loop has been observed in both the rheological and optical properties of the system.

The minimum concentration of agarose required for the formation of a rigid 3-dimensional network varies according to the source and purity of the agarose but lies in the range 0.1-0.5wt.% [12,13,14,].

The hysteresis loops as obtained by optical rotation studies [15], optical absorbance [16] and pulsed proton magnetic resonance [16] are shown in figures 2.3-2.5.

Studies of the optical rotation of more dilute non-gelling agarose solutions have also revealed similar behaviour during temperature cycling (figure 2.6), although this behaviour was not observed by Pines and Prins[13].

Wide band, high resolution and pulsed n.m.r. spectra of agarose sols and gels have been extensively investigated [14,17,18,19,]. These experiments have confirmed the existence of the hysteresis cycle and revealed that the water protons exist in several states. Early studies were analysed in terms of a two phase model for which hydration values of the order of 0.1-3.6g. of water per g. of agarose were obtained. More recent studies, including the use of ^{17}O n.m.r. [20], have shown this to be an oversimplification. A more appropriate model includes consideration of three or more phases with differing correlation times.

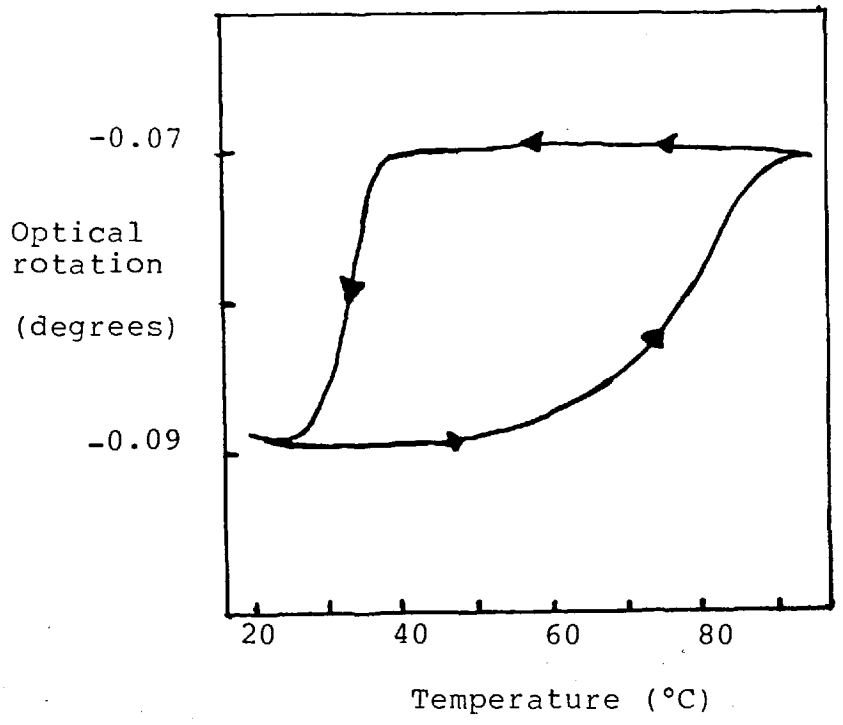


Figure 2.3, Variation of optical rotation with temperature for a 0.2wt.% agarose gel. [15]

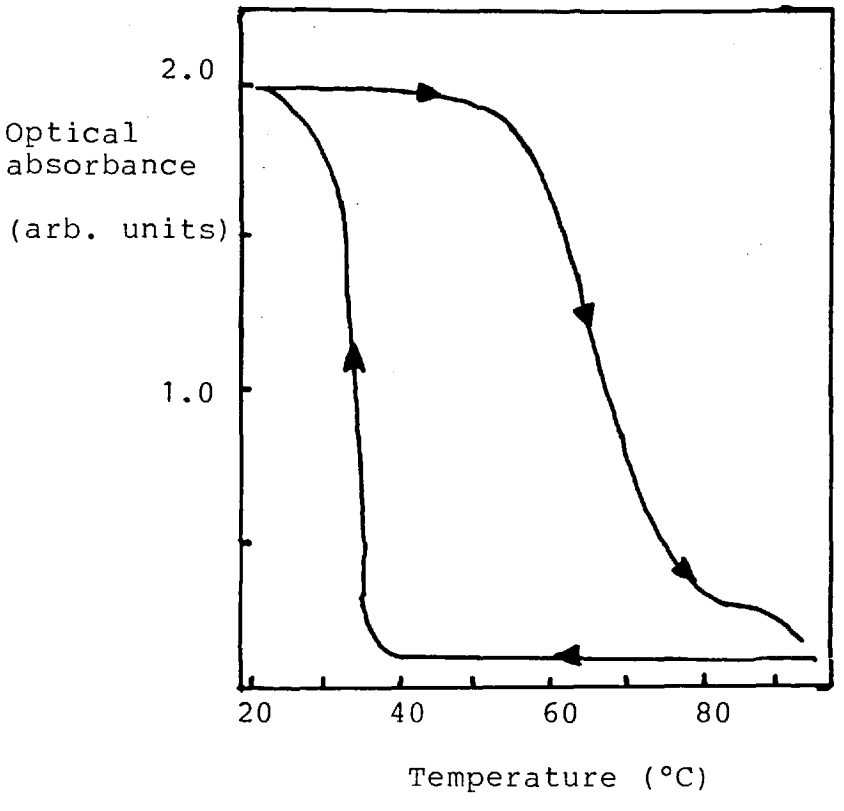


Figure 2.4, Variation of optical absorbance with temperature for a 5.0wt.% agarose gel. [16]

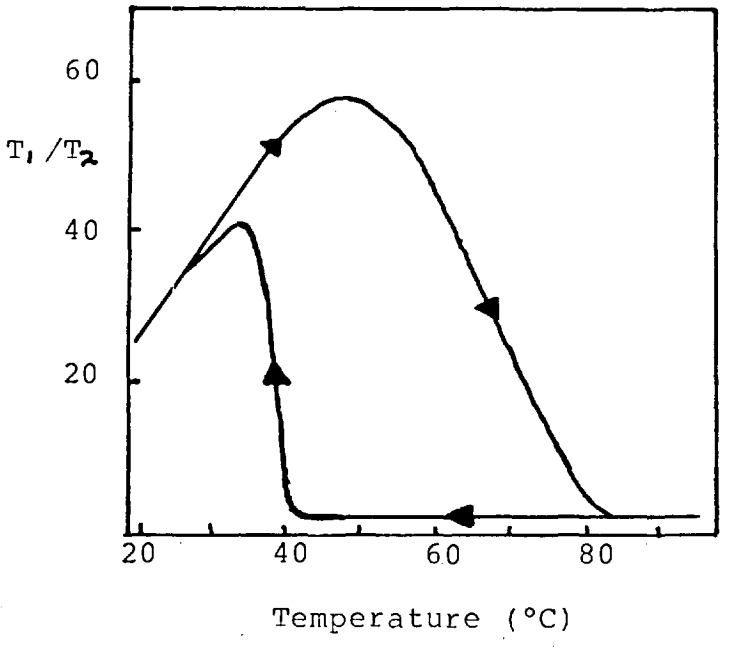


Figure 2.5 Temperature dependence of the longitudinal to transverse relaxation time ratio T_1/T_2 for a 2.0 wt.% agarose solution [16].

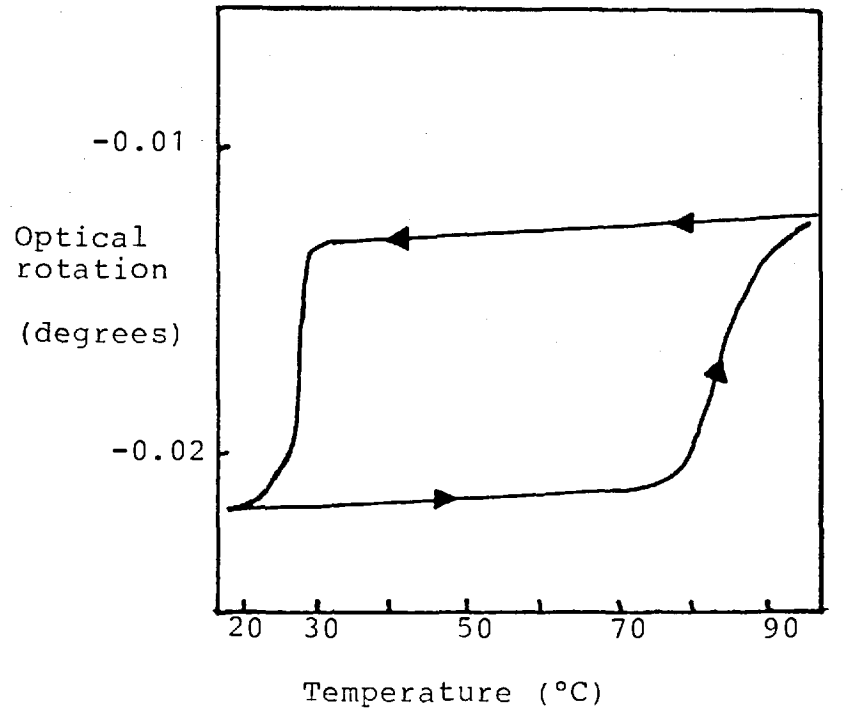


Figure 2.6 Variation of optical rotation with temperature for a 0.05 wt.% agarose solution [15].

A recent study by Hayashi [29] using fluorescence polarisation confirmed the hysteresis cycle (figure 2.7). However, Hayashi also observed a new transition point, T_2, at ~53°C.

This new transition was also observed in measurements of the reduced viscosity, optical rotation and by the technique of differential scanning calorimetry. Hayashi concluded that the new transition, T_2, was associated with helix formation as proposed by Rees (see section 2.3) and that T_1 was associated with a slower gelling reaction. We will dissent from this view.

2.3 The Agarose Molecule

A detailed examination of the physical characteristics of the agarose molecule was undertaken by Hickson and Polson [24]. They concluded from transmission electron microscopy that the chains were linear with a mean length of $(2.6\pm0.3)\times10^3$ Å. The width of the molecule was found to be (15.7±0.9)Å. The molecular weight as evaluated by diffusion/viscosity and sedimentation/viscosity techniques was found to be ~120,000. The molecular weight has been confirmed by Child and Pryce [14] (110,000-170,000)and by Prins [28] (120,000). Laurent [25], using exclusion chromatography, concluded that the diameter of the agarose molecule in the gel state was ~50Å and that the hydrated fibres contained 35-50% water.

X-ray diffraction techniques have been employed to study the packing configuration of many polysaccharides in

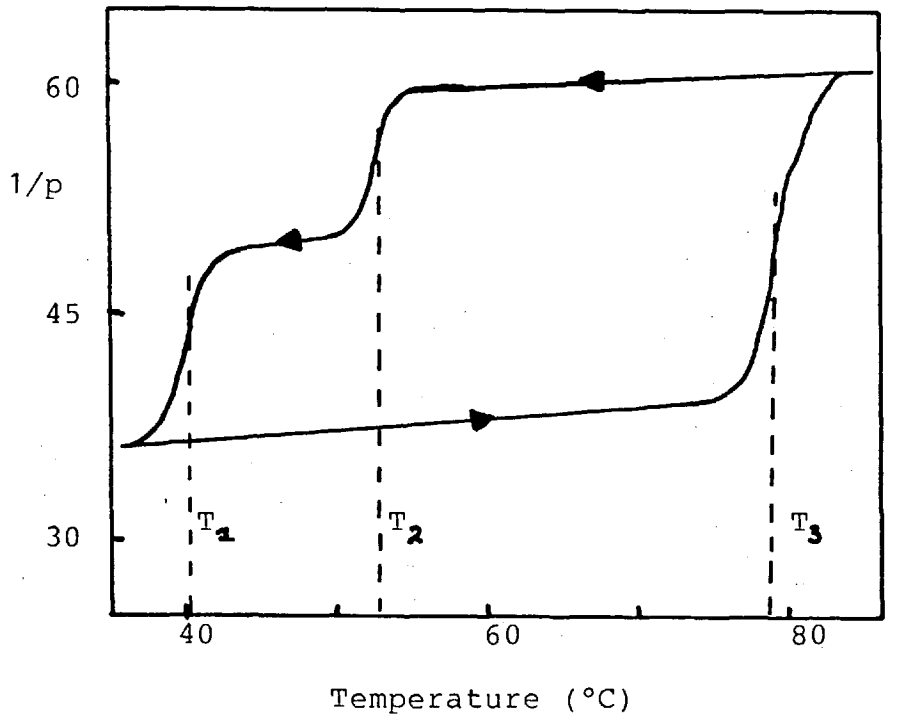


Figure 2.7 Changes in the degree of polarisation of fluorescence (p) with temperature for a 0.3 wt.% agarose solution. [29]

the form of fibres and oriented films. Thus, studies of fibres of k-carrageenan and i-carrageenan [21] have revealed that these polysaccharides exist in the form of double helices with three disaccharide residues per turn of each single chain. X-ray diffraction studies of agarose and several derivatives [11] suggested that double helices were present in fibres and oriented films. Each chain in the double helix was found to form a left-handed 3-fold helix of pitch 1.90 nm. and to be translated axially relative to its partner by exactly half this distance. (Figure 2.8).

Assuming that the ordered structure in such fibres and films is closely related to the ordered configuration that exists in the gel "junction zones", Rees has claimed that the observed changes in optical rotation are consistent with gel formation involving a random coil → double helix conformation change. [2,11,21,22].

The proposed mechanism (figure 2.9) is a two-stage process involving,

1) Coil → double helix transformation resulting in chains crosslinked by isolated double helices.
2) Aggregation of the double helices.

The two stages are thought to be,to some extent, consecutive [22].

This would suggest, considering Laurent's finding of the width of the agarose chains in the gel state, that the postulated aggregates contain 7-11 double helical units.

Since Rees' proposal of the formation of double helices

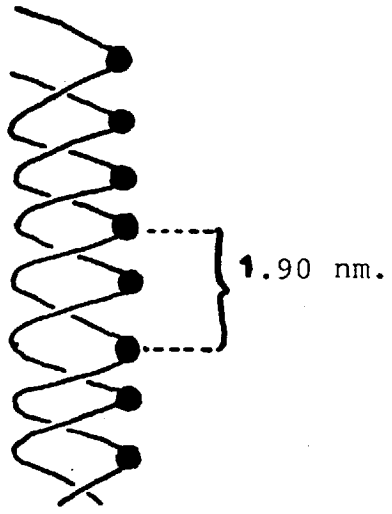


Figure 2.8 The proposed agarose double helix

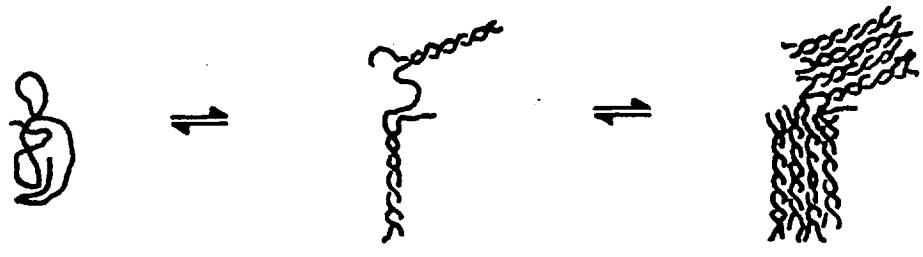


Figure 2.9 Proposed gelation mechanism (Rees)

nearly all experimental observations have been interpreted with reference to this mechanism. However, very recent high resolution X-ray diffraction studies by Atkins [23], which are in general agreement with accepted notions of double and triple helix formation in the carrageenan family, indicate that the association of agarose chains in fibres and oriented films can occur in three distinct crystallographic arrangements, none of which involves the formation of a double helix. Briefly, Atkins' diffraction data, consisting of up to 80 reflections, show that the polysaccharide chains adopt a more elongated conformation. Atkins finds the true layer line spacing to be 28.5Å and that the helices are three-fold with an axial advance of 9.5Å (compared with 6.33Å as found by Rees/Arnott). Such an extended helix cannot intertwine and thus the formation of double helices is ruled out.

Thus the mode of aggregation of the agarose chains during gel formation remains unsolved. However, any "junction zones" or cluster formation in agarose gels must result from the aggregation of single helices in some manner.

CHAPTER 3

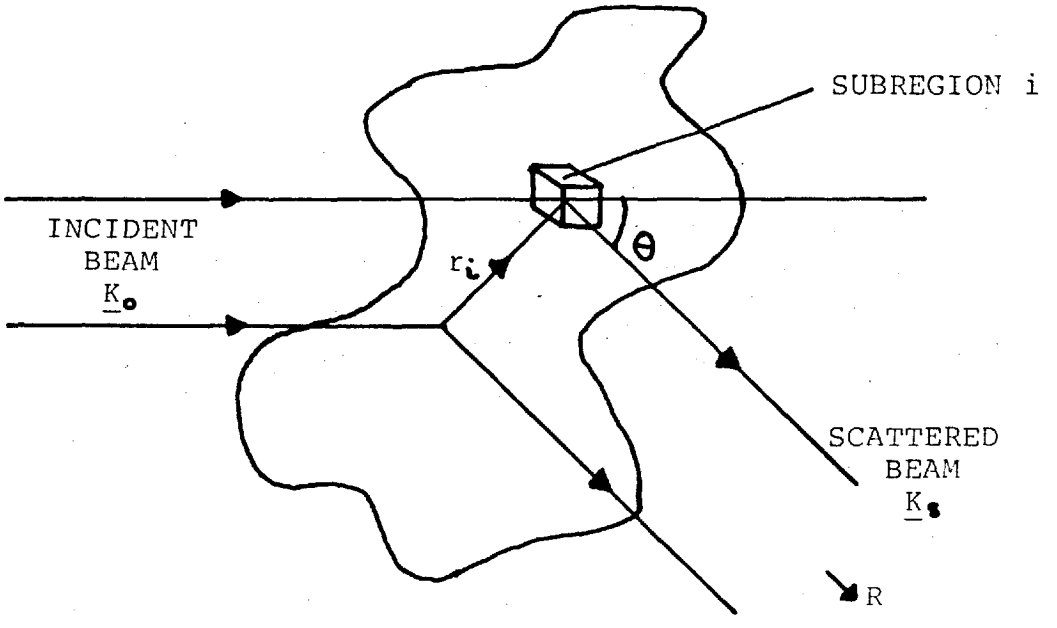
Photon Correlation Spectroscopy

3.1 Principles of Light Scattering

In the classical theory of light scattering an incident beam of polarised light exerts a force on the charges within any dielectric medium. These accelerating charges then radiate light in all directions. If the illuminated volume is considered to be made up of numerous subregions, small in comparison to the incident light wavelength, then the net scattered electric field at any point in space is the vector sum of the scattered field from each subregion. If each subregion, however, is optically identical then the scattered field from each will be identical in amplitude but will differ in phase because of the various spatial positions of the subregions. For a large number of such identical subregions the phase differences at any point in space will cancel out, leaving no net scattered light except in the forward direction. If the subregions are not optically identical then the amplitude of the scattered field from each will no longer be identical and complete cancellation cannot occur.

Accordingly the scattering of an incident light beam occurs because of optical inhomogeneities in the scattering medium. In a liquid these arise because of the translational and rotational motions of the molecules which cause fluctuations in the instantaneous dielectric constant of any given subregion.

Let the incident electric field be a plane wave of the



SCATTERING VECTOR $\underline{K}$: $\underline{K}=\underline{K}_o-\underline{K}_s=\frac{4\pi n}{\lambda_o}\sin\theta/2$

Figure 3.1 Scattering of an incident light beam by a dielectric medium.

form:

$E(\underline{r},t) = E_o \exp i\ (\underline{K}_o.\underline{r}-w_o t)....(1)$

where E_o = amplitude of the field

w_o = angular frequency

$[\underline{K}_o]$ = wavevector = $\frac{2\pi n}{\lambda_o}$

This wave is incident upon a medium whose local dielectric constant is given by:

$\varepsilon(\underline{r},t) = \langle\varepsilon\rangle + \delta\varepsilon(\underline{r},t)....(2)$

In the far field approximation the scattered electric field at an angle θ is given by:

$E_{s,i}(\underline{R},t) = A\ \varepsilon(\underline{r}_i,t) \exp i\ (\underline{K}.\underline{r}_i-w_o t)....(3)$

A = scattering amplitude = $f(\lambda,\underline{R})$, where the detector is a distance R from the scattering volume.

Considering the scattering volume to consist of N subregions:

$$E_s(\underline{R},t) = A' \exp(-iw_o t) \sum_{i=1}^{N} \varepsilon(\underline{r}_i,t) \exp i\ (\underline{K}.\underline{r}_i)....(4)$$

Substituting equation (2).

$$E_s(\underline{R},t) = A' \exp(-iw_o t)\ [\langle\varepsilon\rangle \sum_{i=1}^{N} \exp i\ (\underline{K}.\underline{r}_i) + \sum_{i=1}^{N} \delta\varepsilon(\underline{r}_i,t) \exp i\ (\underline{K}.\underline{r}_i)]....(5)$$

The first summation term will be zero except for scattering in the forward direction. The second term gives the scattering originating from fluctuations of the dielectric constant ($\theta \neq 0$).

Thus:

$$E_{s(\theta\neq 0)} = A' \exp(-iw_o t) \sum_{i=1}^{N} \delta\varepsilon(\underline{r}_i,t) \exp i\ (\underline{K}.\underline{r}_i)$$

$$= A' \exp(-iw_o t) \int_{dv} \delta\varepsilon(\underline{r},t) \exp\left[i\ (\underline{K}.\underline{r})\right] d\underline{r}$$

$$= A' \exp(-iw_o t)\ \ \delta\varepsilon(\underline{K},t)....(6)$$

where $\delta\varepsilon(\underline{r},t)$ and $\delta\varepsilon(\underline{K},t)$ are a fourier transform pair.

Thus in a pure fluid the instantaneous scattered field in a direction Θ ($\theta \neq 0$; $\underline{K} \neq 0$) is proportional to the instantaneous magnitude of the spatial fourier component of the dielectric fluctuation. Thus the perpetual motion of the molecules within the medium causes the total scattered electric field at the detector to fluctuate in time. Since thermal molecular motion is stochastic in nature the total scattered field varies randomly at the detector. These fluctuations, however, may yield important structural and dynamic information about the positions and orientations of the molecules.

Since the scattered field and scattered intensity are simply related:

$I_s = B \langle E_s E_s^* \rangle$ B= constant

Then:

$I_s \propto \langle \delta\varepsilon(\underline{K},t)^2 \rangle$ for fixed R,λ,θ....(7)

Thus the mean square value of the dielectric fluctuations may be obtained from intensity measurements of the scattered light. This may in turn be related to thermodynamic properties of the medium such as the isothermal compressibility and osmotic pressure [30].

When a pure solvent is made more inhomogeneous by the addition of solute the increase in scattered intensity may be used in order to evaluate the number of solute particles per unit volume; in appropriate cases conclusions about the size and shape of these particles can be drawn from observations of the angular distribution of the scattered light [31].

For a dilute non-interacting polymer solution the time averaged scattered intensity may be written:

$\langle I_s \rangle \propto M\ P(K) \ldots . (8)$

where M is the molecular weight of the polymer chain and P(K) is the single particle scattering factor, which is related to the shape of the polymer molecule [32].

For more concentrated solutions the angular variation of scattered intensity also contains information concerning the interactions between solute particles:

$\langle I_s \rangle \propto M\ P(K)\ S(K) \ldots . (9)$

where S(K) is termed the structure factor and is the fourier transform of the pair distribution function g(r):

$$S(K) = 1+4\pi\rho \int_0^\infty r^2 \frac{\sin Kr}{Kr} (g(r)-1)dr \ldots . (10)$$

It can easily be shown for non-interacting systems (for which the pair correlation function is unity) that the above reduces to equation (8).

Thus studies of the angular variation of the scattered light from polymer solutions can be used in order to study the size, shape and geometrical positions of the scattering particles.

3.2 Fluctuations and Correlation Functions

Time dependent correlation functions are familiar tools in the areas of noise analysis and stochastic processes. They provide a concise method of expressing the degree to which two dynamic properties are correlated over a period of time.

Figure 3.2 shows a plot of a random signal, I(t), for example the output current of a photodetector, as a function of time.

An infinite time average for this process may be

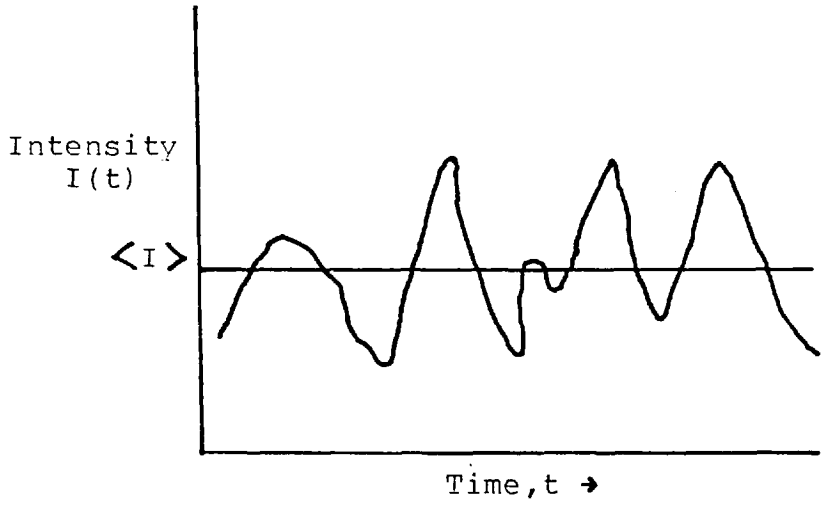


Figure 3.2 A randomly fluctuating intensity signal

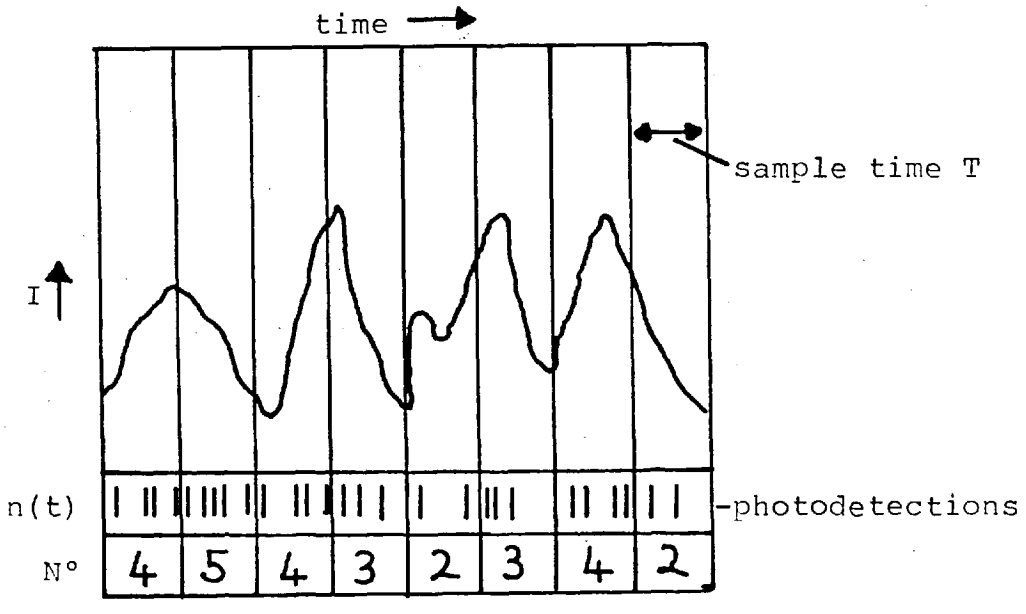


Figure 3.3 Intensity signal and photon counting

expressed:

$$\overline{I\ (t_0)} = \lim_{(T-t_0)\to\infty} \frac{1}{T} \int_{t_0}^{T} I(t)\ dt$$

where t_o is the time at which measurement of I(t) began and T is the time for which measurements were taken.

The process is termed "stationary" provided the infinite time average $\overline{I(t_o)}$ is independent of the time at which measurements began. Then:

$$\langle I \rangle = \lim_{T\to\infty} \frac{1}{T} \int_{0}^{T} I(t)\ dt$$

Thus the value of I(t) fluctuates randomly about its time averaged value $\langle I \rangle$.

The time correlation function for the process is defined:

$$G(\tau) = \lim_{T\to\infty} \frac{1}{T} \int_{0}^{T} I(t)\ I(t+\tau)\ dt$$

$$= \langle I(t)\ I\ (t+\tau) \rangle$$

When τ is very small the values of I(t) and I(t+τ) will be close. However, as τ increases the potential deviations of I(t+τ) from I(t) become greater. Thus at small τ the value of I(t+τ) is highly correlated with I(t) but as τ increases the correlation is lost:

$$\tau\to 0 \quad \langle I(t)\ I(t+\tau) \rangle \quad \to \langle I(t)^2 \rangle$$

$$\tau\to\infty \quad \langle I(t)\ I(t+\tau) \rangle \quad \to \langle I(t) \rangle \langle I(t) \rangle = \langle I(t) \rangle^2$$

Thus the correlation function G(τ) decays from a value of $\langle I(t)^2 \rangle$ to $\langle I(t) \rangle^2$ in the course of time. In many applications the correlation function decays as a single exponential so that:

$$\langle I(t)\ I(t+\tau) \rangle = \langle I(t) \rangle^2 + \left[\langle I(t)^2 \rangle - \langle I(t) \rangle^2 \right] \exp - \frac{\tau}{\tau_r}$$

where τ_r is the relaxation time or correlation time for the process.

By considering a section of the (I(t), time) plot and

then rigorously decomposing the signal into its fourier components it can be shown that the correlation function is the inverse fourier transform of the power spectral density, S(w):

$$\langle I(t)^* I(t+\tau) \rangle = \int_{-\infty}^{\infty} S(w) \exp(-iw\tau)\, dw$$

and thus the power spectral density is the time fourier transform of the correlation function.

$$S(w) = \frac{1}{2\pi} \int_{-\infty}^{\infty} \langle I(t+\tau) I^*(t) \rangle \exp(iw\tau)\, d\tau$$

The above equations relating the intensity correlation function and spectral density are known as the "Wiener-Khintchine Theorem".

3.3 Operation of a Digital Correlator [33,34,35]

Figure 3.3 shows a trace of the fluctuating intensity at a photodetector. In quantum mechanical terms the field at the detector gives rise to a Poisson probability of obtaining a photodetection, in a short time Δt, proportional to the intensity:

$$\overline{n(t)} \propto |E^+(t)|^2 \propto I$$

Thus the output pulse train of the photodetector consists of a Poisson probability process modulated by the fluctuations in scattered intensity. The signal then passes to an amplifier/discriminator which standardises the signal into pulses of a set width. Each pulse corresponds to the detection of a photon at the photodetector.

Thus the number of counts received per sample time, T, is recorded as in figure 3.3. If n(t,T) represents the number of counts received in an interval T centred on time

t, then to obtain the full photocount autocorrelation function the quantity:

$\langle n(0,T)\ n\ (t,T) \rangle$

has to be evaluated. This may be achieved by counting the photodetections occurring during each of a number of consecutive sample times and multiplying the current signal, channel by channel, with the delayed information. However, the above multiplications involving numbers greater than unity are time consuming and therefore limit the speed of operation, as well as being very costly in terms of hardware.

In practice, one generally uses "clipped" rather than full autocorrelation functions. The clipped count is defined as:

$n_k\ (t,T) = 1 \quad \text{if} \quad n(t,T) > k$

$n_k\ (t,T) = 0 \quad \text{if} \quad n(t,T) \leqslant k$

where the integer k is the "clipping level". The clipping level is adjusted to be equal to the mean number of counts per sample time, $\overline{n(t,T)}$, so that there is an equal probability of n(t,T) being above or below a given k.

The accumulation of the single clipped correlation function within the correlator is achieved as follows: (figure 3.4).

The incoming pulses in any given sample time are counted in a scalar which has a preset overflow, k(the clipping level), such that for:

$n(T) > k$ the clipping gate is set into the "1" state

$n(T) \leqslant k$ the clipping gate is set into the "0" state.

The unclipped count is multiplied by the delayed clipped signals (0 or 1) using "and" gates and the

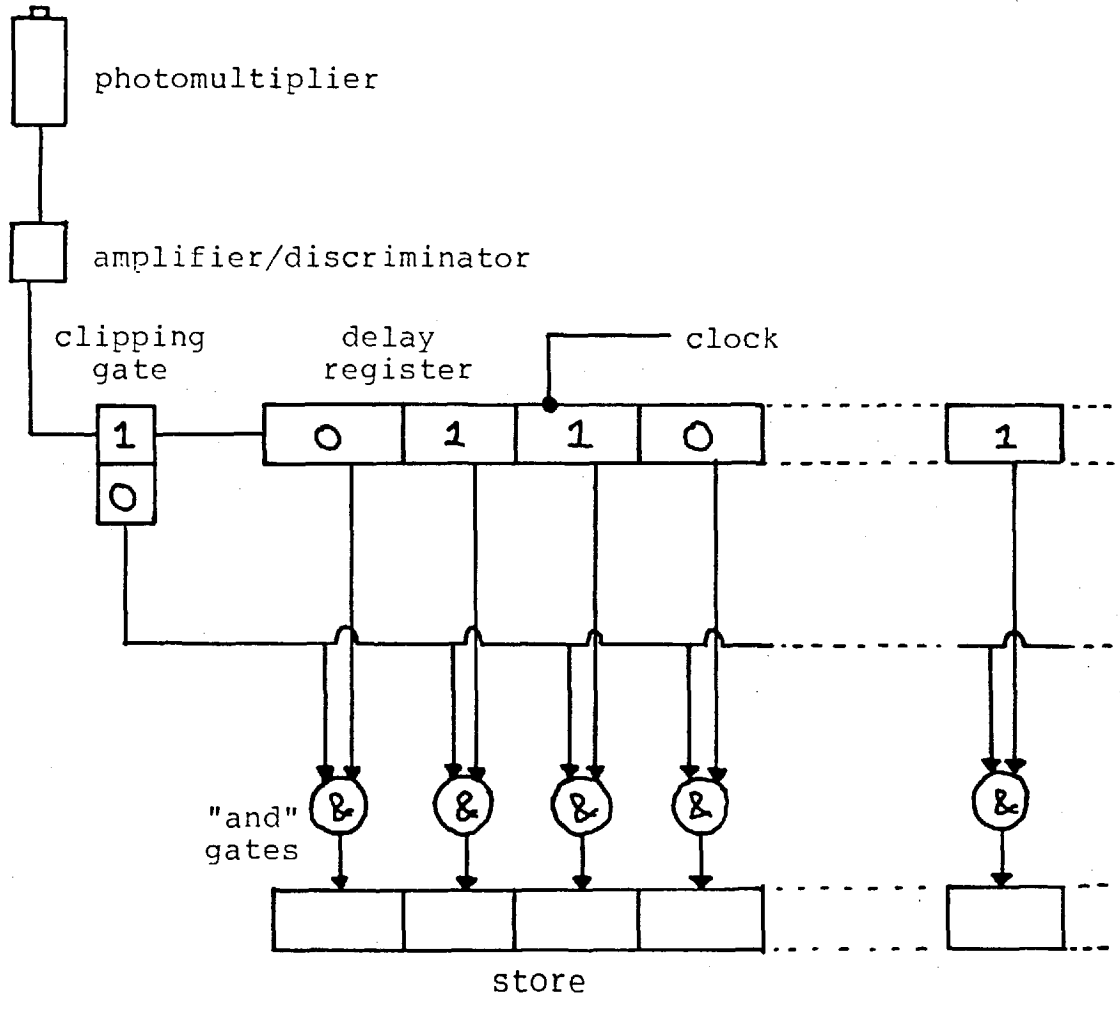


Figure 3.4 Operation of a digital correlator

product added to the channel store. At the end of each sample time the contents of the delay register are moved one position to the right and the contents of the clipping gate (0 or 1) loaded into the first delay register. The clipping gate and scalar are reset and another sample interval commenced.

Thus the single clipped correlator has evaluated

$$G^{(2)}(r,T) = N\langle n(t,T)\ n_k\ (t-rT,T)\rangle$$
$$= N\langle n_k(t)\ n\ (t+rT,T)\rangle$$

where r is the number of stores available in the correlator.

The use of clipped correlation functions leads to considerable simplification in the circuitry and faster operation of the correlator with little loss in the physical information obtained.

Provided the number of scatterers is large and the scattered electric field has a Gaussian amplitude distribution the single clipped function is given by [36,37]:

$$\langle n\ (t)\ n\ (t+\tau)\rangle = \langle n\rangle\ \langle n_k\rangle \left[1+\beta\frac{(1+k)}{1+\langle n\rangle}\left|g^{(1)}(\tau)\right|^2\right]$$

where β is a constant related to the finite aperture size of the photomultiplier detection system and:

$$g^{(1)}(\tau) = \frac{\langle E^*(t)E(t+\tau)\rangle}{\langle E(t)^2\rangle}$$

i.e. the normalised electric field autocorrelation function.

Thus with the single clipped correlation function, a knowledge of the total number of samples taken (N), the total number of counts detected (n_T) and the total number of clipped counts ($n_{T,K}$) the electric field correlation function may be evaluated since:

$$G^{(2)}(\tau) = N\ \langle n_k(t)\ n\ (t+\tau)\rangle$$

is the quantity evaluated experimentally and:

$$1+\frac{\beta(1+k)}{1+\langle n\rangle}\left|g^{(1)}(t)\right|^2 = \frac{\langle n_K(t)\ n\ (t+\tau)\rangle}{\langle n\rangle\quad\langle n_K\rangle} = G^{(2)}(t)\cdot\frac{N}{n_T n_{T,K}}$$

Therefore:

$$G^{(2)}(t)\left[\frac{N}{n_T\cdot n_{T,K}}\right] - 1 = \frac{\beta(1+k)}{1+\langle n\rangle}\left|g^{(1)}(t)\right|^2$$

In the foregoing sections it has been shown that when intensity light scattering and $g^{(1)}(t)$ are taken together, one can obtain important structural and dynamic information about the scattering species [38]. In the following sections the application of photon correlation spectroscopy and the information contained in $g^{(1)}(t)$ in relation to polymer systems and gels will be discussed.

3.4 Ideal Polymer Solutions.

3.4a Light Scattering Studies.

It has been shown in section 3.1 that scattered intensity ($\theta\neq0$; $K\neq0$) arises from fluctuations in the local dielectric constant. For pure liquids these are attributed to the thermal motion of the molecules. In polymer solutions, however, the polarisibility of the solvent molecules can be chosen to be small compared with that of the macromolecules. Thus the macromolecules dominate the behaviour of the dielectric fluctuations.

Thus considering a macromolecule of n_s identical segments then the polarisibility $\alpha(\underline{r},t)$ is given by:

$$\alpha(\underline{r},t) = \sum_{i=1}^{n_s} D_i(t)\quad\delta[\underline{r}-\underline{r}_i(t)]$$

where $D_i(t)$ relates to the orientation of the i^{th} segment and $\underline{r}_i$ is the position of the i^{th} segment relative to an

external frame of reference.

Performing a fourier transform:

$$\alpha(\underline{K},t) = \sum_{i=1}^{n_s} D_i\ (t)\ \exp\ i(\underline{K}.\underline{r}_i(t))$$

The magnitude of the scattered electric field may be obtained:

$$E_S = A'\ \exp\ (-iw_o t) \sum_{i=1}^{n_s} D_i(t)\ \exp\ i(\underline{K}.\underline{r}_i(t))$$

Substituting $\underline{r}_i = \underline{R}+\underline{b}_i$

where $\underline{R}$ is the vector position of the centre of mass of the polymer coil and $\underline{b}_i$ is the vector from the centre of mass to segment i, we obtain:

$$E_S = A'\ \exp(-iw_o t) \sum_{i=1}^{n_s} D_i(t)\ \exp\ i(\underline{K}.\underline{R}(t))$$

$$\times\ \exp\ i(\underline{K}.\underline{b}_i(t))$$

For an optically isotropic molecule D is a scalar and hence:

$$E_S \propto \sum_{i=1}^{n_s} \exp\ i(\underline{K}.\underline{R}(t))\ \exp\ i(\underline{K}.\underline{b}_i(t))$$

Thus the temporal electric field correlation function may be written:

$$\langle E_S^*(0)\ E_S(t)\rangle \propto \Big\langle \sum_{i=1}^{n_s} \exp\ i(\underline{K}.\underline{R}(t))\ \exp\ i(\underline{K}.\underline{b}_i(t))$$

$$\times \sum_{j=1}^{n_s} \exp -i(\underline{K}.\underline{R}(0))\ \exp\ -i(\underline{K}.\underline{b}_j(0))\Big\rangle$$

$$\propto \Big\langle \sum_{i,j=1}^{n_s} \exp\ i(\underline{K}.(\underline{R}(t)-\underline{R}(0)))$$

$$\times\ \exp\ i(\underline{K}.(\underline{b}_i(t)-\underline{b}_j(0))\Big\rangle$$

For small molecules $\left|\underline{b}_i(t)-\underline{b}_j(0)\right|$ will be small. Also at small scattering angles $\underline{K}$ is small. Then:

$$\sum_{i,j=1}^{n_s} \exp\ i(\underline{K}.(\underline{b}_i(t)-\underline{b}_j(0)) \approx n_s^2$$

Thus :

$$\langle E_S^*(0)\ E_S(t)\rangle \propto \langle \exp\ i(\underline{K}.(\underline{R}(t)-\underline{R}(0)))\rangle$$

which is determined solely by the translational motion of the centre of mass of the macromolecule.

We define:

$$F(\underline{K},t) = \langle \exp i(\underline{K}.(\underline{R}(t)-\underline{R}(0))) \rangle$$

where $F(\underline{K},t)$ is termed the intermediate scattering function which is related to the self component of the Van Hove space time correlation function, $G_s(\underline{r},t)$, via an inverse fourier transform:

$$F_s(\underline{K},t) = \int d^3\underline{r}\ e^{i\underline{k}.\underline{r}}\ G_s(\underline{r},t)\ d\underline{r}$$

where $G_s(\underline{r},t)$ is the probability that a particle at the origin at time t=0 will be at a position $\underline{r} \rightarrow \underline{r}+d\underline{r}$ at time t, and is thus the Green's function solution of a diffusion equation.

Solving the appropriate Brownian diffusion equations:

$$\frac{\partial G_s(\underline{r},t)}{\partial t} = D\ \nabla^2 G_s(\underline{r},t)$$

then:

$$\frac{\partial F_s(\underline{K},t)}{\partial t} = -K^2 D\ F_s(\underline{K},t)$$

Therefore:

$$F_s(\underline{K},t) = \exp(-K^2Dt)$$

where D is the translational diffusion coefficient of the species.

Thus:

$$\langle E_s^*(0)E_s(t)\rangle \propto P(K)\exp(-K^2Dt)$$

The single particle scattering factor, P(K), is unity for scattering species whose dimensions are smaller than $\sim\lambda/20$. For larger dimensions, P(K) is determined by the shape of the scattering species[32].

The normalised electric field autocorrelation function $g^{(1)}(t)$ is related to the intermediate scattering function

by:

$$g^{(1)}(\underline{K},t) = \frac{\langle E_s^*(0)\ E_s(t)\rangle}{\langle E_s(t)^2\rangle}$$

where $\langle E_s(t)^2\rangle = \langle I(\underline{K},0)\rangle = \langle I(\underline{K},t)\rangle$, the time averaged intensity.

The time averaged intensity is given by: (section 3.1)

$$\langle I(\underline{K},t)\rangle \propto P(K)\ S(K)$$

Thus

$$g^{(1)}(\underline{K},t) = \frac{\langle E_s^*(0)E_s(t)\rangle}{\langle I(\underline{K},t)\rangle} = \frac{F_s(K,t)\ P(K)}{P(K)\ S(K)}$$

$$= \frac{F_s(K,t)}{S(K)}$$

Thus for the case of simple brownian diffusion:

$$g^{(1)}(\underline{K},t) = \frac{\exp - K^2Dt}{S(K)}$$

$S(K)$ is determined by the pair distribution function and for a dilute non-interacting solution $S(K) \rightarrow 1$.

Thus for a system of dilute, spherical, non-interacting species undergoing brownian motion:

$$g^{(1)}(\underline{K},t) = \exp - K^2Dt$$

Considering the experimentally determined quantity, the photocount autocorrelation function, then for such a system:

$$G^{(2)}(\underline{K},t)\ \frac{N}{n_T n_{T,k}} = 1 + \frac{\beta(1+k)}{(1+\langle n\rangle)}\ \exp -2K^2Dt$$

where the left-hand side of this equation is termed the normalised second order electric field autocorrelation function:

Then:

$$\ln\left\{g^{(2)}(\underline{K},t) - 1\right\} = -2K^2Dt + \ln\ R$$

where $R = \frac{\beta(1+k)}{(1+\langle n\rangle)}$

Thus a plot of the natural logarithm of $\left\{g^{(2)}(\underline{K},t) - 1\right\}$; t

should be linear with a gradient of $-2K^2D$. Accordingly the translational diffusion coefficient may be directly evaluated from the correlation function of the scattered light.

3.4b Polydispersity

All synthetic macromolecules possess some degree of polydispersity. For a monodisperse system of small, spherical, non-interacting species undergoing Brownian diffusion it has been shown that:

$$g^{(1)}(\underline{K},t) = \exp - K^2Dt = \exp - \Gamma t$$

However, for a polydisperse system Γ will now contain contributions from all the various macromolecular chains:

$$g^{(1)}(\underline{K},t) = \int_0^\infty G(\Gamma)\, e^{-\Gamma t}\, d\Gamma$$

where $G(\Gamma)d\Gamma$ is the fraction of the total scattered intensity which obeys $\Gamma=DK^2$ within the increment $d\Gamma$.

The standard approach to such a polydisperse system is based on the method of cumulants as devised by Koppel [39]:

$$g^{(1)}(\underline{K},t) = \overline{\exp - \Gamma t}$$

where the bar denotes an average over Γ weighted by the distribution function $G(\Gamma)$.

The moments of the distribution are given by:

$$\mu_m(\Gamma) = \frac{d^m}{d(-t)^m}\, g^{(1)}(\underline{K},t)\Big|_{-t=0}$$

The cumulants of Γ are then given by:

$$K_m(\Gamma) = \frac{d^m}{d(-t)^m} \ln g^{(1)}(\underline{K},t)\Big|_{-t=0}$$

Thus: $K_1 = \overline{\Gamma}$; $K_2 = \overline{(\Gamma-\overline{\Gamma})^2}$

and: $\overline{D} = \overline{\Gamma}/K^2$

If the intensity of light scattered by the

macromolecules is proportional to the molecular weight multiplied by the weight concentration then:

$$G(\Gamma) = \sum_i c_i M_i^w (\delta\Gamma - \Gamma_i) \Big/ \sum_i c_i M_i^w$$

where M^w is the molecular weight.

Therefore:

$$\bar{D} = \bar{\Gamma}/K^2 = \sum_i c_i M_i^w D_i \Big/ \sum_i c_i M_i^w$$

$$= D_z$$

where D_z is the so-called z-average diffusion coefficient. The second cumulant K_2 when normalised by $(K_1)^2$ is related to the width of the distribution and can thus give a measure of polydispersity. For a Gaussian distribution all higher moments are zero.

A simpler but less rigorous approach has been proposed by Pusey [40]:

$$g^{(1)}(\underline{K},t) = \exp -\bar{\Gamma}t \left\{1 + \frac{\mu_2 t^2}{2!} + \frac{\mu_3 t^3}{3!} + \ldots\right\}$$

where μ_i is the i^{th} moment of the distribution about the mean of $G(\Gamma)$.

Thus the initial slope of a $(\ell n\, g^{(1)}(K,t); t)$ plot gives the negative mean decay rate, $-\bar{\Gamma}$. The second moment is obtained by differentiation:

$$\lim_{t \to 0} \frac{\partial^2}{\partial t^2} \ell n\, g^{(1)}(\underline{K},t) = \mu_2$$

Pusey also defined a quality parameter, Q, where:

$$Q = \mu_2/\bar{\Gamma}^2$$

i.e. for a single exponential decay Q = 0.

Although these techniques are commonly employed in the analysis of experimental data, it must be stated that photon correlation spectroscopy is relatively insensitive to the multiple decay times arising from polydispersity and the

determination of the detailed form of $G(\Gamma)$ is not normally possible. It should also be noted that the 24-channel correlator used in this work did not provide data suitable for moment analysis. Only during the last few weeks of the project did 96 channels become available. Their use demonstrated that non-exponentiality is not a major problem.

3.4c Internal Motions

In the foregoing derivation for the physical interpretation of the photocount autocorrelation function of a macromolecular solution it was assumed that $\left|\underline{K}.(\underline{b}_i(t)-\underline{b}_j(0))\right| \ll 1$ This need not be the case.

For large molecules this intramolecular factor must be considered, when evaluation of the rotational diffusion coefficient becomes possible.

Considering the case of a rigid rod [41,42].

$$g^{(1)}(K,t) = P_0(KL)\ \exp -D_T K^2 t + P_1(KL)\ \exp -(D_T K^2 + 6D_R)t + \ldots\ldots$$

where P_i is the relative integrated scattered intensity. P_0 refers to pure translation. P_1 refers to the first non-zero term that contains the rotational diffusion coefficient. L is the length of the rigid rod.

Pecora has shown [43] that, for $KL < 3$, P_1 contributes less than 1% to the total scattered intensity, when measurements in this regime may be analysed in terms of:

$$g^{(1)}(K,t) \propto \exp - D_T K^2 t$$

For $KL > 5$ the contribution of P_1 is significant and the spectral width is related to both D_T and D_R.

Hence having obtained the translational diffusion

coefficient at low K (KL<3) the rotational diffusion coefficient may be evaluated from measurements at higher K (KL>5).

In this treatment, however, the translational and rotational motions are not coupled. The coupling of these motions has been studied by Maedo and Saito [44] who calculated that the coupling term contributes less than 1% at small K but may become significant (~8%) at higher K values.

In addition to rigid rods, the internal modes of flexible coil macromolecules have also been investigated theoretically. For the internal motions of flexible coil macromolecules:

$$g^{(1)}(K,t) = \sum_{m,n} R_{m,n} \exp - (DK^2 + \frac{m}{\tau_n})t$$

where τ_n is the decay time of the n^{th} normal mode. The double summation is necessary since each normal mode contributes an infinite series of Lorentzian functions. Pecora [42] has shown that for coils of radius of gyration less than 2000 Å the internal motions cannot be observed by means of quasi-elastic light scattering.

However, the internal motions of smaller molecules may be investigated using neutron scattering techniques.

Thus much attention has been focused on the internal motions of flexible coil polymers both experimentally [45,46,47] and theoretically [47,48,49,50,51,52]. Much of this work has been concerned with the wavevector dependence of the characteristic time τ_n i.e.

$$g^{(1)}(K,t) \propto \exp - \frac{t}{\tau_n} \qquad \text{i.e.} \frac{1}{\tau_n} = \Gamma$$

The findings, both theoretical and experimental, are summarised below:

1) For $KR \ll 1$ (where R is the radius of gyration of the coil) a single exponential decay is obtained with $\Gamma = D_T K^2$. Thus the translational diffusion coefficient only may be evaluated in this regime.

2) At higher values of KR the internal modes contribute to the total scattered intensity and Γ is found to increase faster than K^2. Theoretical predictions for this regime have shown a high degree of consistency. For a Rouse coil (free-draining) it has been shown that Γ should vary as K^4. For Zimm-type coils with the inclusion of hydrodynamic interactions between segments Γ should vary as K^3. However, the predictions differ on the point of whether the decay should be exponential in time . Experimental evidence has shown good agreement with the Zimm-type coil predictions ($\Gamma \propto K^3$) and suggests that the decay is non-exponential [46].

Thus we may conclude that when the scattering vector, $K > 1/R$ internal motions within the polymer chain contribute significantly to the scattered intensity. In this regime the characteristic time is found to vary as K^{-3} (as predicted by the more realistic Zimm-coil model), although the detailed nature of the temporal correlation function has not been satisfactorily established.

3.5 Complex Systems

In the previous sections the spectrum of scattered

light for a system of dilute, non-interacting molecules was discussed. When many particles are present the interactions between particles become important. These interactions may be direct, such as charge effects, or indirect such as that mediated by the motion of solvent molecules. Thus the resulting motion for the many-particle system may be quite different from that of the single diffusing particle.

The effects of intermolecular interactions on diffusion have been considered by numerous authors [53,54, 55,56]. Phillies [57] predicted that when the inverse wavevector was of the order of the interparticle separation, r, then a significant wavevector dependence of the diffusion coefficient should be observed provided $\frac{\partial U}{\partial r}$ is non-zero (U is the interparticle interaction energy). In 1974 Brown et. al. [58] found such a wavevector dependence of the effective diffusion coefficient when studying aqueous dispersions of charged polystyrene spheres. Using the techniques of intensity light scattering and photon correlation spectroscopy they concluded that the effective diffusion coefficient obtained from the mean decay rate exhibited a similar angular dependence to that of $S(K)^{-1}$ [59] i.e.,

$$-\overline{\Gamma} = \frac{d}{dt}\left| g^{(1)}(K,t)\right|_{t\to 0} = \frac{-K^2 D_o}{S(K)}$$

This empirical relationship has been derived theoretically and discussed by several workers [60,61,62], but in the form quoted there is no allowance for the influence of hydrodynamic interactions on D_o.

The various types of interactions may be considered according to different time scales:

1) For times short compared to the collision time between Brownian particles and solvent molecules i.e. $\tau < \tau_B$: equivalent frequency $\sim > 10^{10}$ Hz. This is beyond the range of the time-domain correlation techniques available, the internal correlation time of the photomultiplier being $\sim 0.4\mu s$.

2) Intermediate times which are long compared to the time between solvent molecule and Brownian particle collisions but short compared to the time between Brownian particle collisions i.e. $\tau_B < \tau < \tau_I$: equivalent frequency $\sim 10^3 - 10^6$ Hz.

3) Long times greater than the time between collisions between Brownian particles i.e. $\tau > \tau_I$: equivalent frequency $\sim 10^2$ Hz.

Quasi-elastic light scattering may be used to study both the intermediate and long time scales, but neutron scattering techniques have to be employed to probe short times. We are principally concerned with the intermediate time scale.

Ackerson [60] employed the generalised Smoluchowski equation to calculate the first two cumulants of the decay of the intermediate scattering function for interacting colloidal particles. The result obtained for the first cumulant agreed with that found experimentally by Brown et.al.. It was shown that the second cumulant should provide information about the effective inter-colloidal potential. These findings refer to the intermediate time scale, since the first cumulant is obtained from the initial

decay of the normalised correlation function and the interaction enters through normalisation by the static structure factor, $S(K)$.

The separation between intermediate and long time scales has been exhibited by Brown et. al. (figure 7). For large values of the wavevector, $\underline{K}$, the characteristic time will be small compared with the interaction time and the small excursions of the particle will be Brownian in character. The correlation function should then tend towards a single exponential of the form:

$$g^{(1)}(\underline{K},t) \propto \exp\left[-\frac{K^2 D_0}{S(K)}\right]$$

However, for smaller K the excursions of the particles will be greater and $\tau \leq \tau_I$. In this regime the decay rate of the exponential will be a complicated function of the interaction. For small enough K where $\tau \gg \tau_I$, however, the intermediate scattering function will again be a single exponential but it may be difficult to observe the initial decay by P.C.S. methods. The form of the decay for $\tau \gg \tau_I$ has been discussed by Ackerson [62].

In the foregoing discussion we have been principally concerned with interacting colloidal particles which are large and massive compared with other fluid molecules. De Gennes [51,63] has presented a dynamic scaling argument approach to the dynamics of entangled polymer solutions. However, in these concentrated solutions or in melts and gels one expects only collective motion to be observed by light scattering since the distances available for Brownian diffusion are restricted by the high density of material present. In order to observe the

Brownian motion of segments in such cases one would have to resort to neutron scattering techniques.

3.6 Gels

Light scattering has proved to be an invaluable technique for the study of viscoelastic gels. The technique is non-intrusive, non-destructive and all the viscoelastic parameters of the gel may be obtained. The experimental techniques may be considered in two sections:

a) Light scattering from thermally excited displacement fluctuations of the gel network.

b) Light scattering from distortions of the gel network caused by macroscopic displacement waves.

a) In 1973 Tanaka, Hocker, Benedek [64] first reported measurements of the spectrum of light scattered by thermally excited displacement fluctuations in polyacrylamide gels. A detailed theory of the amplitude and time dependence of displacements responsible for the scattered spectrum was also presented. The findings of Tanaka, Hocker, Benedek are outlined below:

1) Longitudinal and transverse displacements of the gel fibre network are responsible for the polarised and depolarised scattered light respectively.

2) The correlation functions for the displacements at a given wavevector have the form of a single exponential decay:

$g^{(1)}(\underline{K},t) \propto \exp -\Gamma t$

where the decay rate is given by:

$\Gamma = G_L \underline{K}^2/f$ for longitudinal displacements

$\Gamma = G_T \underline{K}^2/f$ for transverse displacements

where f is a frictional force; G_L is the longitudinal compressional modulus of the fibre network and G_T is the shear modulus of the fibre network.

Thus from the polarised and depolarised light spectra of the gel all the viscoelastic parameters of the gel (K (the bulk modulus), μ (the shear modulus) and f) can be evaluated.

For the polarised component:

$$\Gamma = 2\,[(K+\tfrac{4}{3}\mu)/f]\,K^2$$

For the depolarised component:

$$\Gamma = (2\mu/f)\,K^2$$

Unfortunately, for most gels the intensity of the depolarised spectrum is very weak : measurement of the depolarised component is not normally possible. This difficulty in the characterisation of gels using this technique may be overcome by considering the nature of the gel under study. The gels are generally rather weak and can be compared in certain respects to a sponge i.e. under a uniaxial compression the gel will shrink in the direction of compression but will not increase markedly in directions perpendicular to the applied compression. Under such circumstances Poisson's ratio for the gel is ~0 and the gel may then be characterised solely by its Young's Modulus. Thus:

$$E = 3K = 2\mu \text{ ; or } K + \tfrac{4}{3}\mu = 2\mu$$

In this case measurement of the polarised spectrum will

be sufficient to characterise the gel [65,66].

A further extension of the theoretical aspects of light scattering from gels has been given by Wun and Carlson [67] who considered the incorporation of static scattering due to the spatial structuring of the Rayleigh scatterers.

b) Nossal et.al. [68,69,70,71] reported measurements of the elastic moduli of gels by probing the standing displacement waves set up in the samples by mechanical or acoustic excitation. The gel was modelled as a continuum and the elasticity equations solved subject to appropriate boundary conditions. The resulting photocount autocorrelation function was found to be of the form:

$$g^{(2)}(\underline{K},t) = f(\underline{K}) \cos (w_{p,q,\gamma} t)$$

where $f(\underline{K})$ is an amplitude factor.

Thus it can be seen that the resulting autocorrelation functions are cosusoidal with a frequency which should be independent of scattering angle.

The solution of the elasticity equation for a gel of dimensions (axbxc) whose top surface is free is given by:

$$w_{p,q,\gamma} = \pi C_{LONG} \left[\frac{p^2}{a^2} + \frac{q^2}{b^2} + \frac{\gamma^2}{c^2} \right]^{1/2}$$

where: C_{LONG} = longitudinal sound velocity

p,q - arbitrary integers which cannot simultaneously be zero

γ - arbitrary constant which may be half-integer or zero.

The longitudinal sound velocity may be written in terms of Young's Modulus:

$$C_{LONG} = \left[\frac{E(1-\sigma)}{\rho(1+\sigma)(1-2\sigma)} \right]^{1/2}$$

where σ is the Poisson ratio and ρ is the gel density;

or the elasticity coefficients:

$$C_{LONG} = \left[\frac{K + \frac{4}{3}\mu}{\rho}\right]^{1/2}$$

As before one has to consider the type of gel under study to simplify the interpretation. If the gel structure is loose (i.e. sponge-like) then :

$\sigma \simeq 0$ and $C_{LONG} = \left[\frac{E}{\rho}\right]^{1/2}$

If the gel is highly cross-linked (rubber-like) then $K \gg \mu$ and:

$$C_{LONG} = \left[\frac{K}{\rho}\right]^{1/2}$$

Thus again the viscoelastic parameters of the gel may be obtained from a non-destructive probe.

Nossal considered the variation of Young's modulus with concentration for both agarose and polyacrylamide gels and obtained the relationship:

$E \propto c^m$

where $m \approx 3$.

A similar relationship has also been found by Hecht and Geissler [72] in studies of the scattered light from concentrated polystyrene solutions. This exponent is in close agreement with that predicted by Daoud and Jannink [73] for semi-dilute polymer solutions in poor solvents using a tricritical point analogy [74].

CHAPTER 4

Experimental Techniques

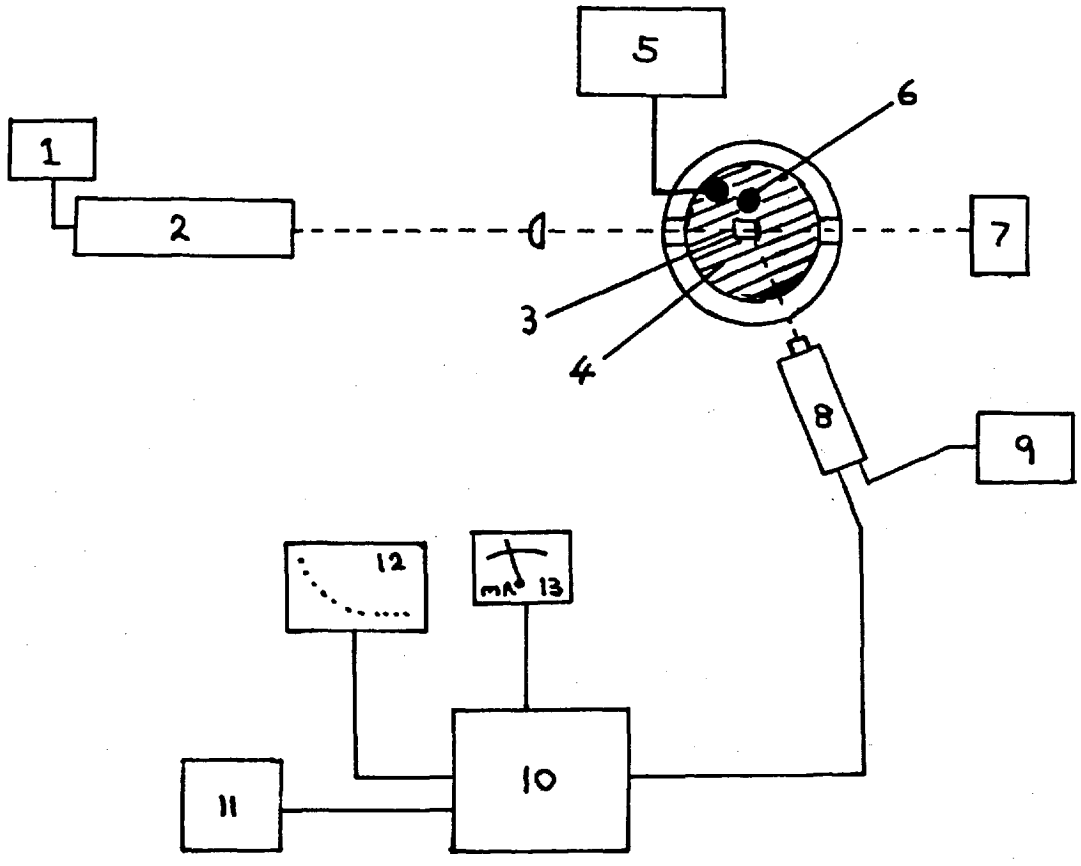
4.1 Photon Correlation Spectroscopy

4.1a Apparatus

The apparatus used in this study was a Malvern system 4300 photon correlation spectrometer. The system is shown diagrammatically in figure 4.1.

The sample was contained in 10x10x40 mm. (internal dimensions) optical cells which were surrounded by an index matching bath of filtered m-xylene (refractive index 1.4972 at 20 °C). The temperature of the sample was controlled by passing current through heating resistors embedded in the spectrometer bath unit. The magnitude of the heating current was controlled by thermistors also embedded in the spectrometer unit. In this manner the temperature of the sample could be maintained to within 0.2 °C. The temperature was recorded using a mercury-in-glass-thermometer or thermocouple immersed in the index matching bath.

The sample was illuminated by a Spectra Physics model 124 A helium-neon laser (operating at ~5mW) giving laser light of wavelength 6328 Å. The laser beam was collimated and focused to pass through the centre of the specimen cell and finally terminated in a light trap. The scattered laser light was monitored using a photo-multiplier which could be rotated to angles θ=5-135° from the main beam. The spectrometer assembly comprising sample,index matching bath, laser and photomultiplier was mounted on a 2 inch. thick concrete slab fitted



1. Laser power supply
2. Laser
3. Sample cell
4. Index matching bath
5. Heater controller
6. Thermometer
7. Light trap
8. Photomultiplier
9. H.T. supply for photomultiplier
10. Malvern K 7023 digital correlator
11. Punch
12. Oscilloscope
13. Ratemeter

Figure 4.1 Photon correlation spectroscopy apparatus

with anti-vibration mounts.

The autocorrelation functions were obtained using a Malvern K 7023 24-channel digital correlator. This system enabled the data to be monitored in several modes:

1) A dynamic display of the autocorrelation function was available on an oscilloscope.
2) A permanent record of the data could be made using a high speed punch facility.
3) The output of the photomultiplier could be monitored by means of a ratemeter.

Thus the scattered intensity could be monitored using the ratemeter or by photocount collections in the correlator over a fixed period of time. The correlation function could be observed as it was accumulated using the oscilloscope and calculations could be made from the function as recorded on papertape.

4.1b Index Matching

In order to minimise flare and internal reflections within the sample cell an index matching liquid with the same refractive index as the glass windows of the cell should be used. In the present work filtered m-xylene was normally used, but for temperatures in excess of 100 °C filtered glycerol was substituted for the m-xylene. Because of the variation of refractive index of the sample solution and the surroundings a refraction correction must be applied to the measured scattering angle, θ_{MEAS}

Considering Snell's Law the following relationships

were obtained:

For $\theta_{MEAS} \geq 90°$ $\quad \frac{n_1}{n_2} = \frac{\text{Sin } (\theta_{MEAS} - 90)}{\text{Sin } (\theta_{TRUE} - 90)}$

For $\theta_{MEAS} = 60 \rightarrow 90°$ $\quad \frac{n_1}{n_2} = \frac{\text{Sin } (90 - \theta_{MEAS})}{\text{Sin } (90 - \theta_{TRUE})}$

For $\theta_{MEAS} < 40°$ $\quad \frac{n_1}{n_2} = \frac{\text{Sin } \theta_{MEAS}}{\text{Sin } \theta_{TRUE}}$

Using values for the refractive indices of water (1.3325) and m-xylene (1.4972) the above correction has been considered. Results are shown in table 1, with values of the wavevector, $|K|$, where:

$$|K| = \frac{4\pi n_1}{\lambda_0} \text{ Sin } \theta_{TRUE}/2$$

where n_1 is the refractive index of the solution and λ_0 is the laser wavelength in free space.

Further corrections due to the temperature variation of the refractive indices and the finite thickness of the cell windows may be applied but since these result in only a small correction (1-2%) they have been omitted.

Experimental measurements were confined to the range 20-120°. The lower limit of 20° was used in order to minimise the effect of scattering from any dust particles present in the sample. The upper limit was to ensure that measurements were not taken from the face of the cell through which the incident beam passed, as flare and internal reflections were considered to be greatest from this face. Measurements could not be taken between 40 - 60° as the corner of the square sample cell obscured the scattered light beam.

Table 4.1

Corrected Values for Scattering Angles and Wavevector

$\theta_{MEAS}/^{o}$	$\theta_{TRUE}/^{o}$	$K/10^{4}cm^{-1}$	$K^{2}/10^{9}cm^{-2}$	$K^{3}/10^{14}cm^{-3}$
20	22.6	5.19	2.69	1.4
25	28.4	6.48	4.20	2.7
30	34.2	7.78	6.05	4.7
35	40.1	9.08	8.24	7.5
40	46.2	10.39	10.80	11.2
60	55.8	12.39	15.34	19.0
65	61.6	13.55	18.35	24.9
70	67.4	14.68	21.56	31.7
75	73.1	15.75	24.81	39.1
80	78.8	16.79	28.18	47.3
90	90	18.71	35.01	65.5
100	101.3	20.46	41.84	85.6
110	112.6	22.01	48.46	106.7
120	124.2	23.38	54.68	127.9

4.1c Operation

Before each set of runs the alignment of the laser beam was checked by monitoring the scattered intensity of the m-xylene bath at 30,60,90, and 120°. The laser beam was adjusted in position so that the scattered intensity remained constant over this angular range. This ensured that the laser beam was indeed traversing the sample horizontally and that the incident beam, scattering volume and aperture of the photomultiplier were in the same horizontal plane.

The windows of the sample cell were rinsed with filtered m-xylene and wiped with lens tissue before the sample cell was placed in the index matching bath which was already at a temperature above that required for the planned experiment. The temperature was then set as required and the sample left to equilibrate.

In order to obtain a statistically accurate correlation function there are three parameters that may be varied:

1) The effective photocathode area which is determined by the size of the iris of the photomultiplier.
2) The sample time of the correlator.
3) The clipping level applied to the output signal of the photomultiplier.

The effect on the statistical accuracy of the autocorrelation function of these parameters has been studied in detail [75].

The iris of the photomultiplier was normally set at the

smaller aperture sizes since the light flux was such that the optimum number of photodetections could easily be obtained.

The sample or channel time was chosen so that the last 4-6 points of the 24-channel correlator gave a constant value. The time was chosen using the dynamic display on the oscilloscope. This procedure was found to be necessary in order to normalise each function since the normalisation factor calculated by the correlator was usually 5-15% in error. This apparent failure of machine normalisation is thought to arise mainly from flare within the sample cell because of the large variation in refractive index water→ glass.

Having set the aperture and channel time, the clipping level is easily obtained using the probability analysis mode of the correlator.

This facility plots a trace of the distribution of counts received per sample time. The clipping level was then set equal to the mean number of counts received per sample time. The correlator clip facility only permitted clip levels of ≤ 9. For higher clip levels an external clipping counter model RR95 was employed, which extended the clipping range to 99×10^4.

Having set the above parameters the accumulation of the autocorrelation function was begun. The correlator could either be set to run for a specified time or could be stopped manually once the oscilloscope displayed a function of adequate statistical accuracy.

4.1d Analysis of Results

Figure 4.2a shows a typical photocount autocorrelation function for a 0.1wt.% agarose sol at 63°C.

The function is normalised with respect to the constant value of the function at high t.

Thus:

$$g^{(2)}(t) = \frac{G^{(2)}(t)}{\lim_{t \to \infty} G^{(2)}(t)}$$

Each individual function was normalised in this manner.

For scattered light conforming to Gaussian statistics the normalised photocount autocorrelation function is related to the normalised electric field autocorrelation function via the Siegert relationship:

$$g^{(2)}(t) = 1 + \left| g^{(1)}(t) \right|^2$$

Thus for a single exponential decay :

$$g^{(1)}(t) \propto \exp\left[-\frac{\Gamma}{2} t \right]$$

and

$$\ln\left[g^{(2)}(t) - 1 \right] = -\Gamma t$$

A plot of the data in this form is given in figure 4.2b. The data show good agreement with a single exponential relaxation of characteristic time 1/436 s..

The single exponential behaviour was not so evident in all the functions. Figure 4.3 shows data for a nominally identical run. Here it can be seen that the decay can no longer be fitted by a single exponential. This deviation may occur because of numerous factors i.e. polydispersity,

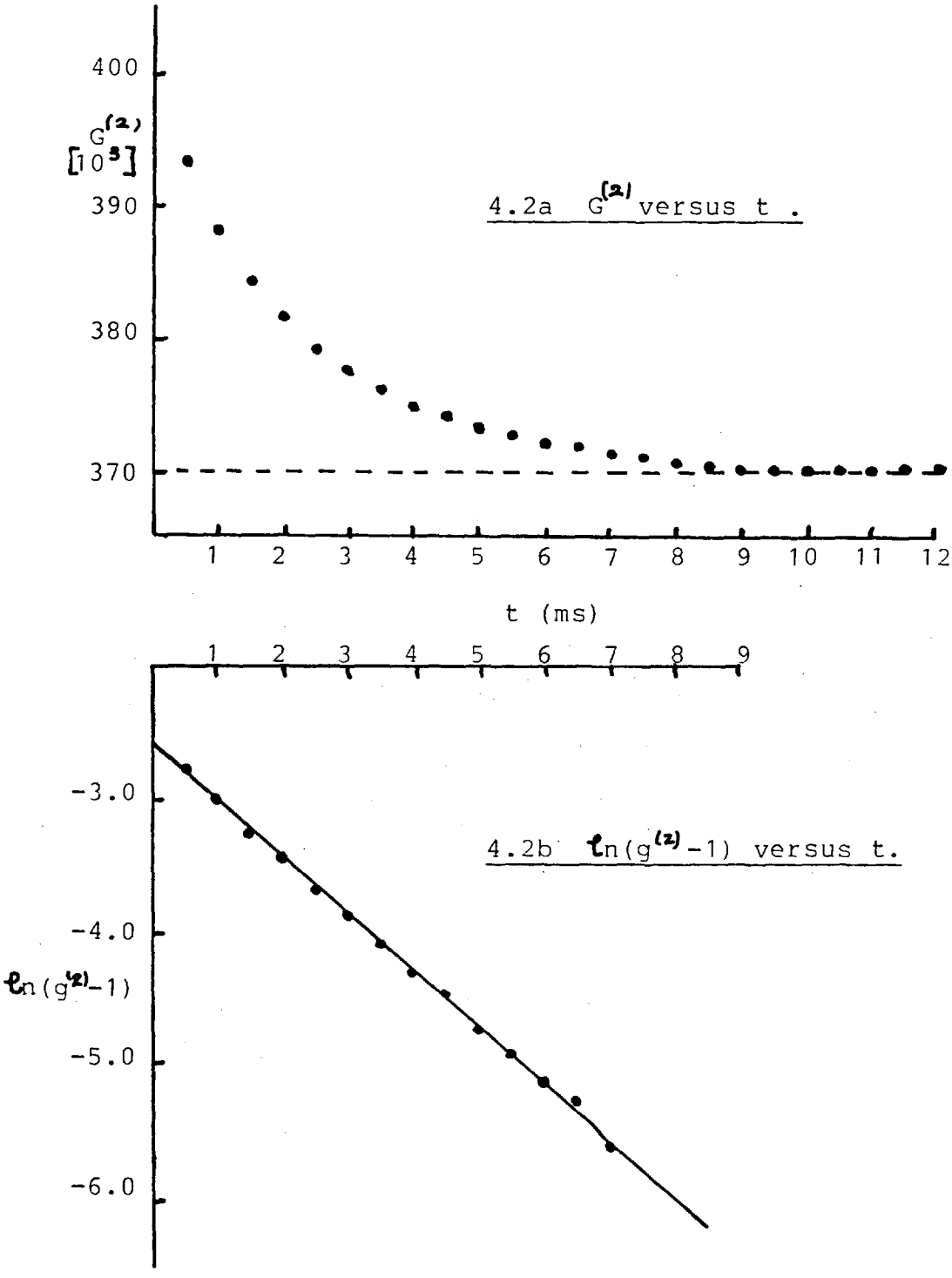


Figure 4.2 Autocorrelation function obtained from a 0.1 wt% agarose sol at 63 °C.

[Angle= 60° ; Channel time = 500 μs ;Clip level= 57; Aperture =3]

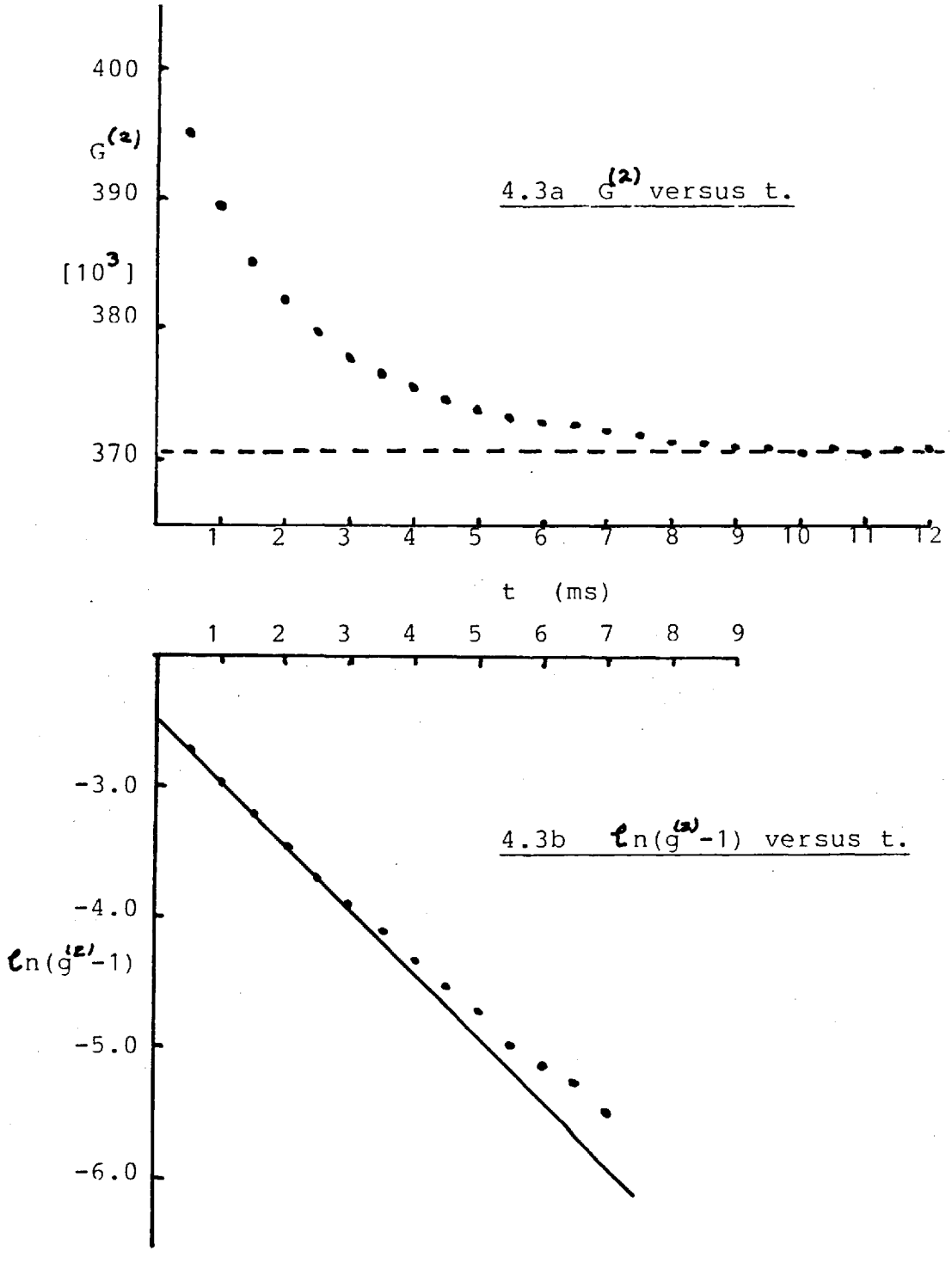


Figure 4.3 Autocorrelation function obtained under identical conditions to that shown in Figure 4.2.

dust, flare, convection currents etc..

To compensate for the possible deviation from single exponential behaviour the data have been analysed by using the first cumulant, Γ_1, where:

$$\Gamma_1 = \lim_{t \to 0} - \frac{\partial}{\partial t} \ln [g^{(2)}(t) - 1]$$

Thus the initial slopes of the autocorrelation functions, where statistical accuracy is highest, have been studied. Several measurements were made at each angle and the mean value of the first cumulant, Γ_1, determined.

A photocount autocorrelation function for a 0.75wt.% agarose sol at 52.3°C is shown in figure 4.4 as obtained from a 96-channel correlator.

This plot also shows the deviations from single exponential behaviour occurring in the intermediate time region, although overall the data are in excellent agreement with a single exponential decay.

4.2 Optical Rotation Studies

4.2a Apparatus

Measurements of the rotation of plane polarised light by agarose solutions were made using a Bendix-N.P.L. model 143D polarimeter. The polarimeter is shown diagrammatically in figure 4.5.

A beam of plane polarised light is formed by the tungsten filament lamp, interference filter , collimator and polariser. The analyser and polariser are crossed so that

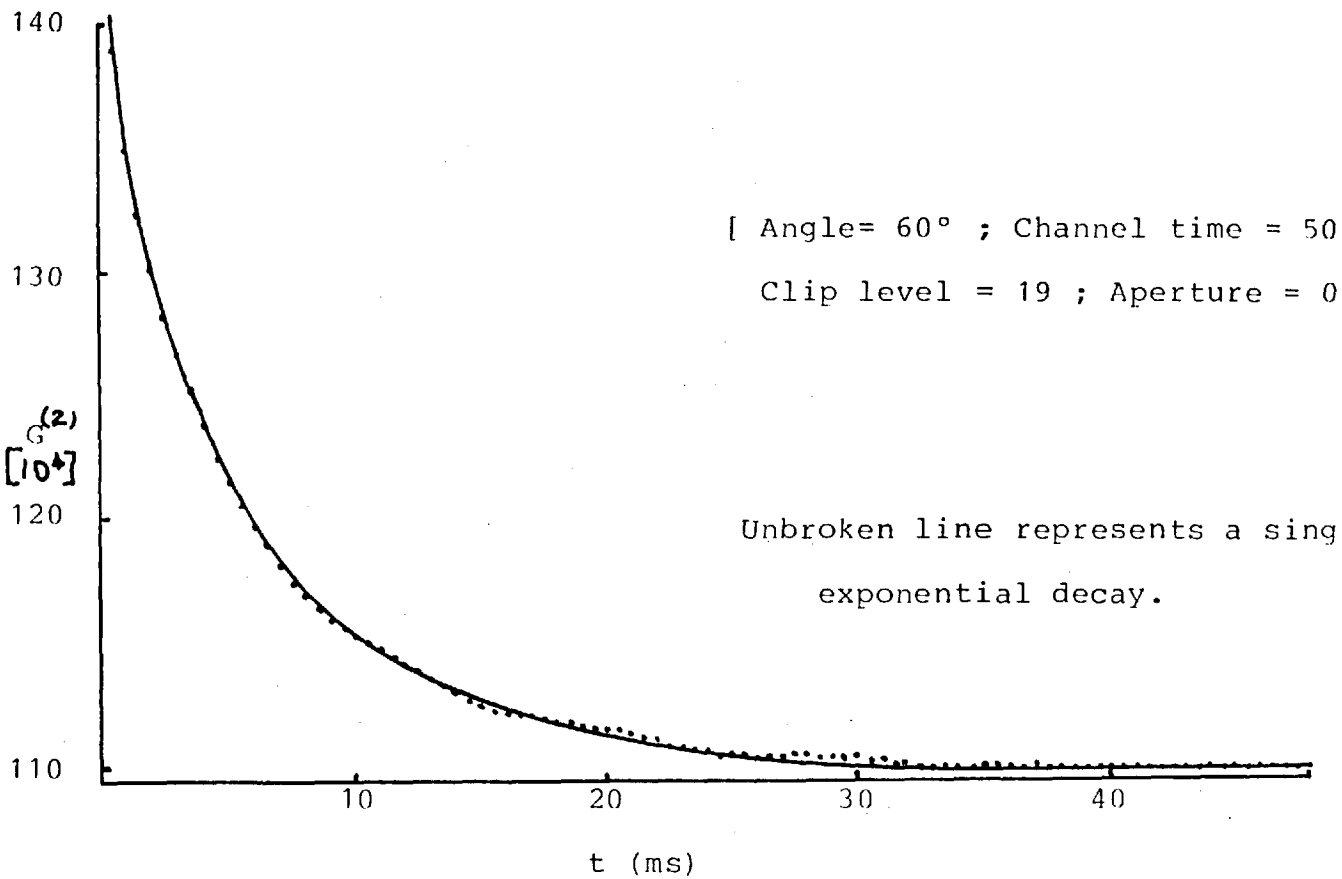
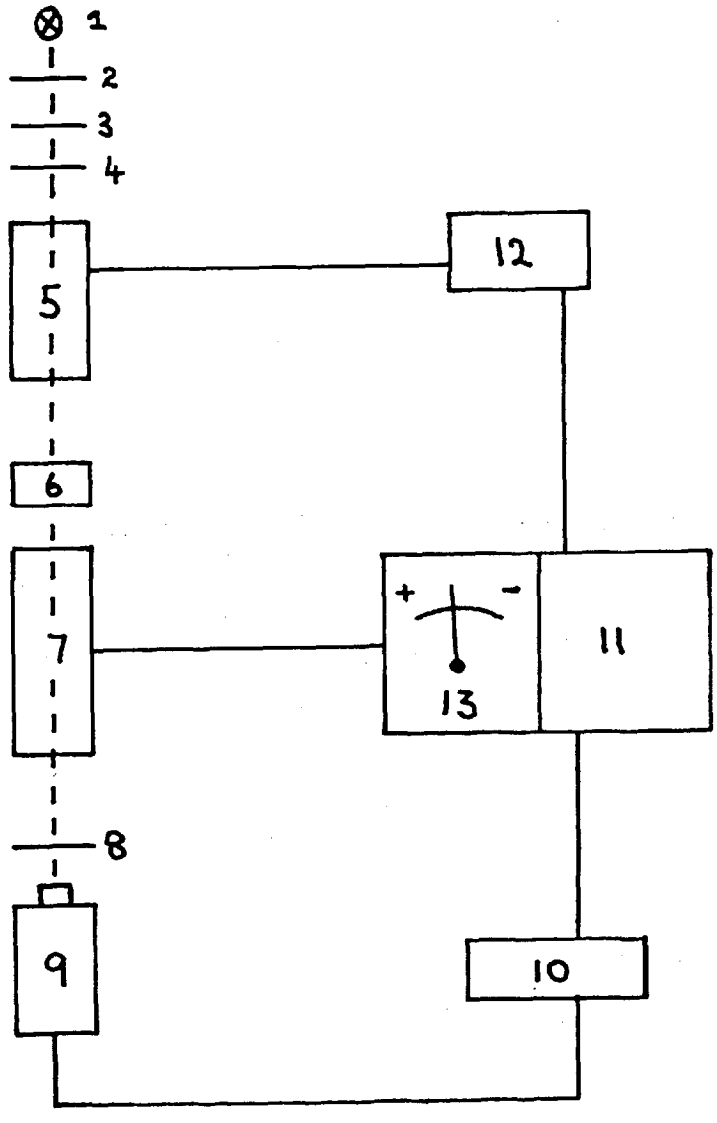


Figure 4.4 Autocorrelation function obtained from a 0.75 wt% agarose solution at 52.3°C.



1. Tungsten filament lamp
2. Filter (5461 Å)
3. Collimator
4. Polariser
5. Faraday modulator
6. Sample cell
7. Compensating Faraday cell
8. Analyser
9. Photomultiplier
10. Amplifier
11. Phase sensitive detector
12. Oscillator
13. D.C. output

Figure 4.5 Diagrammatic representation of the polarimeter.

the intensity at the photocathode is zero. The Faraday modulator causes the plane of the polarised light to oscillate (380 Hz.) about its mean position. Thus the intensity at the photocathode nulls twice per oscillation i.e. with a frequency of 760 Hz.. A narrow band amplifier centred at 380 Hz. amplifies the output signal from the photocathode. Thus with no sample in the beam there is no output from the amplifier. When an optically active sample is placed in the beam it causes the signal from the photocathode to be asymmetrical, thus introducing a 380 Hz. component into the amplifier. The phase sensitive detector detects the 380 Hz. component and a d.c. current is applied to the compensating Faraday cell to restore the output of the photocathode to symmetry. The d.c. current needed to restore symmetry depends on the direction and extent of rotation of the beam by the sample. The ammeter used is calibrated in terms of angle of rotation. The maximum rotation that may be measured being $\pm 0.5°$.

4.3b Sample Cell

A special sample cell (Hellma product n° 165) was used in order to study the variation in the optical rotation as a function of temperature. The cell, of path-length 2 cm. , was surrounded by a heating jacket through which was circulated distilled water from a thermostatted bath. A thermocouple placed in the filling neck of the sample cell enabled the temperature of the sample to be monitored. The cell was surrounded by a specially constructed tufnol jacket which acted as an insulator

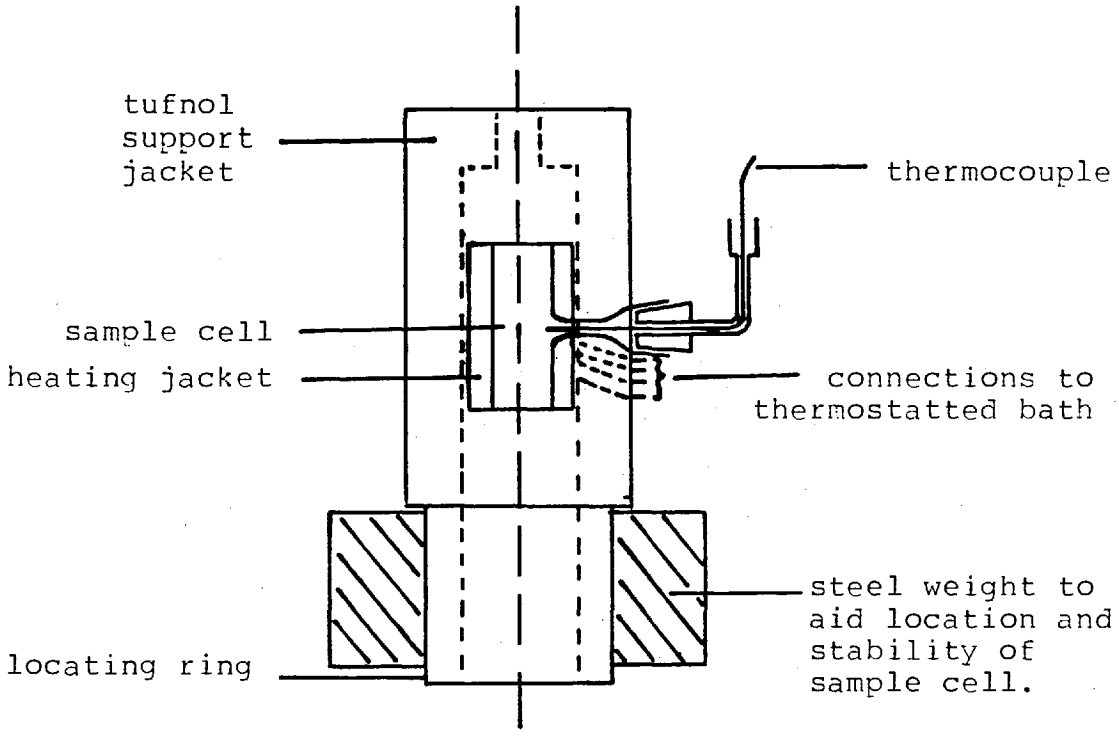


Figure 4.6 Sample holder for polarimetry experiments

and also provided a rigid mounting which could be accurately located in the polarimeter housing (figure 4.6) .

4.2c Measurements

Before commencing experiments the polariser and analyser were checked so that zero rotation was observed with no sample in the polarimeter. The cell was first filled with distilled, de-ionised, filtered water and the angle of rotation studied as a function of temperature. The angle of rotation was found to vary with temperature in a consistent and reproducible manner. These variations may be attributed to the effects of stress in the cell windows as the cell is heated or cooled.

For solution measurements the cell was preheated to ~60 °C and hot agarose solution (pre-heated in a pressure cooker) decanted into the cell. After the sample had equilibrated measurements were taken as the sample was temperature cycled in the range 20→95 °C. The heating and cooling rates were ~2 °C/ minute. The solution results were corrected for the effects of window stress.

4.3 Sample Preparation

The agarose used in this work was obtained from B.D.H. Chemicals Ltd.. It was of electrophoresis grade (product n° 33006) and hence had a low sulphate content and low electroendosmosis effect. Agarose solutions were prepared using distilled,de-ionised, filtered (0.45 μm millipore filter) water.

Samples were prepared by weighing the appropriate

amount of agarose into a graduated flask and then pipetting the required volume of distilled, de-ionised, filtered water into the flask. The flask was then placed in a domestic pressure cooker and heated to ~122 °C for 15-20 minutes. With more concentrated samples a further period of heating was required to ensure complete dispersion of the agarose.

For spectroscopic measurements the gels were dispersed by heating in the pressure cooker at ~122 °C and then decanted into clean preheated optical sample cells.

All glassware was cleaned in a sulphuric/chromic acid bath. Light scattering cells were cleaned in a nitric/ chromic acid bath. Before use glassware was washed thoroughly with distilled water, then acetone and finally dried in an oven.

The experimental results relate to two agarose batches - 2091970 and 6409620. The main body of the results relate to batch 2091970: when the second batch has been used it is specified in the text.

CHAPTER 5

Results

The experimental results are presented in two sections. The first section deals with the investigation of the agarose system throughout the hysteresis cycle as studied using photon correlation spectroscopy, optical rotation and viscosity measurements. The second section contains additional experimental data from investigations designed to test hypotheses arising from the study of the gelation cycle and in general terms to advance our understanding of the behaviour of the agarose system.

5.1 The Hysteresis Cycle

The results in this section are further subdivided into five sections:

5.1a The Gel State

5.1b Gelling Solutions

5.1c Non-gelling Solutions

5.1d Optical Rotation Studies

5.1e Aggregation Temperatures.

This separation helps to emphasize the importance and implications of each set of results when one considers their interpretation and the possible models for the gelation process.

5.1a The Gel State

When gelling solutions (concentration $>$ 0.1wt.%) were cooled to the region of the gelation temperature (30-35°C) photon scattering correlations were observed over far longer time scales than had been noted at higher temperatures (figure 5.1). This implies the formation of larger, more slowly moving, domains or aggregates. Similar observations have been made on the P.V.A.-Congo Red System [76]. However during a more detailed quantitative study of this phenomenon, low frequency oscillations in the autocorrelation functions were observed (figure 5.2). Although these oscillations initially seemed to be of a transient nature as reported by Prins [77] it was soon established that they were undamped cosusoidal oscillatory functions which persisted for days or even weeks after the gelation process had begun. Thus they appeared to be characteristic of the fully developed gel.

Since a Tanaka-Hocker-Benedek type autocorrelation function of exponential form could not be obtained, we commenced a systematic study of the temperature, angular and concentration dependences of these functions (figure 5.3 and 5.4). It was during these investigations that a paper reporting the observation and origins of such functions was published by Nossal et. al.[68,69].

In agreement with Nossal, we had been able to show that the oscillations could be initiated, sustained and varied in amplitude by building vibrations, machine noise and even human speech in the low audio-frequency range.

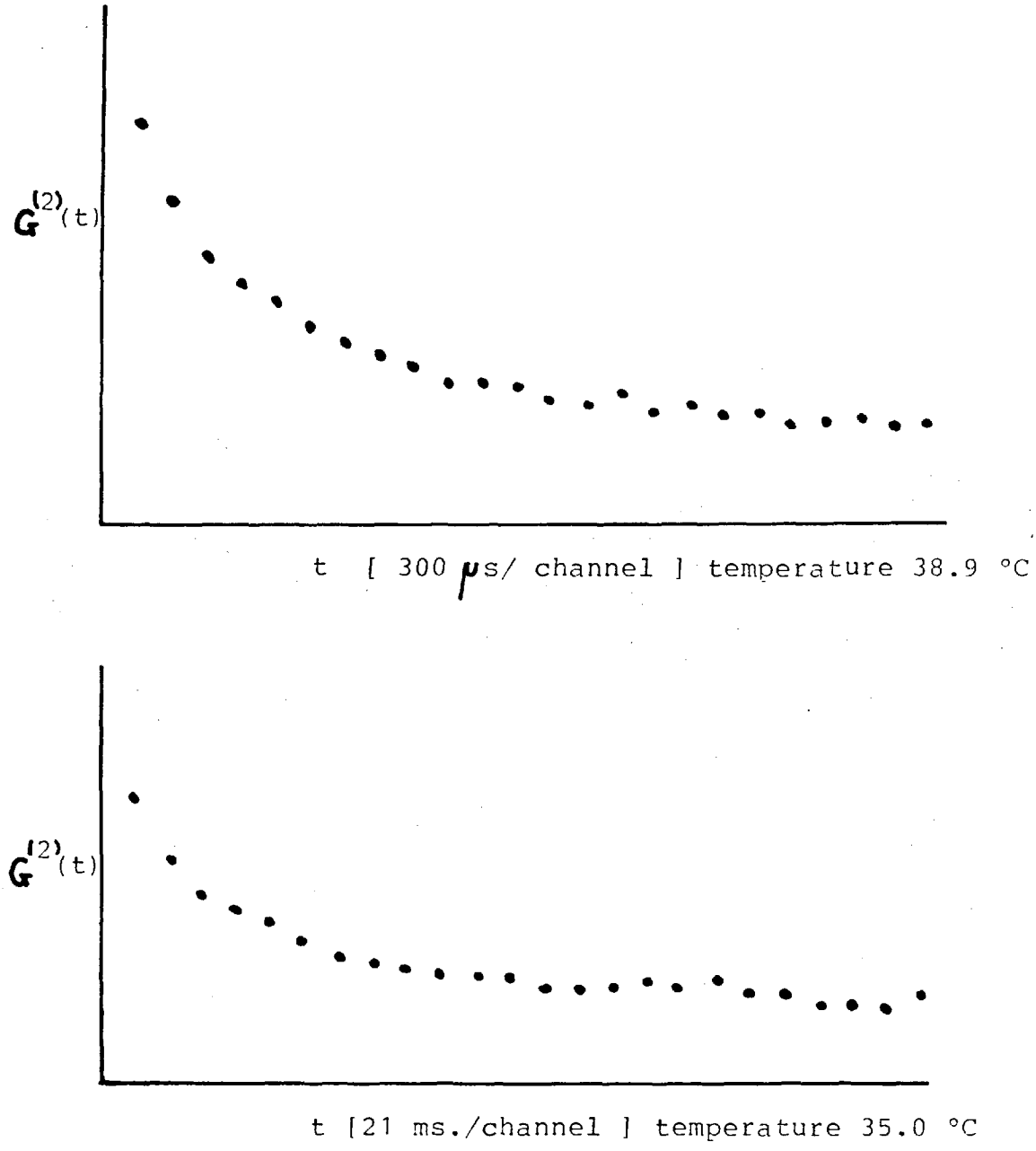


Figure 5.1 Autocorrelation functions obtained from a 0.5wt% agarose solution near the sol/gel transition.

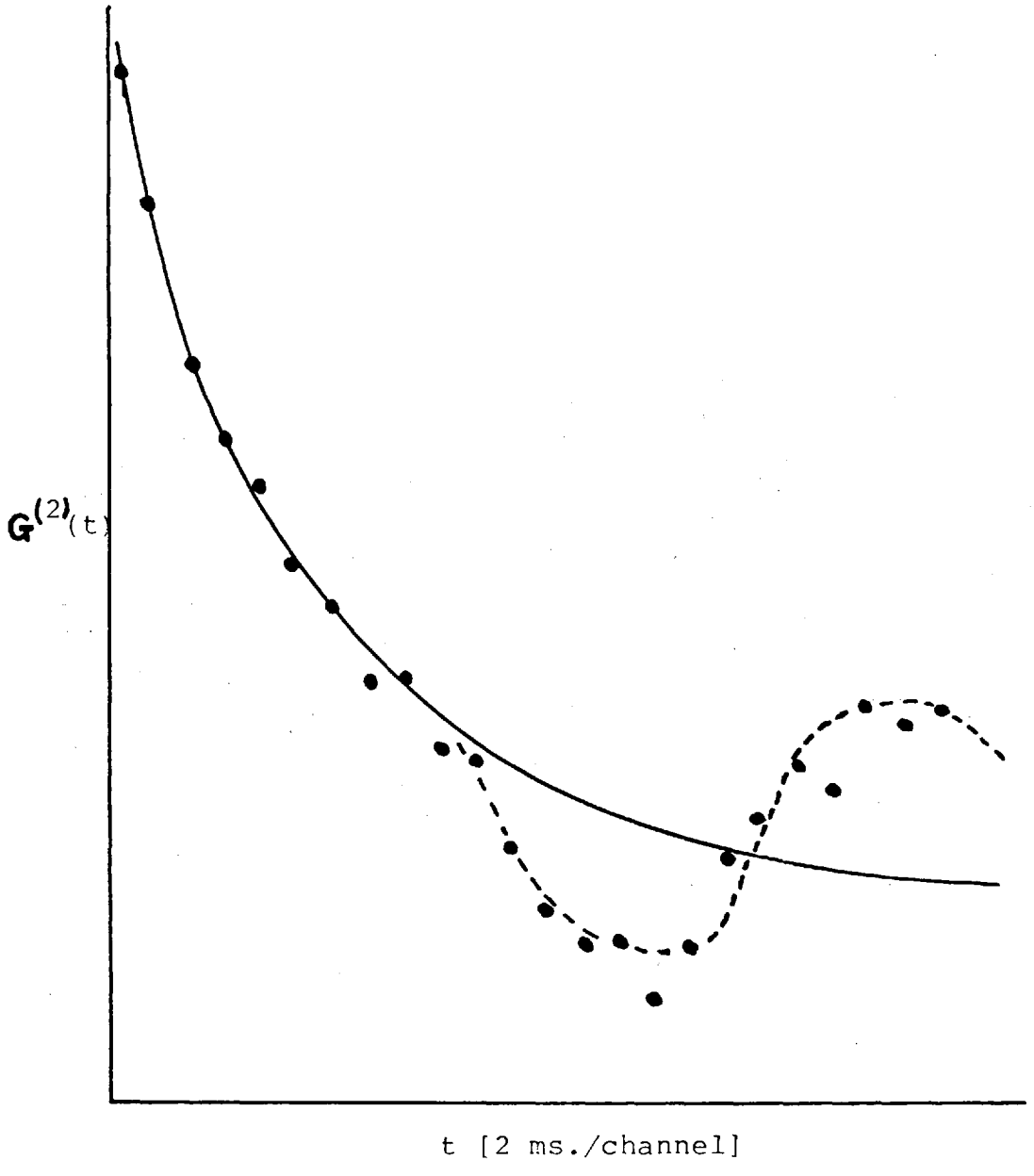


Figure 5.2 Oscillatory autocorrelation function observed when cooling a 0.75 wt% agarose solution through the sol/gel transition.

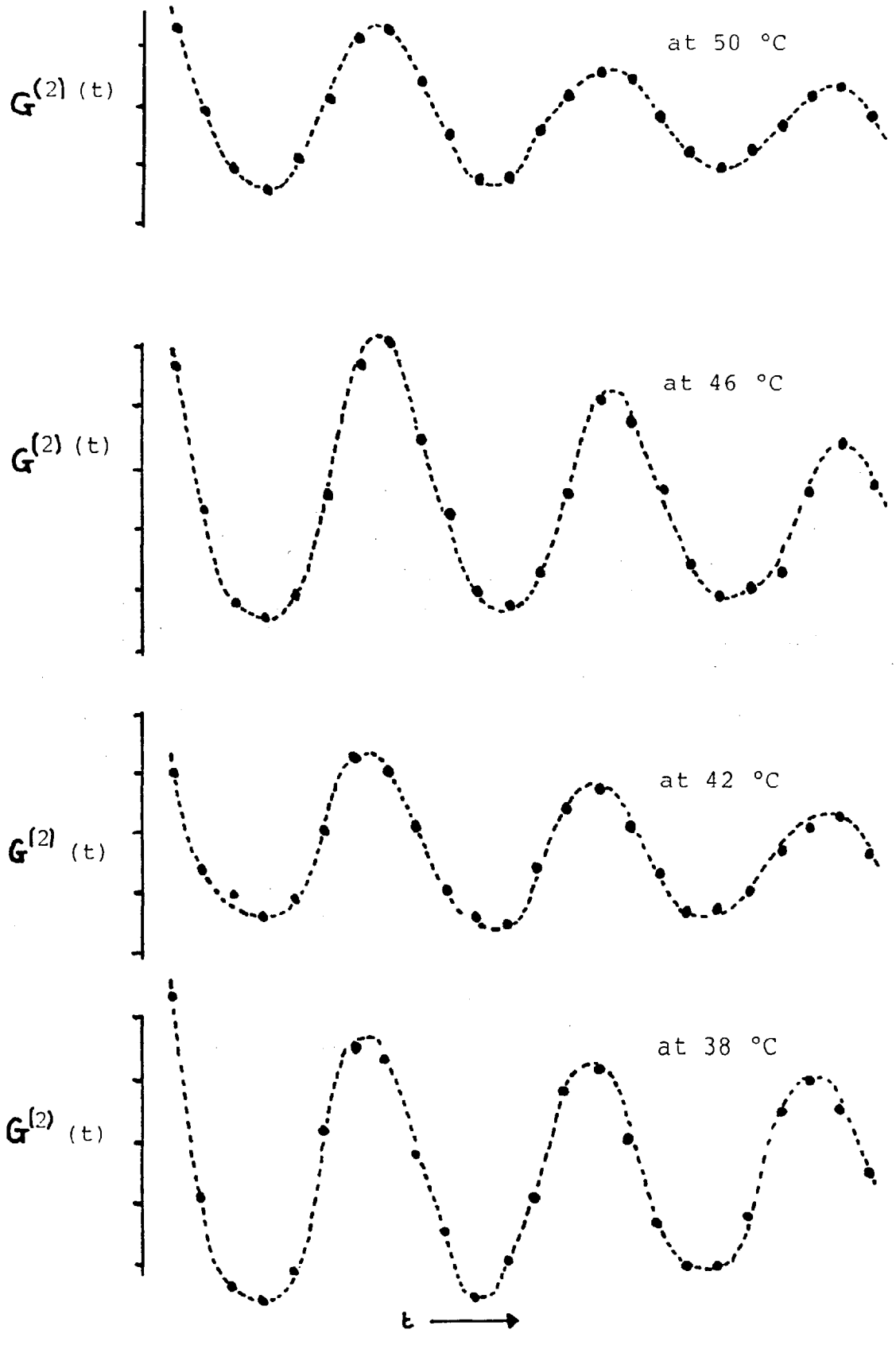


Figure 5.3 Temperature dependence of oscillatory autocorrelation function as a gel is cooled from 50 °C. [all at 6 ms/ channel].

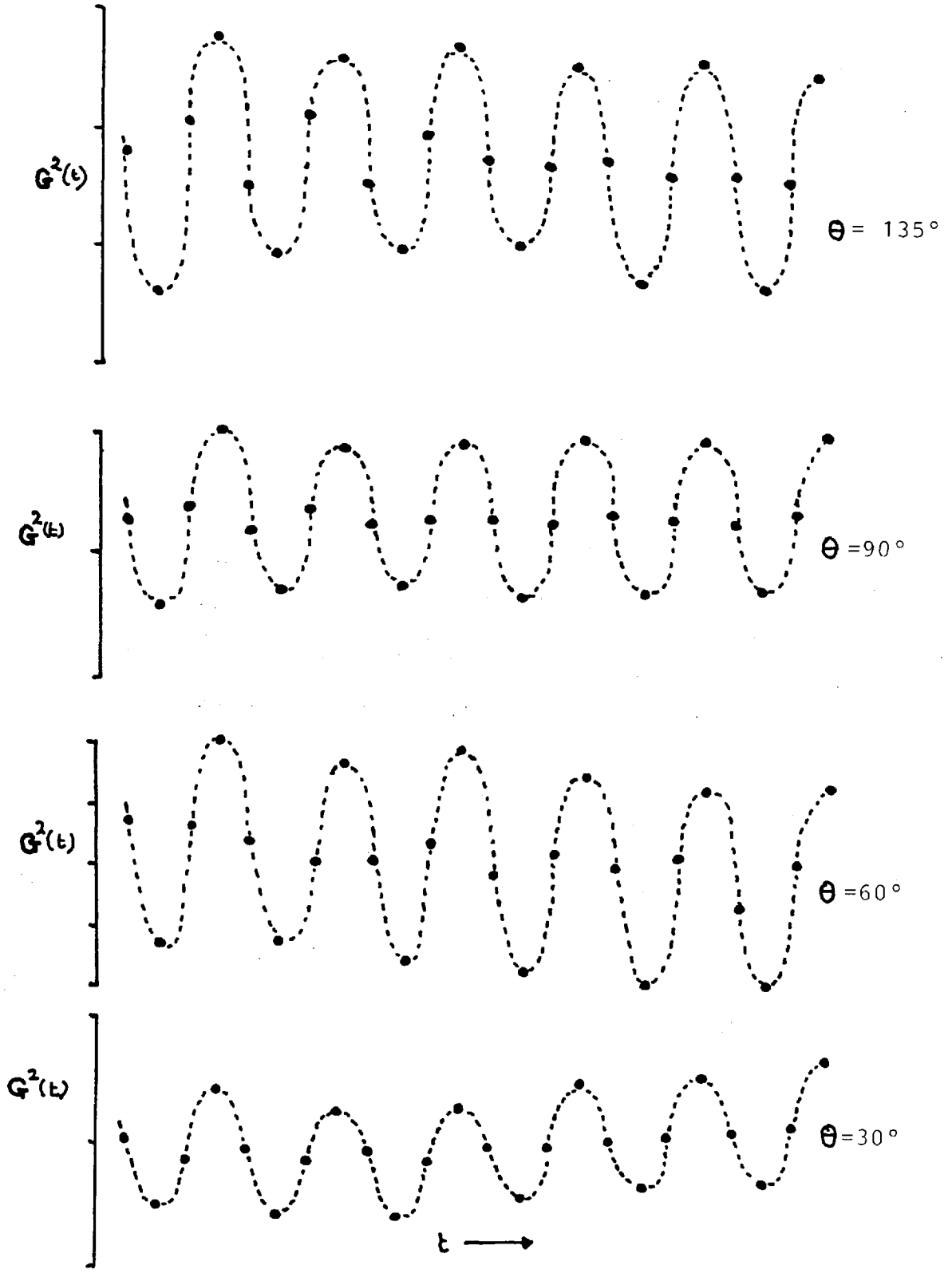


Figure 5.4 Angular dependence of oscillatory autocorrelation functions. [All at 5 ms/channel].

These experiments were therefore brought to a conclusion and analysed using Nossal's theoretical approach. The observed frequencies and corresponding C_{LONG} for various agarose gels are tabulated in table 5.1 and compared with prediction in figure 5.5. Figure 5.6 shows the dependence of the derived elastic constant, E, with concentration.

The result obtained ($E \propto c^{2.9\pm0.1}$) is in excellent agreement with that determined by Nossal.

Table 5.1

Observed frequencies and longitudinal sound velocity for agarose gels.

	Concentration of agarose/wt.%				
	0.1	0.2	0.3	0.5	0.75
observed frequencies /Hz	7.8-8.4	20	31.5-35	70	139
	12.5	33	49	87.5	190
	14.2	40.7	56	139	204
	15.6	49.2	69	160	285
	21	55		183	312
	25			203	
calculated longitudinal sound velocity C_{LONG} / cm s^{-1}	15.6	40.7	69	139	284
calculated elastic modulus E dyne/cm^{-2}	243.7	1660	4.76 $\times 10^3$	1.94 $\times 10^4$	8.12 $\times 10^4$

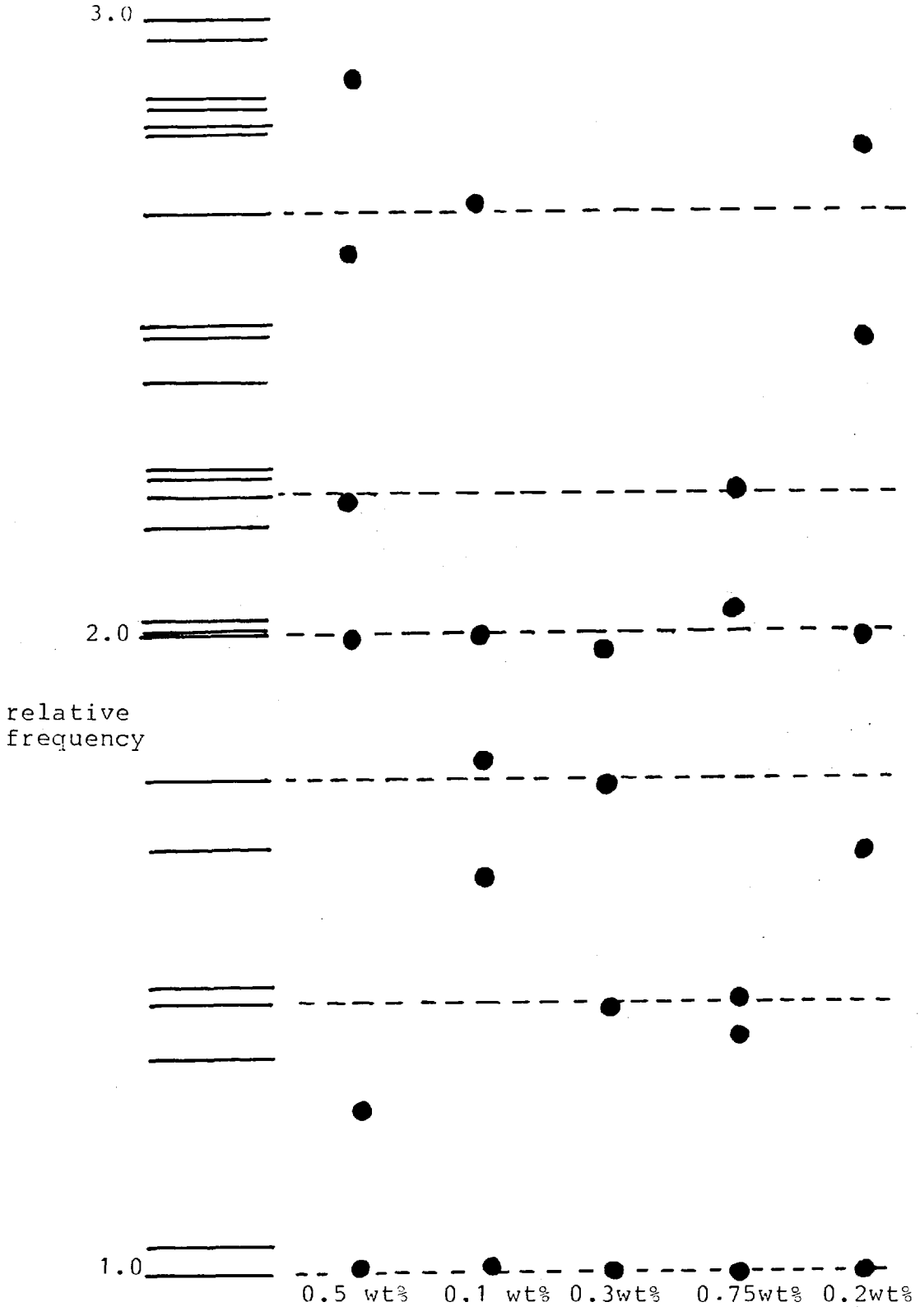


Figure 5.5 Observed and predicted frequency spectrum for agarose samples.

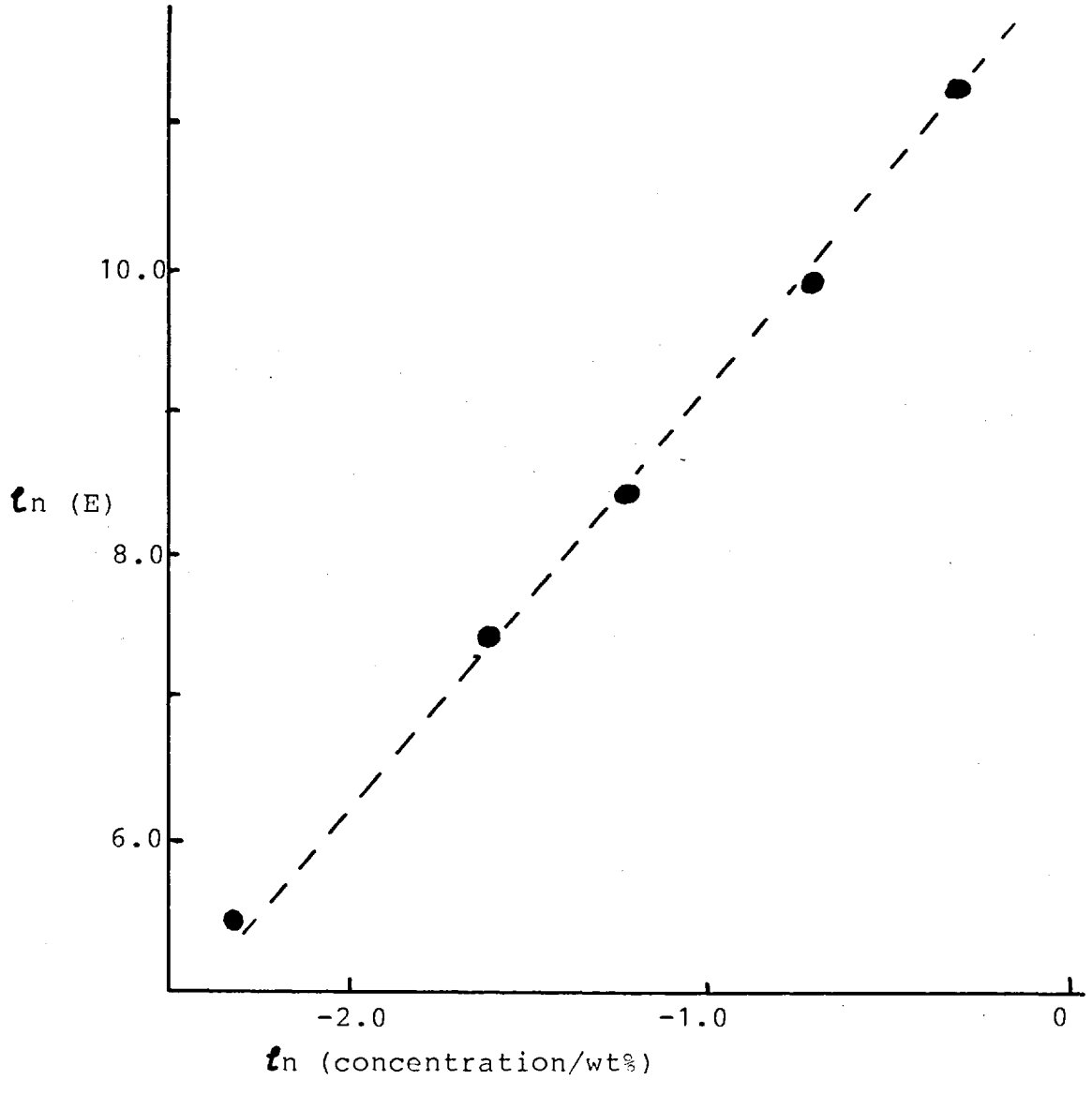


Figure 5.6 ℓn (elastic constant,E,) versus ℓn (concentration) for agarose gels.

5.1b Gelling Solutions

5.1b(i) Scattered Intensity Data

Measurements of the intensity of scattered light as a function of temperature were made at a fixed wavevector (θ = 60°) using the photon correlation apparatus. Figures 5.7 and 5.8 show the results obtained on cooling a fully homogenised solution from temperatures above 92°C for a 2.5wt.% and 0.1wt.% sample respectively.

Both plots show four distinct patterns of behaviour:

1) As the sample is cooled (100→40°C) the scattered intensity remains constant at a relatively low level with good reproducibility. This is region I of the cycle, termed the sol state.
2) A dramatic increase in scattered intensity occurs at 30-40°C, dependent on concentration. This corresponds to the onset of gelation as indicated by the development of elastic properties, and is termed region II.
3) A smoothly curved, but less reproducible decrease in scattered intensity is observed as the sample is reheated from region III, the fully developed gel, though region IV, the dispersing gel, until,
4) the scattered intensity returns to a level characteristic of the agarose solution at 90-95°C.

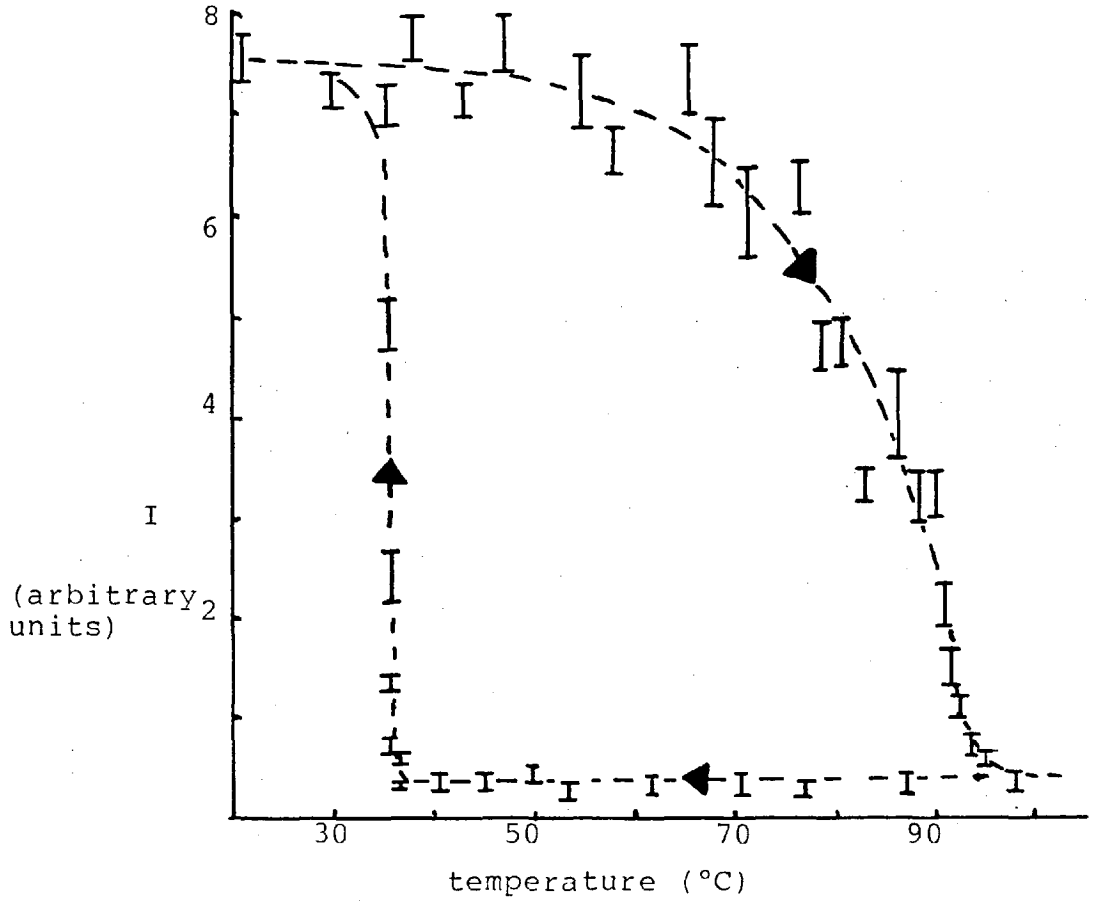


Figure 5.7 Scattered intensity versus temperature for a 2.5 wt% agarose solution.

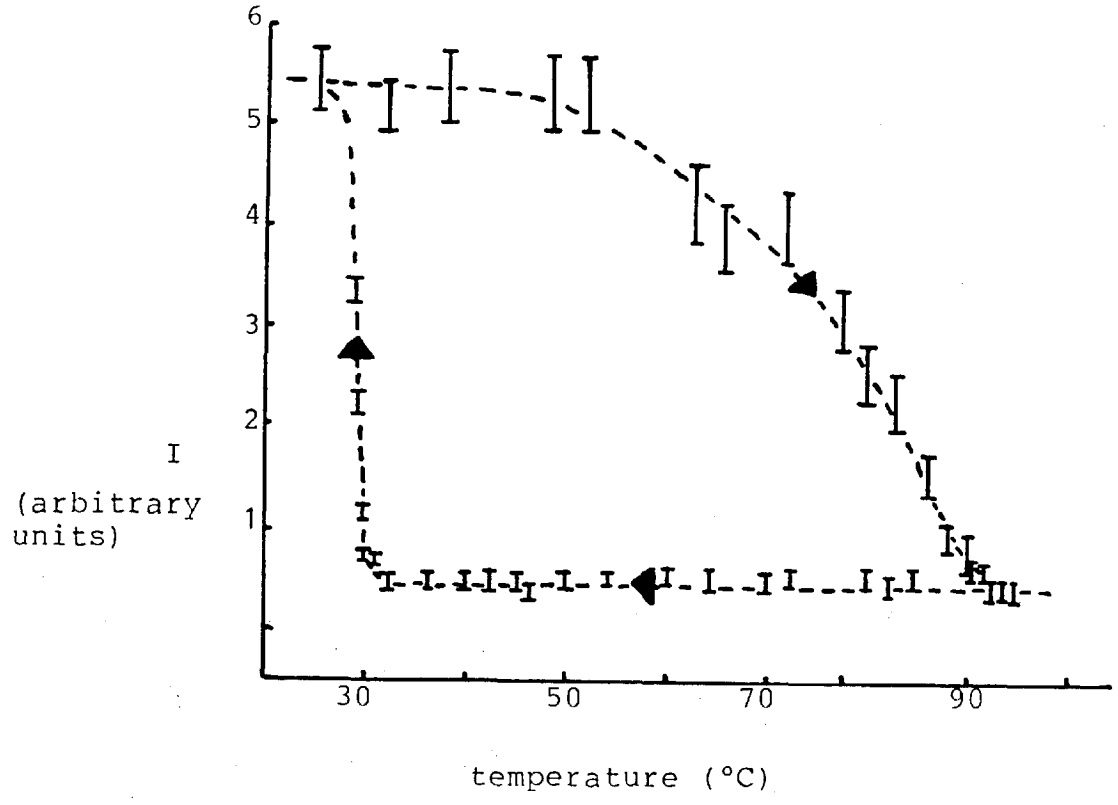


Figure 5.8 Scattered intensity versus temperature for a 0.1 wt%agarose solution.

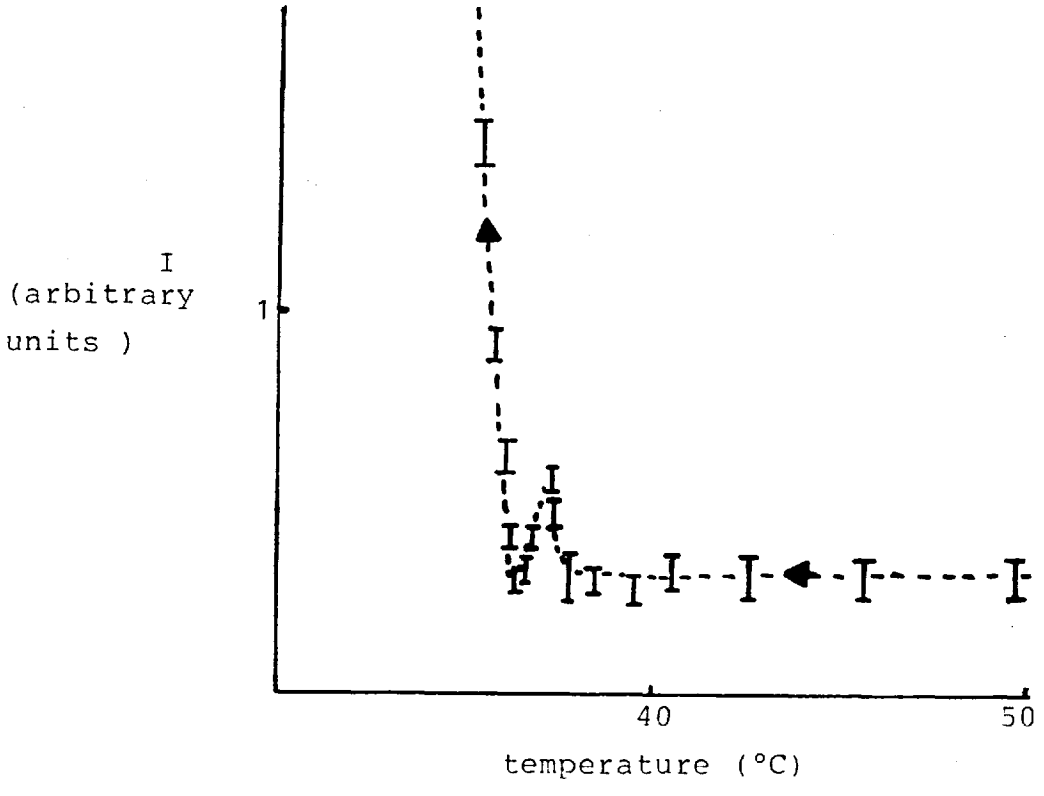


Figure 5.9 Intensity fluctuations above the aggregation temperature.

The aggregation temperature, T*, deemed to correspond to the onset of gelation, is easily evaluated from these measurements and will be discussed in section 5.1e. The above phenomena are intrinsic to the system. However, in some samples transient and irreproducible fluctuations in intensity were observed at a few degrees above the dramatic rise that occurred upon gelation (figure 5.9). These fluctuations are undoubtedly caused by extrinsic or heterogeneous gel formation creating aggregates capable of sedimentation. It was noted that after such fluctuations had ceased the scattered light signal became very steady, even steadier than throughout the main section of region I, as befits a homogeneous sol.

In all cases it was observed that the loop closed perfectly at high temperatures. The closure at low temperatures, however, was less reproducible. This is, no doubt, caused by ageing of the gel involving some slow molecular rearrangement.

The low level of intensity in region (I) remained constant when the sol was temperature cycled (40-95°C). However, when an unfiltered agarose solution (0.5wt.%) was held at a constant temperature a few degrees above T* a weakly scattering soft gel was formed during a period of 3-6 days. Filtered gelling solutions appear not to show these extrinsic phenomena, which are seemingly enhanced by the addition of colloidal Ca(Mg) SO_4 (SiO_4,PO_4).

Thus the gel formed at T* is only characteristic of cooling rates down to about 1°/hr. It does not represent

a truly stable gel.

A preformed gel (0.5wt%) was heated to ~50°C and an agarose sol (region I) of the same concentration and at the same temperature was decanted onto the surface of the gel.

After two days no signs of gelation whatsoever could be observed in the sol layer and there was no increase in height of the gel/sol interface, indicating no adsorption of the free agarose chains in the sol state onto the surface of the preformed gel.

5.1b(ii) Photon Correlation

Measurements of the autocorrelation functions obtained from gelling agarose solutions in region I of the hysteresis cycle were made in the temperature range 50-95°C. The autocorrelation functions were analysed in terms of the first cumulant (section 4.1d) and figures 5.10 and 5.11 show typical plots of the first cumulant versus (wavevector)^2. These plots exhibit increasingly large deviations from a simple linear (wavevector)^2 dependence as the wavevector is increased. In figures 5.12 and 5.13 the same data are plotted against (wavevector)^3. This linear dependence with (wavevector)^3 was found for all gelling agarose solutions in region I studied over this temperature range.

Experimentally the data were characterised by the equation:

$$\Gamma_1 = \Phi K^3$$

The concentration and temperature dependence of the

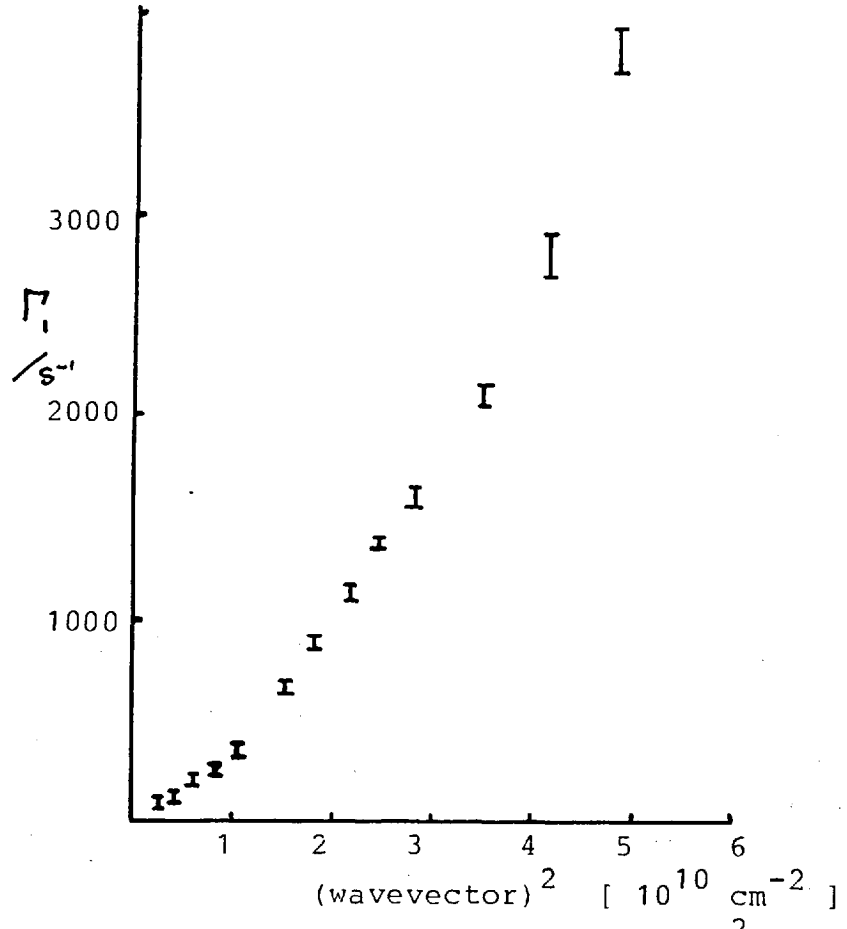


Figure 5.10 First cumulant versus (wavevector)^2 for a 0.1wt% agarose solution at 92.5 °C.

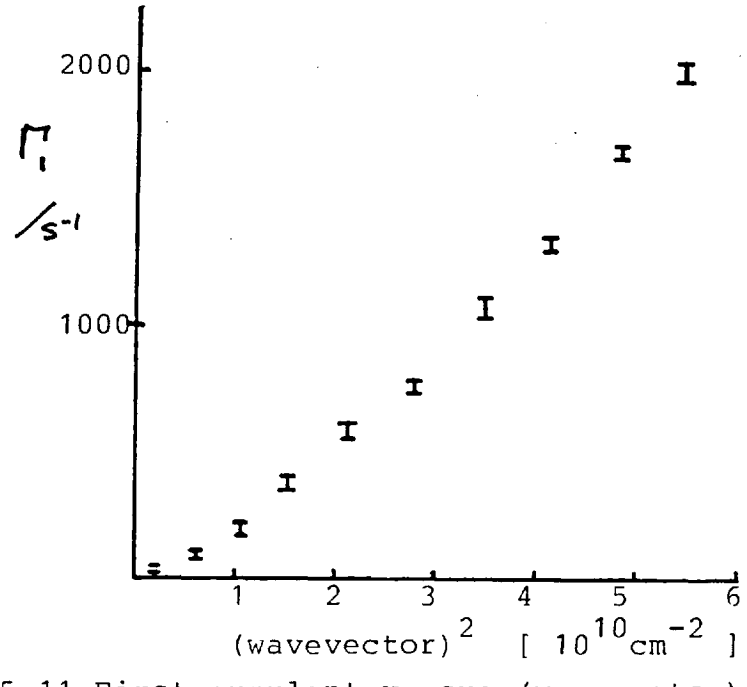


Figure 5.11 First cumulant versus (wavevector)^2 for a 0.5wt% agarose solution at 79 °C.

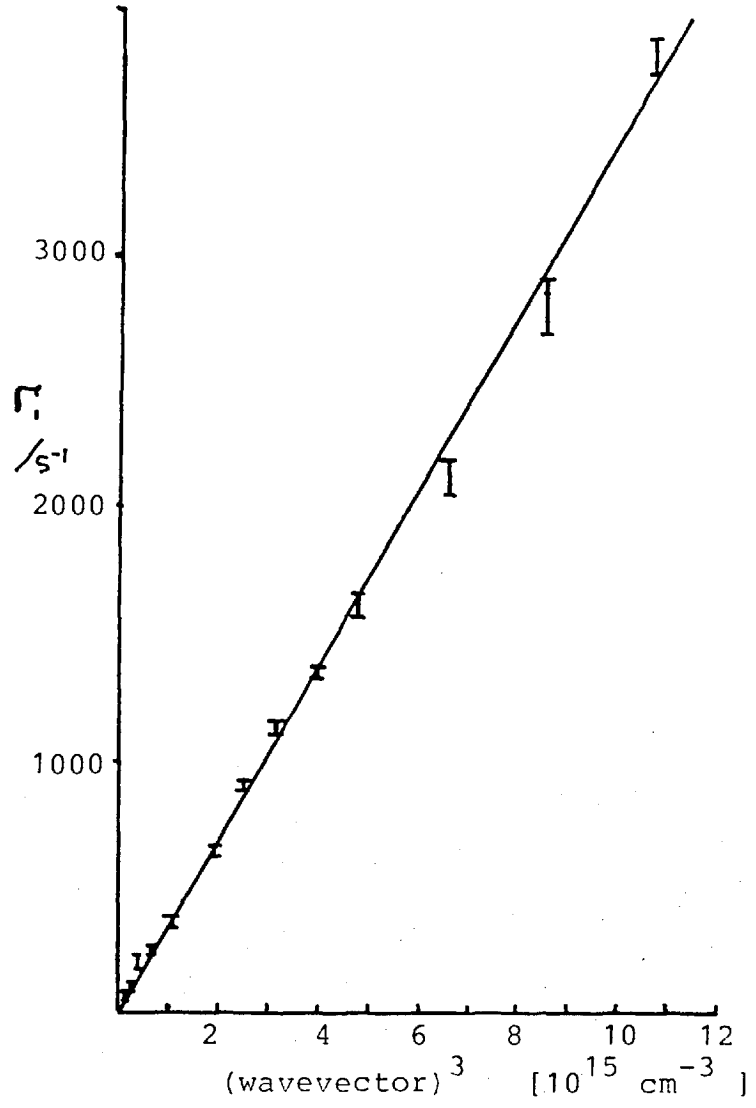


Figure 5.12 First cumulant versus (wavevector)^3 for a 0.1wt% agarose solution at92.5 °C.

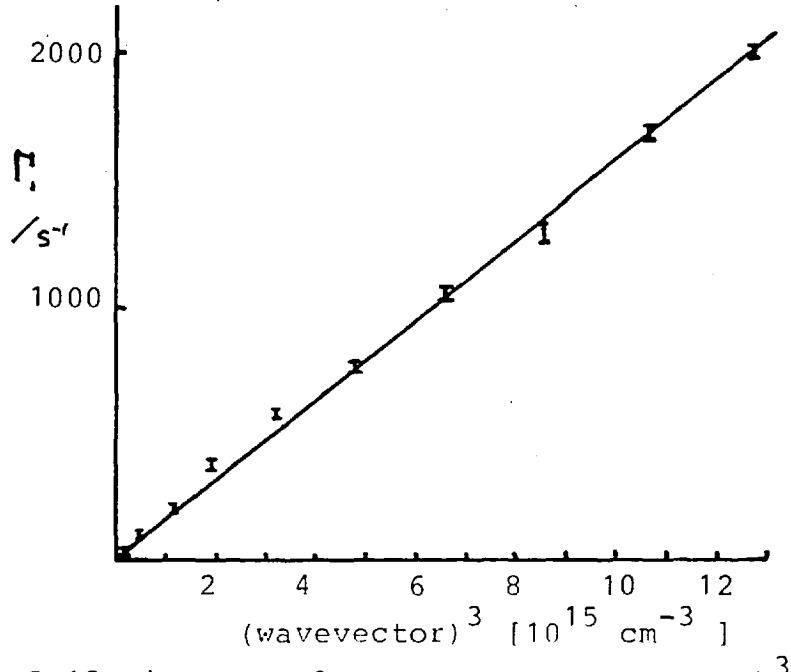


Figure 5.13 First cumulant versus (wavevector)^3 for a 0.5wt% agarose solution at79 °C.

parameter Φ are well represented in figure 5.14 where it is seen that Φ increases with temperature at all concentrations, but at fixed temperature increases with decreasing concentration, in the gelling range.

5.1b (iii) Viscosity

The viscosity of gelling agarose solutions in region I was studied as a function of concentration and temperature using an Ubbelohde type viscometer.

Calibration

The viscometer (ASTM D445) had a nominal constant given by the manufacturers of 0.01 cS/s.. However, it was necessary to calibrate for use in the temperature range 30-100°C by measuring the flow times for distilled, deionised, filtered water at various temperatures and comparing with the standard values for the viscosity of water [78]. The comparison was made using a quadratic equation allowing for the kinetic energy of the emerging fluid from the capillary [79].

Thus:

$$\eta\rho = \nu = \frac{1}{2A}\left[t + (t^2 - 4AB)^{\frac{1}{2}}\right]$$

where: A,B = calibration constants

t = flow time/s

η = dynamic viscosity/cp

ν = kinematic viscosity/cS

ρ = density/gcm^{-3}

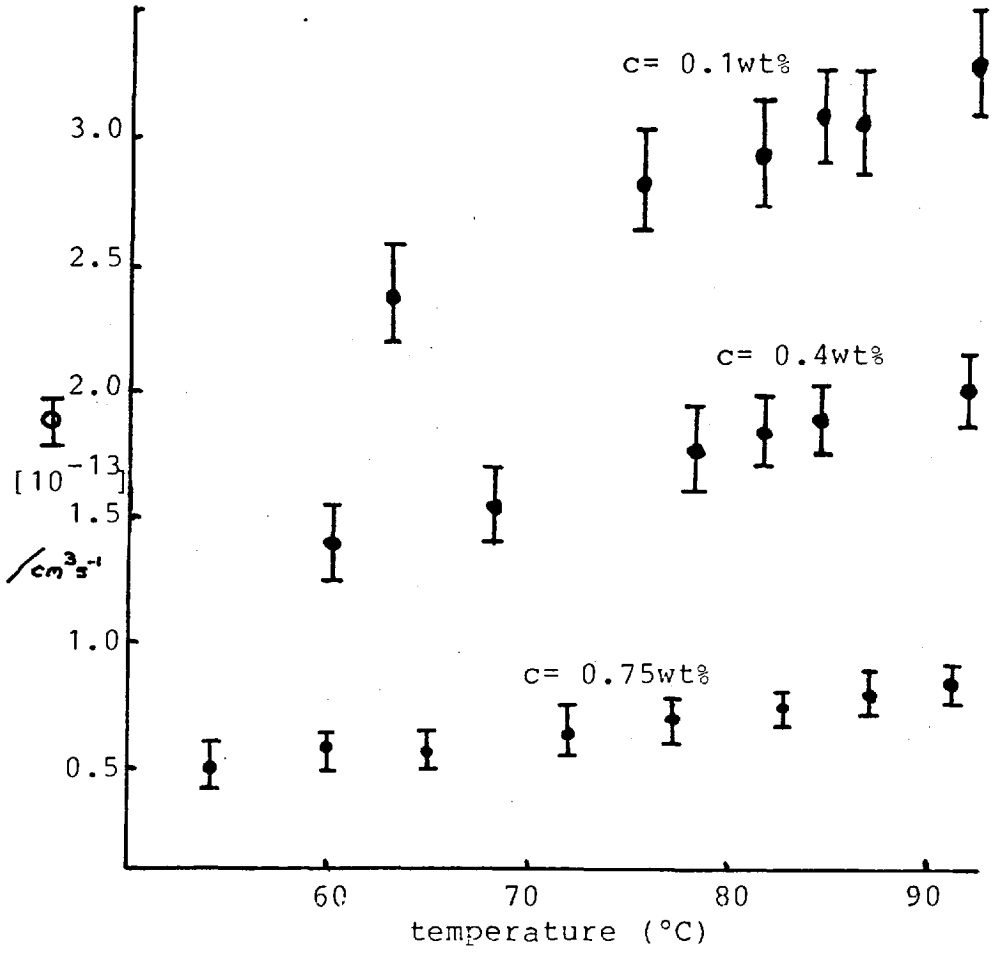


Figure 5.14 Variation of the parameter Φ with temperature for various agarose solutions.

The flow times for the solvent are presented in table 5.2.

Table 5.2

Calibration of the Ubbelohde Viscometer

Temperature/°C	flow time/s
19.8	100.3
29.9	80.6
40.4	66.4
50.0	57.1
60.2	49.7
70.1	44.4
80.1	40.0
90.1	36.7

Using the above values the calibration equation was found to be:

$$\eta\rho = \nu = \frac{1}{197.3}\,[t+(t^2-812.88)^{\frac{1}{2}}]$$

By application of this equation the viscosity of water could be evaluated between 20-90°C with a maximum error of ±0.5%.

The most concentrated agarose solution studied was 0.75wt.%; therefore the solvent and solution densities at any given temperature were taken to be equal. Hence by use of the calibration equation absolute values of the viscosity of agarose solutions could easily be determined with an error of ±1%.

Solution Results

The tables below present the flow time, t, kinematic viscosity, ν, and relative viscosity with respect to the solvent, η/η_0, of agarose solutions at temperatures in the range 50-95°C.

Table 5.3

Viscosity Results for Agarose Solutions

Table 5.3a 0.75wt.% Agarose Solution

Temperature /°C	flow time /s	kinematic viscosity/cS	relative viscosity
50.3	255.2	2.58	4.80
55.8	228.0	2.30	4.68
60.6	209.4	2.11	4.63
66.4	185.8	1.87	4.50
72.6	167.0	1.68	4.46
77.7	153.4	1.54	4.37
82.6	141.9	1.42	4.32
86.0	135.0	1.35	4.28
90.0	125.3	1.25	4.13
92.2	122.2	1.22	4.16

Table 5.3b 0.5wt.% Agarose Solution

Temperature /°C	flow time /s	kinematic viscosity/cS	relative viscosity
51.4	142.0	1.43	2.69
57.1	127.9	1.28	2.66
61.8	117.5	1.17	2.62
67.2	107.8	1.07	2.60
71.7	100.4	0.997	2.58
77.6	92.0	0.910	2.55
82.6	85.7	0.844	2.50
87.2	79.7	0.781	2.49
90.3	76.6	0.749	2.47
93.0	73.9	0.720	2.45

Table 5.3c 0.3wt.% Agarose Solution

Temperature /°C	flow time /s	kinematic viscosity/cS	relative viscosity
47.4	102.3	1.02	1.77
52.8	93.3	0.923	1.80
58.0	85.6	0.843	1.78
63.0	79.2	0.776	1.77
67.8	73.9	0.720	1.77
73.0	68.8	0.666	1.77
77.9	64.5	0.620	1.76
83.1	60.5	0.577	1.75
87.8	57.0	0.539	1.74
89.9	55.7	0.525	1.73
92.9	53.9	0.505	1.73

Table 5.3d 0.2wt.% Agarose Solution

Temperature /°C	flow time /s	kinematic viscosity/cS	relative viscosity
47.7	81.2	0.797	1.40
52.9	74.4	0.725	1.41
58.0	68.8	0.666	1.41
63.1	64.3	0.618	1.41
70.5	58.3	0.553	1.42
73.5	56.3	0.531	1.42
78.1	53.3	0.498	1.42
82.0	51.0	0.473	1.42
85.8	48.8	0.448	1.41
88.5	47.4	0.432	1.41
91.9	45.9	0.415	1.40
93.1	45.3	0.408	1.40

Table 5.3e 0.1wt.% Agarose Solution

Temperature /°C	flow time /s	kinematic viscosity/cS	relative viscosity
58.0	58.7	0.558	1.18
63.0	54.9	0.516	1.18
68.0	51.7	0.481	1.18
74.0	48.0	0.439	1.18
79.0	45.7	0.413	1.19
84.1	43.4	0.386	1.18
89.7	41.2	0.360	1.18
93.0	39.9	0.344	1.17

Figures 5.15 and 5.16 show the viscosity, ν, and relative viscosity, η/η_o, of several agarose solutions as a function of temperature.

The variation of viscosity with concentration at both 50°C and 80°C is displayed in figure 5.17. From this plot the following relationships have been obtained:

At 50°C $\eta/\eta_o = 1+1.0c+5.4c^2$

At 80°C $\eta/\eta_o = 1+1.33c+3.84c^2$

where c is concentration of agarose in wt.%.

5.1c Non-gelling Solutions

5.1c(i) Scattered Intensity Data

The dependence of the scattered intensity of a 0.05wt.% agarose solution was studied as a function of temperature just as for the gelling solutions (figure 5.18). Unexpectedly it seemed to show identical features to those of a gelling solution. The dramatic increase in intensity must therefore be associated with aggregation of the agarose units and we may again evaluate an aggregation temperature, T*, without, however, defining the detailed nature of this aggregation. The hysteresis cycle is thus centred about two states of the agarose system:

1) A "sol" state, region I, in which the agarose system is stable between 40-100°C.

2) An aggregated state which occurs below 30°C (RegionIII) and once formed exists, albeit with steadily decreasing turbidity, to ~90 °C when the sol state (I) is restored.

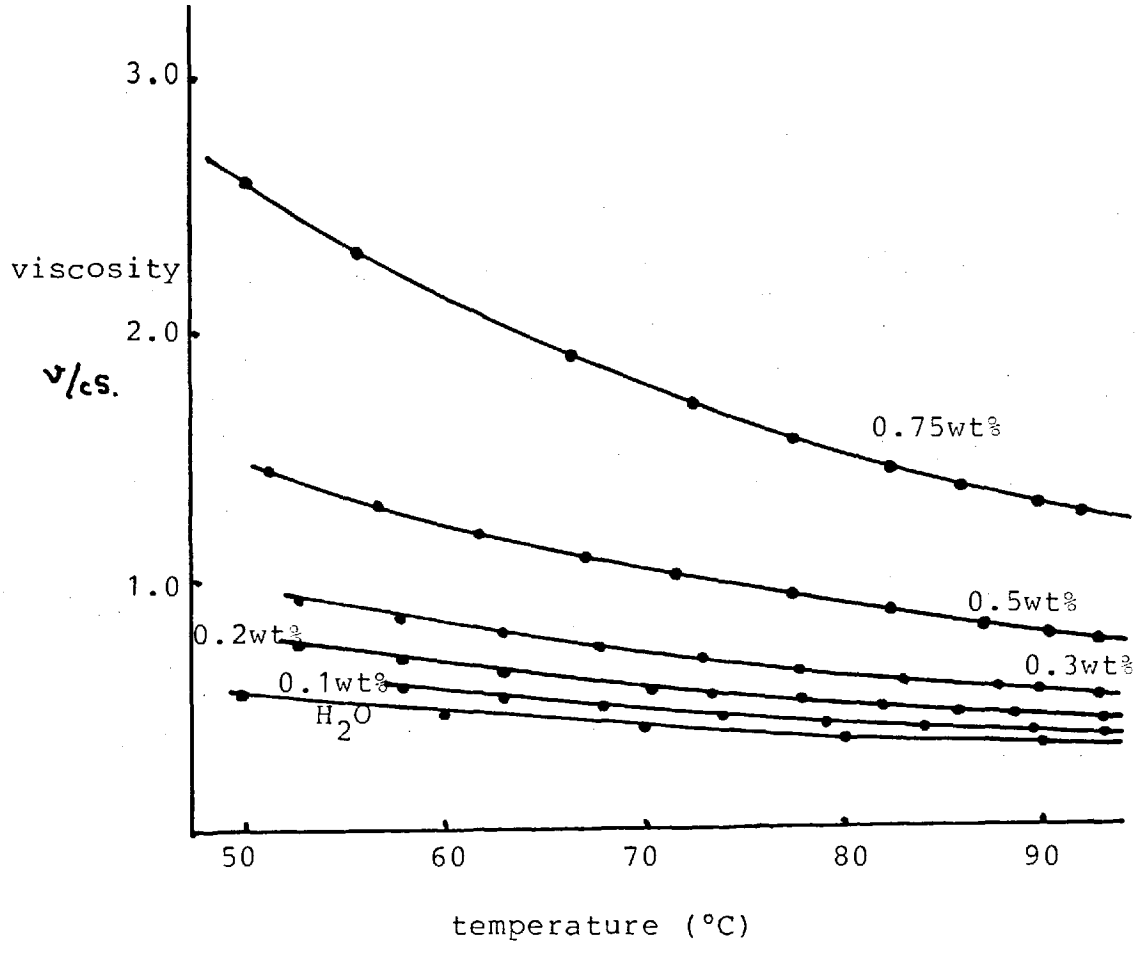


Figure 5.15 Temperature dependence of the solution viscosity for agarose solutions.

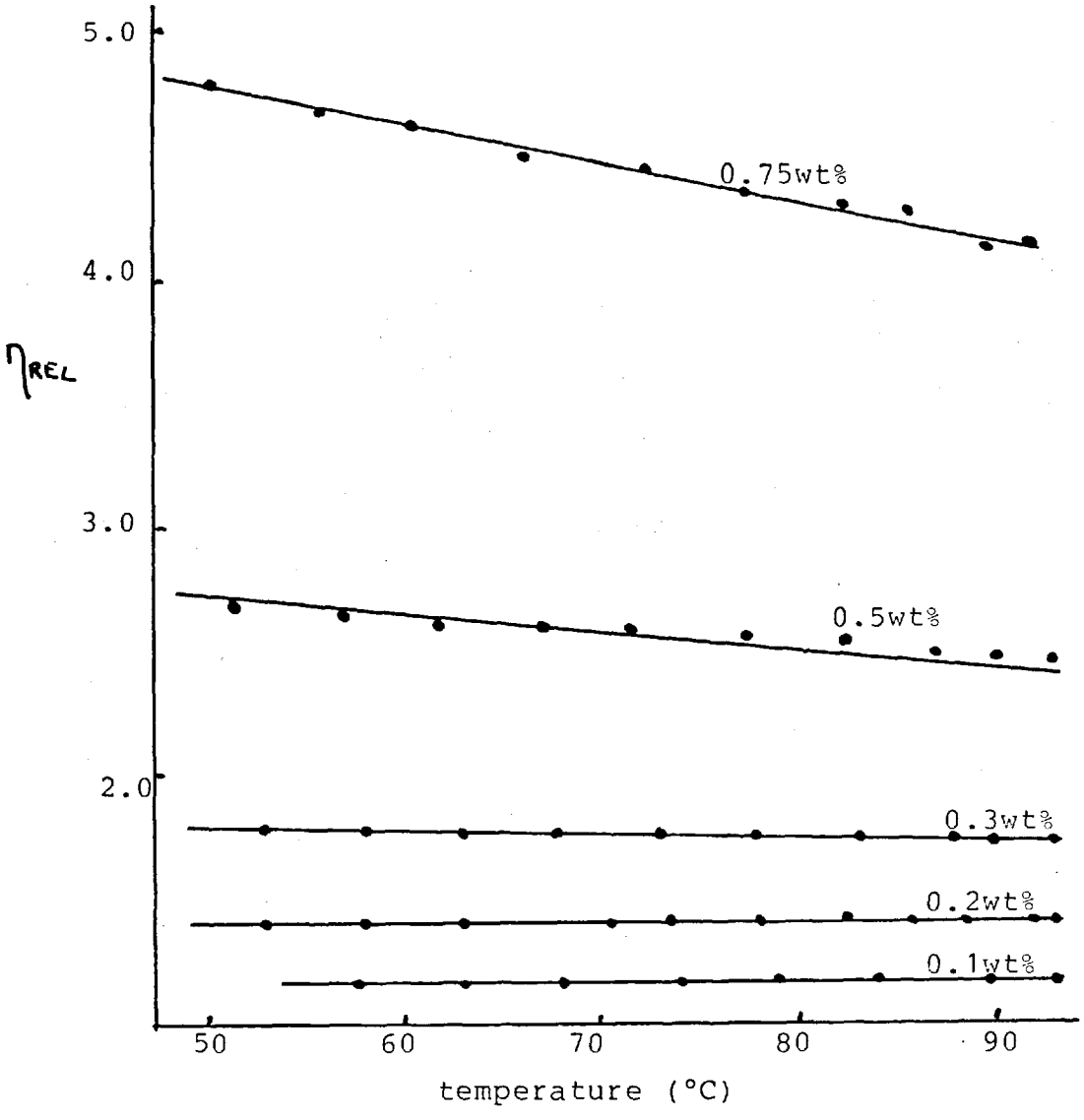


Figure 5.16 Temperature dependence of the relative viscosity of agarose solutions.

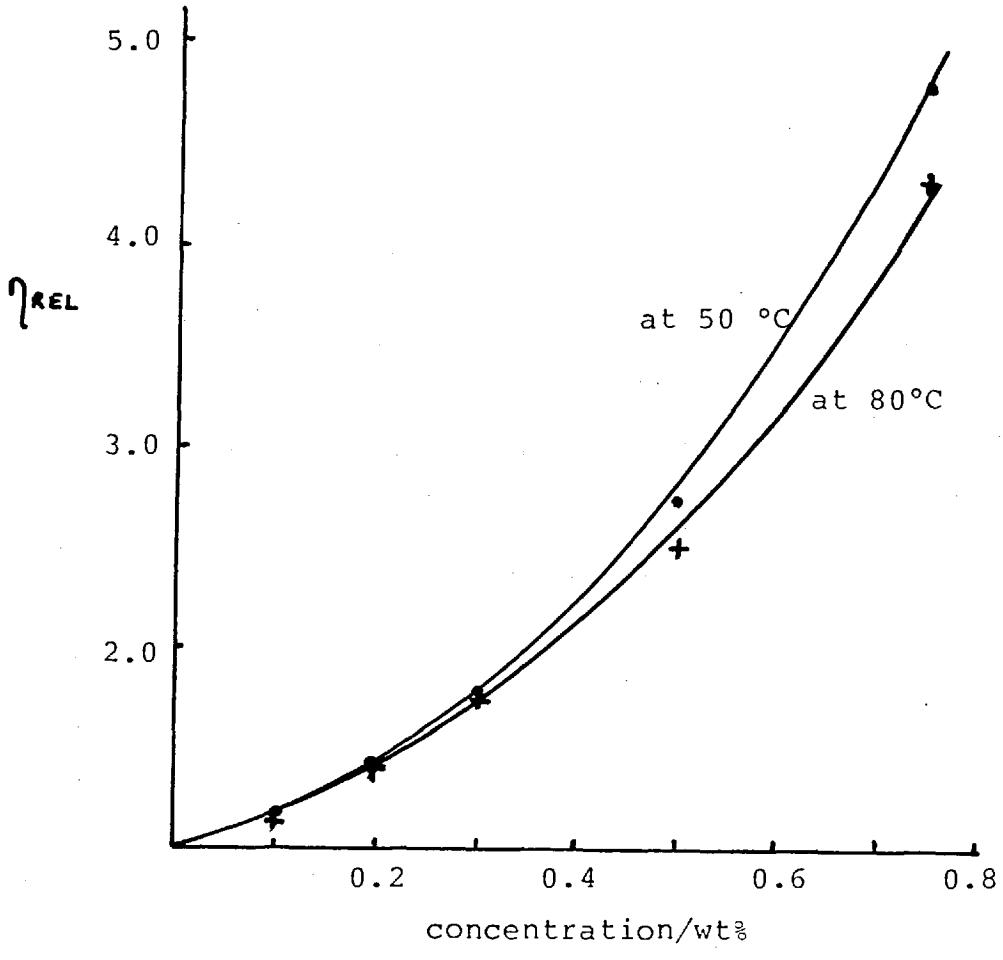


Figure 5.17 Concentration dependence of the relative viscosity of agarose solutions.

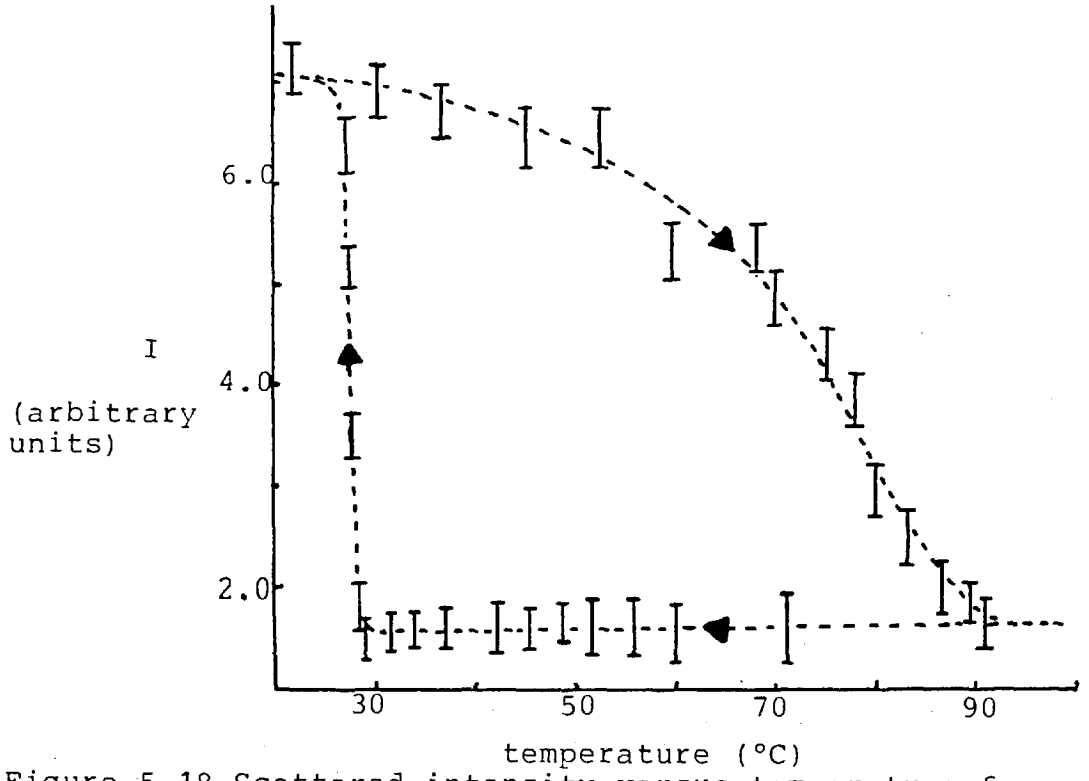


Figure 5.18 Scattered intensity versus temperature for a 0.05 wt% agarose solution.

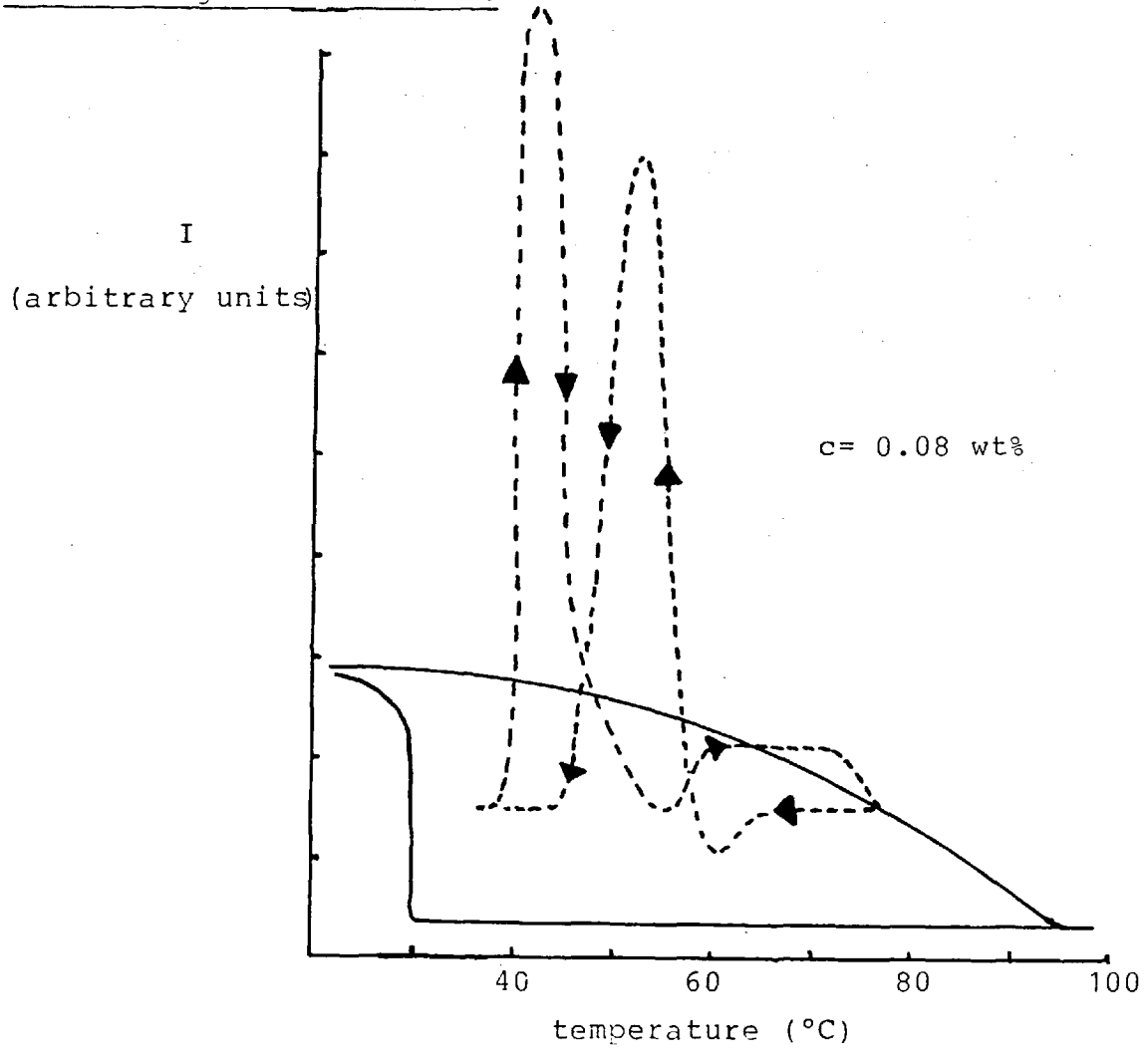


Figure 5.19 Intensity fluctuations on cooling a sample in the aggregated state.

The aggregation at concentrations above 0.1 wt% leads to the formation of a three-dimensional network occupying the whole of the solution. Evidently this is not so for non-gelling solutions. However, after standing in a closed flask for several months at room temperature non-gelling solutions will form a gel layer in the lower part of the solution.

Studies of the reversibility of this cycle have shown that in the sol region (I) the intensity is constant, at a low level, whether the sample is heated or cooled. However, when one cools a sample already in the aggregated state (IV) at 75 °C intensity fluctuations as shown in figure 5.19 were observed. Thus in the aggregated state (IV) the system does not exhibit complete reversibility upon heating and cooling. These fluctuations are consistent with the heterogeneous formation of aggregates which settle out of the solution.

5.1c(ii) Photon Correlation

Measurements were first made in the sol state (region I) for a 0.05 wt% non-gelling agarose solution. The plot of the first cumulant versus (wavevector)^2 is shown in figure 5.20 . Here the results obey the simple (wavevector)^2 dependence symptomatic of a Brownian motion.

On cooling the same dependences were found (figures 5.21-5.23). However, as the sol/gel transition temperature was approached deviations from this dependence were observed (figure 5.24) until at lower temperatures major changes in

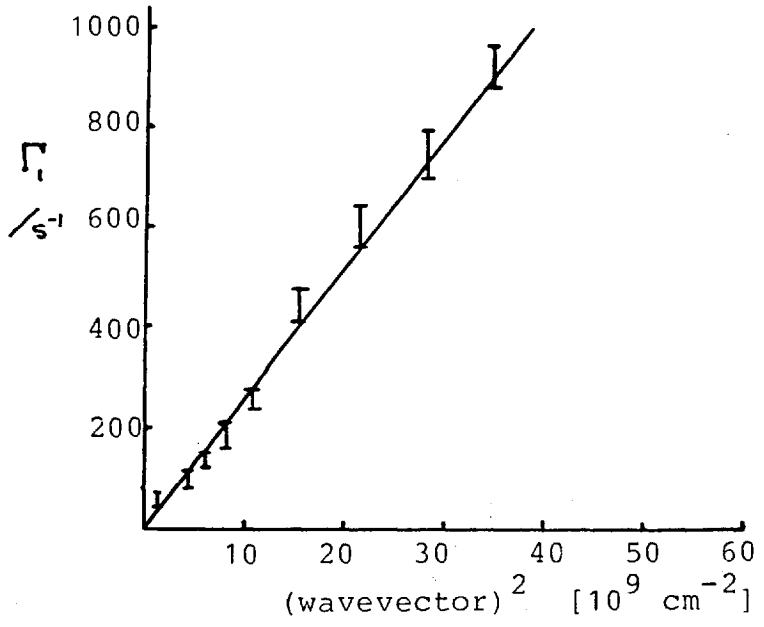


Figure 5.20 First cumulant versus (wavevector)^2 for a 0.05 wt% agarose solution at 92.5 °C.

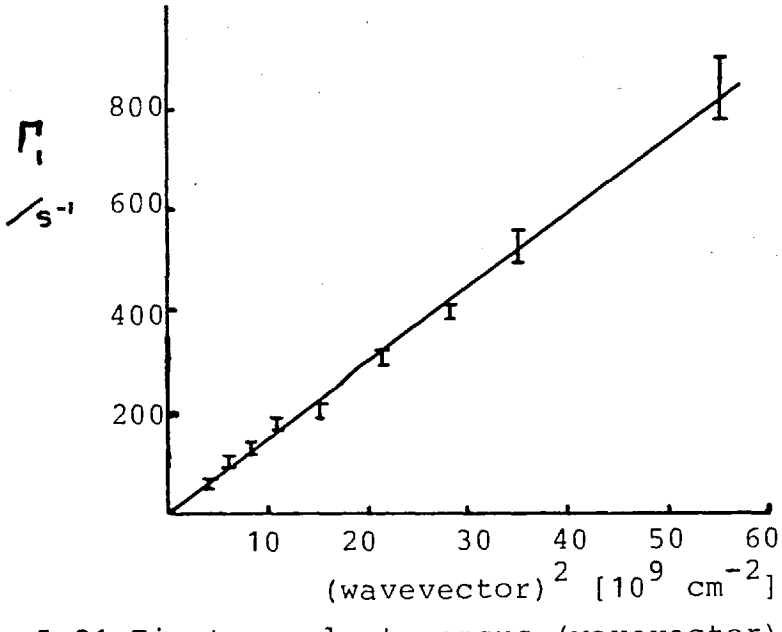


Figure 5.21 First cumulant versus (wavevector)^2 for a 0.05 wt% agarose solution at 59 °C.

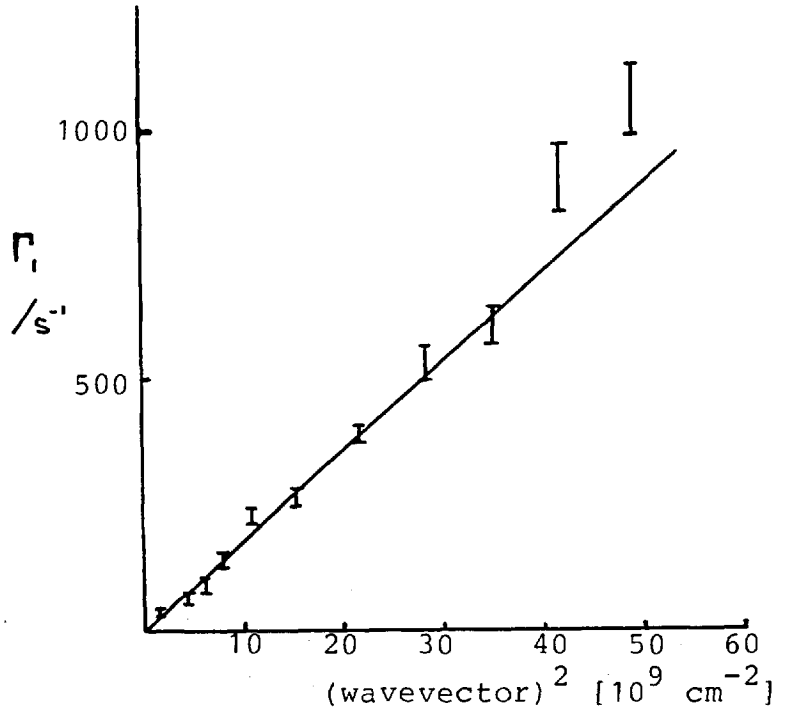


Figure 5.22 First cumulant versus (wavevector)^2 for a 0.05 wt% agarose solution at 45 °C.

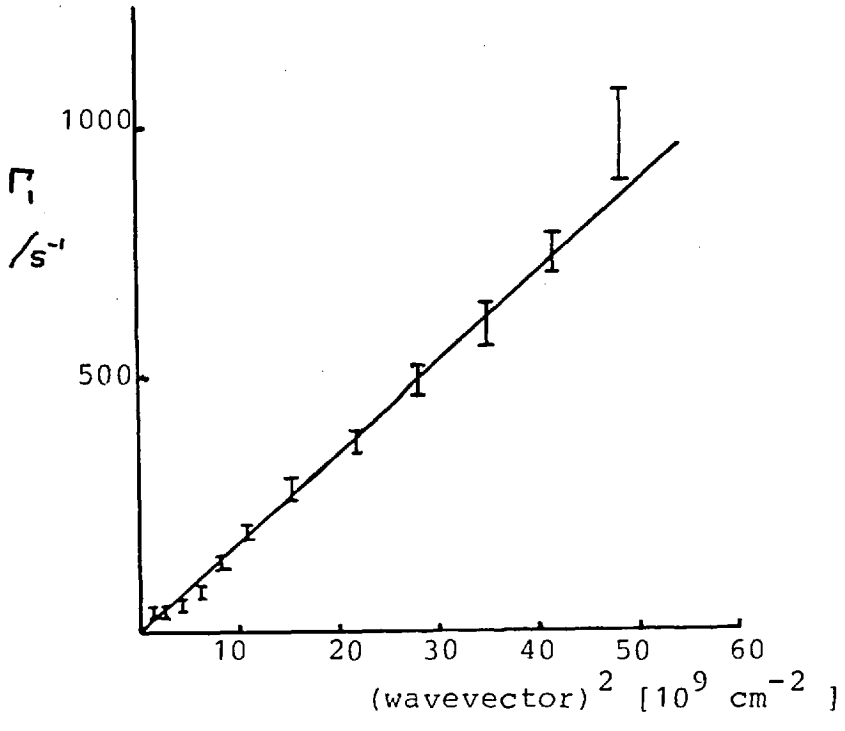


Figure 5.23 First cumulant versus (wavevector)^2 for a 0.05 wt% agarose solution at40 °C.

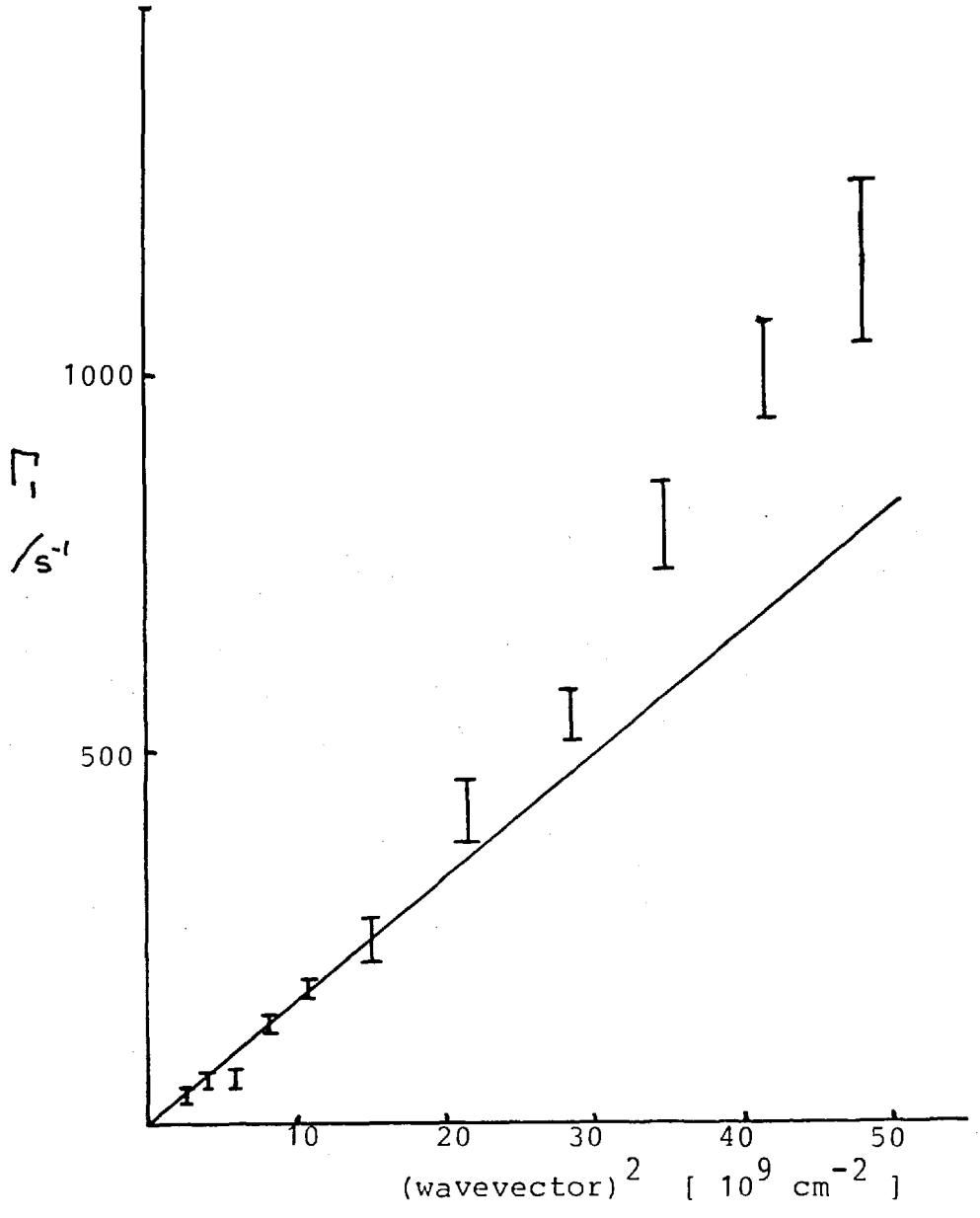


Figure 5.24 First cumulant versus (wavevector)^2 for a 0.05 wt% agarose solution at 33.4 °C.

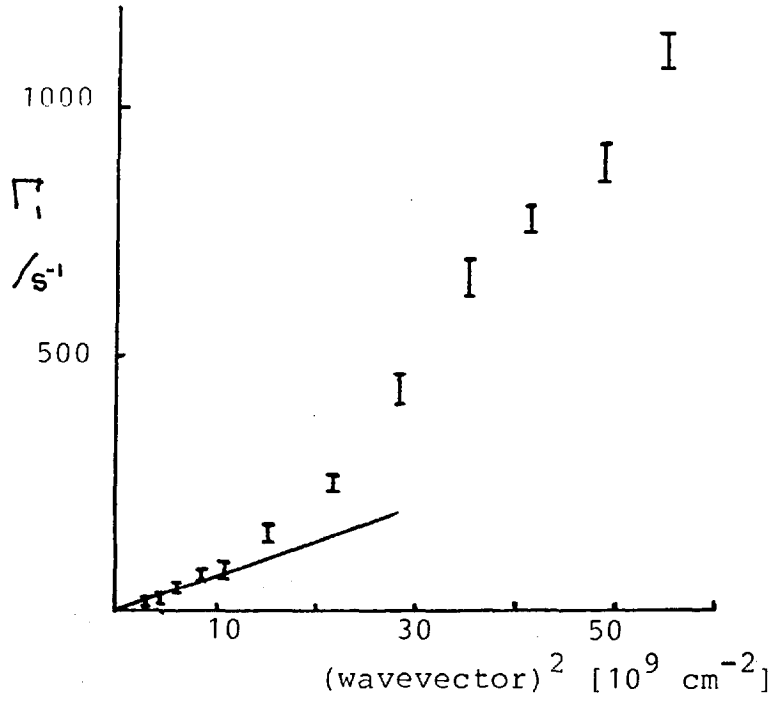


Figure 5.25 a

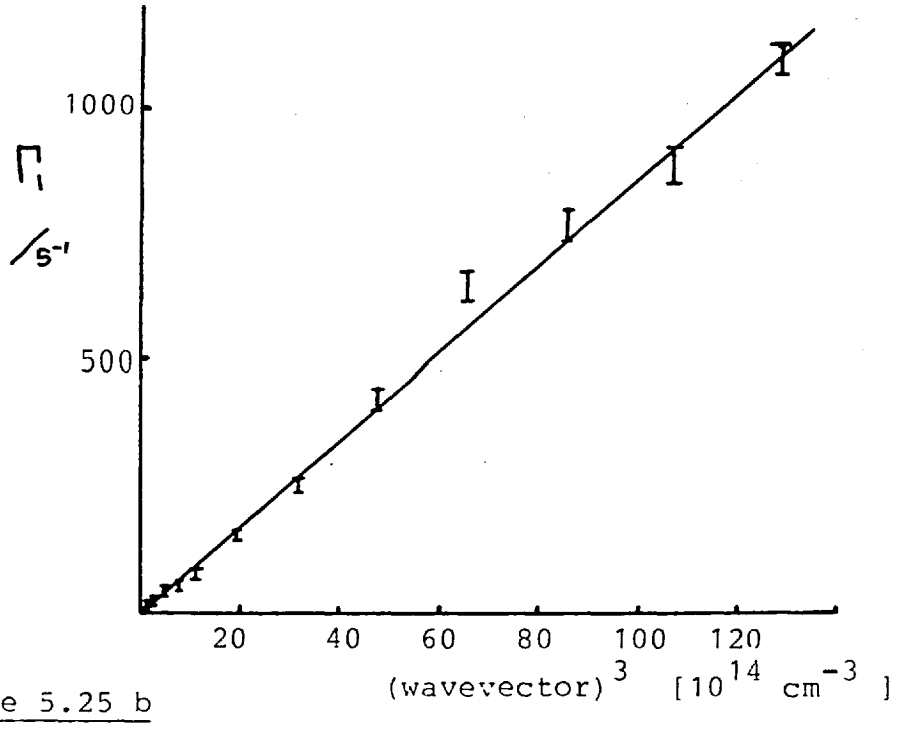


Figure 5.25 b

Figure 5.25 First cumulant versus (wavevector)^2 [5.25a] and (wavevector)^3 [5.25 b] for a 0.05 wt% agarose solution at 23°C.

functional form became apparent. These data were then plotted against (wavevector)^3 and a linear fit obtained (figure 5.25). The (wavevector)^3 dependence persisted as the temperature was raised through region (IV), until the sol state was restored at ~90°C (figures 5.26 and 5.27).

In the region where the autocorrelation functions obey a (wavevector)^2 dependence an effective diffusion coefficient was evaluated and by applying the Stokes-Einstein equation an effective hydrodynamic radius, r, was obtained. In the region obeying a (wavevector)^3 dependence a maximum effective diffusion coefficient was evaluated from the slope of the K^2-plots as wavevector, $K \to 0$ and hence a minimum effective hydrodynamic radius was determined.

Figure 5.28 shows the results for the calculated effective hydrodynamic radius, r, as a function of temperature. The values at temperatures greater than 95°C were measured with the agarose solution enclosed in sealed cylindrical glass tubes.

It is of great importance to note that the effective hydrodynamic radius decreases as the temperature is reduced, and that the hydrodynamic radius in region IV is about twice the value obtained in region I. The smooth return of region IV to region I as observed in turbidity plots is not seen in these results.

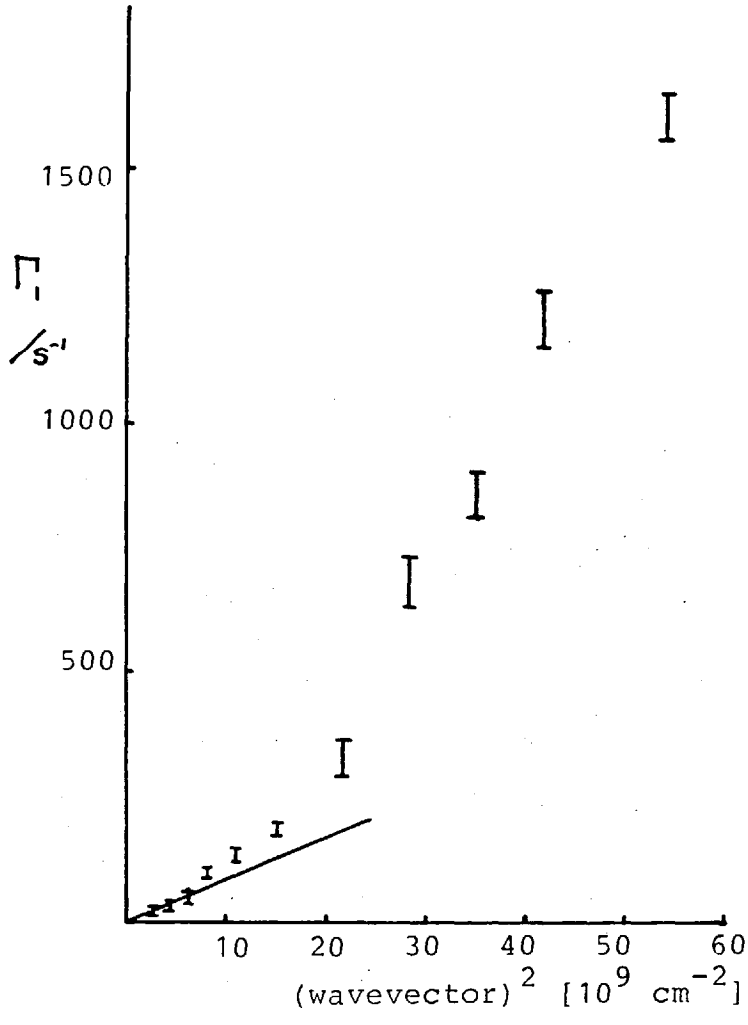


Figure 5.26 First cumulant versus (wavevector)^2 for a 0.05 wt% agarose solution in the aggregated state at 50 °C.

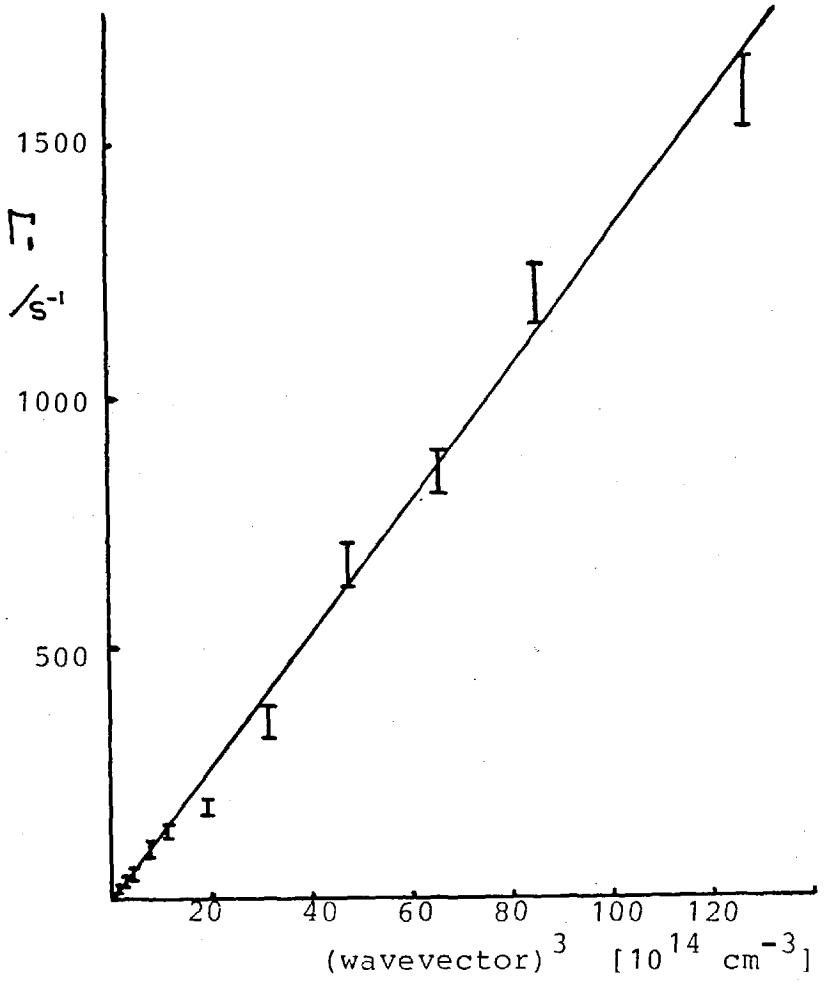


Figure 5.27 First cumulant versus (wavevector)^3 for a 0.05 wt% agarose solution in the aggregated state at 50 °C.

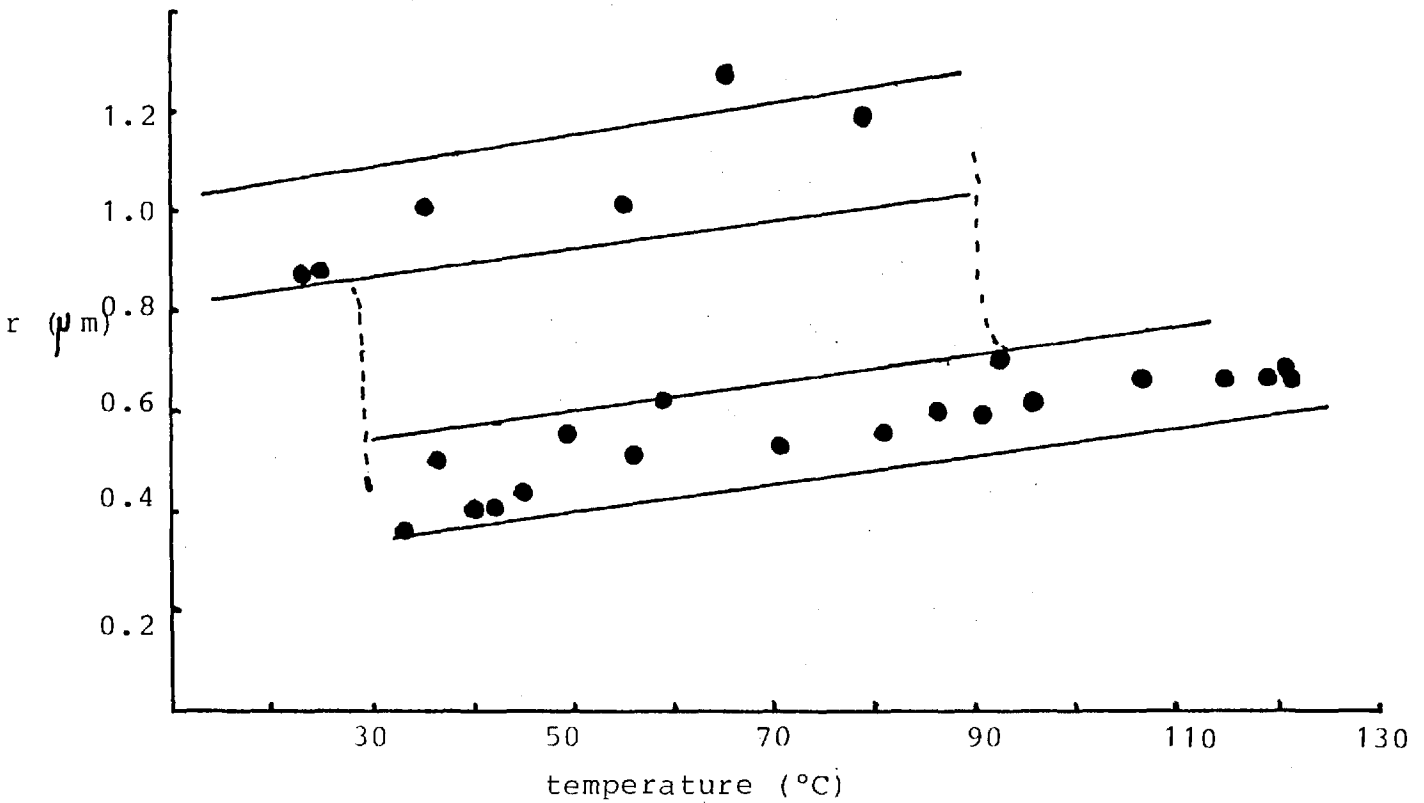


Figure 5.28 Temperature variation of the effective hydrodynamic radius for non-gelling agarose solutions.

5.1d Optical Rotation Studies

Because of the set pathlength (2 cm.) imposed by the design of the thermostat jacket it was not possible to determine the optical rotation of plane polarised light by very dilute solutions. Also, with more concentrated solutions, as the solution neared the sol/gel transition oscillations in the readings of the angle of rotation were observed (figure 5.29). This is thought to arise from a combination of circumstances including:

1) multiple scattering of the light beam as the turbidity of the sample increased, which will depolarise the light and thus reduce detection sensitivity and:
2) strain birefringence in samples constrained to gel in a fixed volume.

As a consequence of these limitations accurate determinations of the rotation of plane polarised light at the sol/gel transition could only be obtained in a rather limited concentration range (0.2-0.4 wt%). Figures 5.30 and 5.31 show the results obtained for the optical rotation as a function of temperature for 0.2 and 0.3 wt% solutions respectively, corrections having been made for any stress imposed upon the cell windows due to temperature variations.

This technique supplied further information concerning the aggregation temperature which is discussed in the following section. Despite difficulties with the more concentrated gels, sensible values of T* could be obtained after calibration of the thermometer.

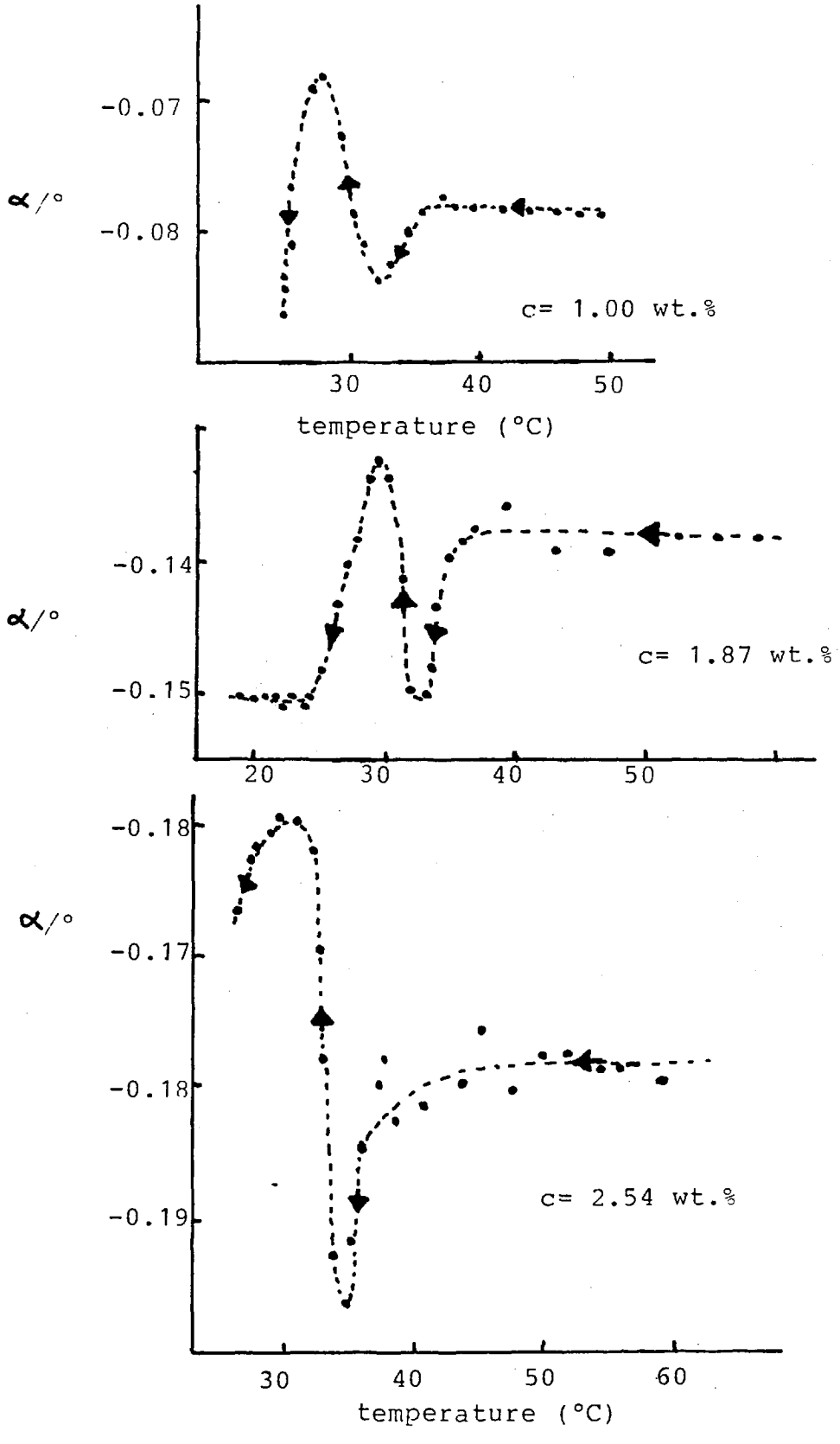


Figure 5.29 Behaviour of optical rotation for gelling agarose solutions near the sol/gel transition.

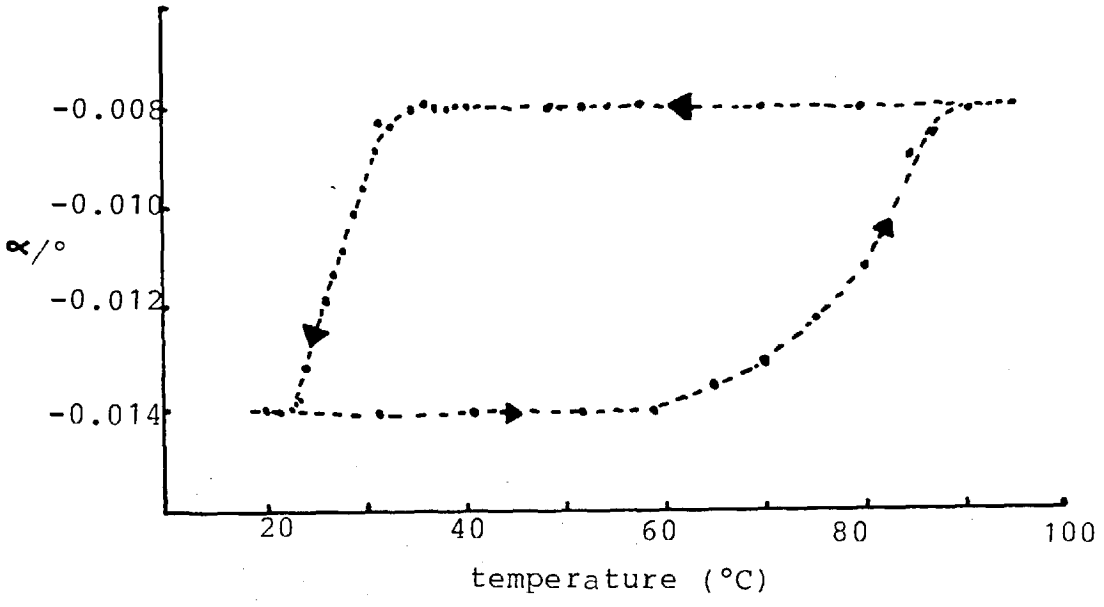


Figure 5.30 Temperature variation of optical rotation for a 0.2 wt% agarose solution.

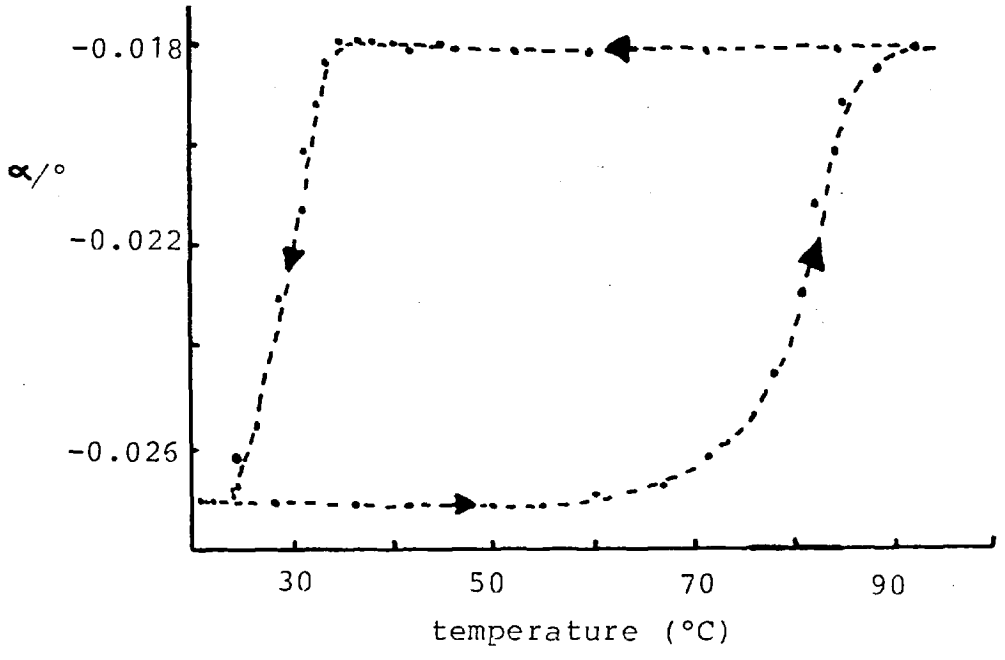


Figure 5.31 Temperature variation of optical rotation for a 0.3 wt% agarose solution.

5.1e Aggregation Temperature

In both optical rotation measurements and intensity measurements dramatic changes in properties are seen as gelation occurs. A study of the temperature at which these changes occur has shown that consistent results may be obtained from both techniques and that there is a concentration dependence of this aggregation temperature (table 5.4).

Table 5.4 Concentration Dependence of the Aggregation Temperature.

Concentration of agarose/wt.%	Aggregation temperature/°C from intensity measurements	from optical rotation studies
0.05	28.5	
0.08	29.9	
0.10	30.0	
0.20	31.6	30.7
0.30	32.4	31.5
0.40	33.1	
0.50	33.6	
0.75	34.9	
1.00	35.6	36.0
1.40	36.1	
1.87	36.4	35.8
2.54	36.6	36.5

These data are plotted in figure 5.32.

Colloidal Ca(Mg) SO_4 (SiO_4,PO_4) was added to a 0.57wt.% agarose solution and the solution slowly cooled in

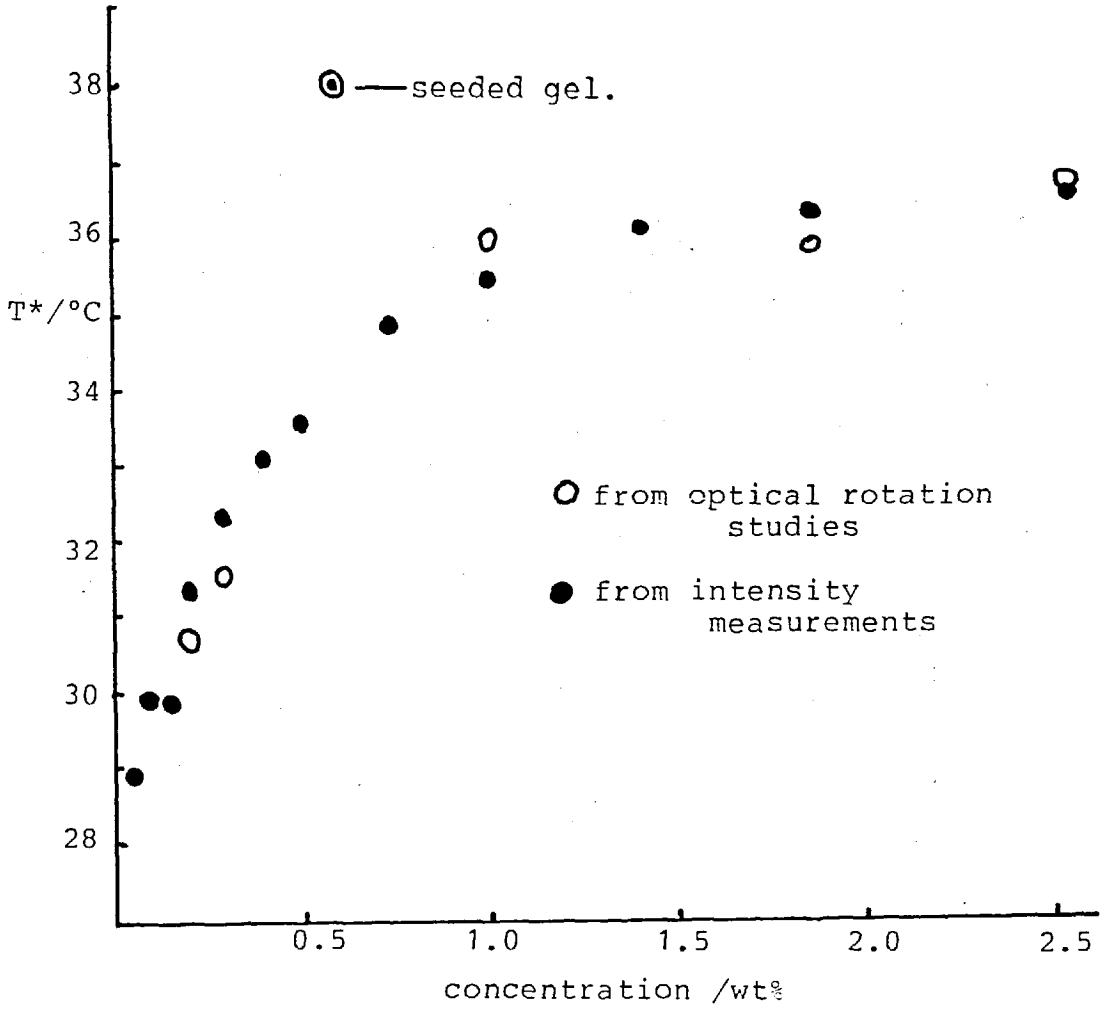


Figure 5.32 Concentration dependence of the aggregation temperature, T*.

a thermostatted bath. The onset of turbidity for this solution occurred at 38.0°C thus indicating an elevation of the gelling temperature by addition of these colloidal particles.

5.2 Complementary Experimental Data

5.2a Batch and Pretreatment Dependence

A second agarose batch (N°6409620) was checked to verify that the basic hydrodynamic properties found in section 1 are batch-independent. The agarose was also dissolved in water and then precipitated with polyethylene glycol as in the commercial purification of agarose to verify that this process did not cause any change in the relevant parameters under study.

Characterisation

Three main features were used to characterise the newly delivered sample:

1) A gelling solution (0.5wt.%) was made and its autocorrelation functions at ~50°C in the sol state (I) were studied (figure 5.33a).
2) A non-gelling solution was prepared and its autocorrelation functions at ~50°C in the sol state (I) were studied (figure 5.33b).
3) The autocorrelation functions of the non-gelling solution at room temperature were studied (figure 5.33c).

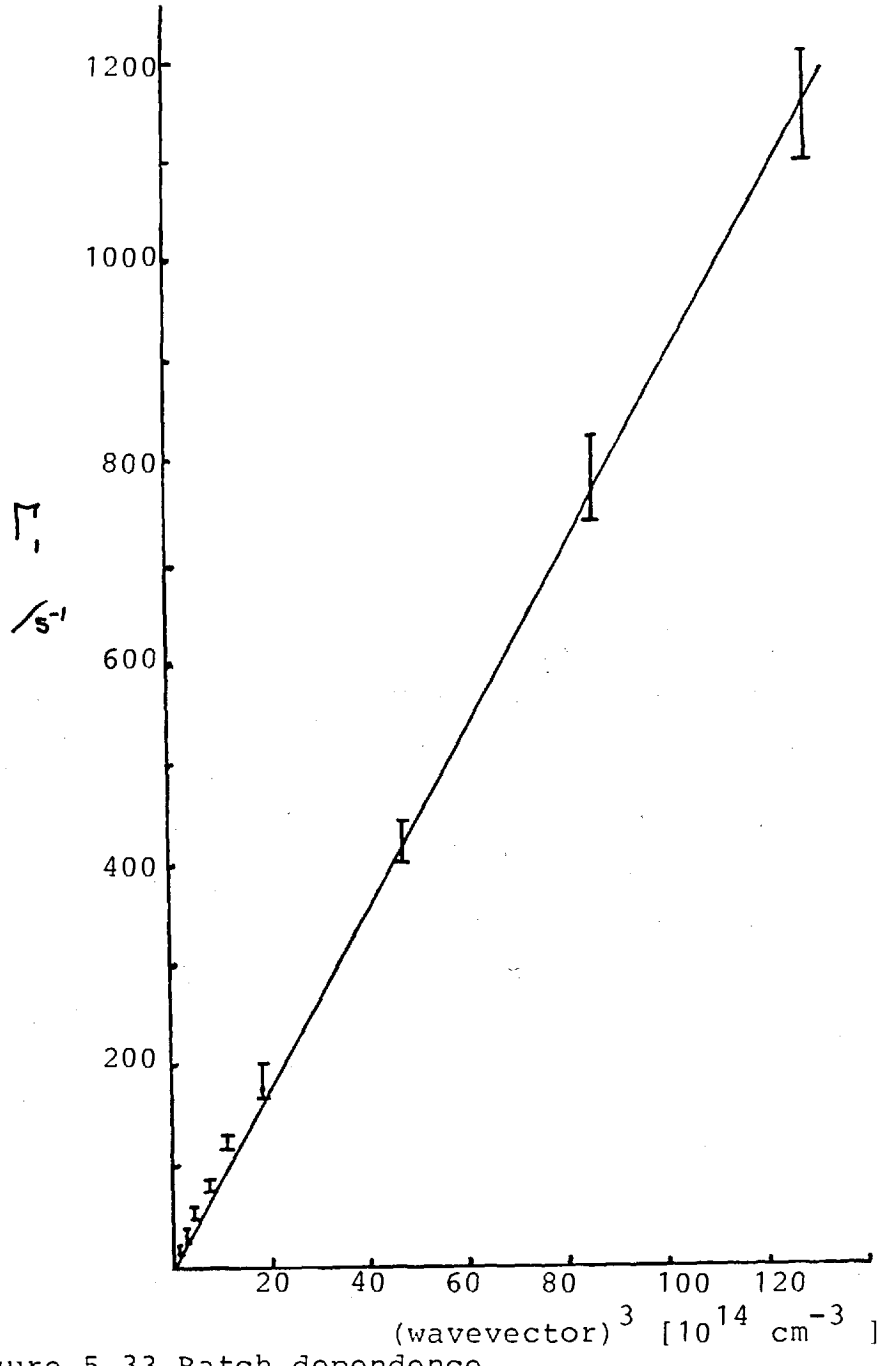


Figure 5.33 Batch dependence.

Figure 5.33a First cumulant versus (wavevector)^3 for a 0.5 wt% agarose solution (batch 6409620) at 50 °C.

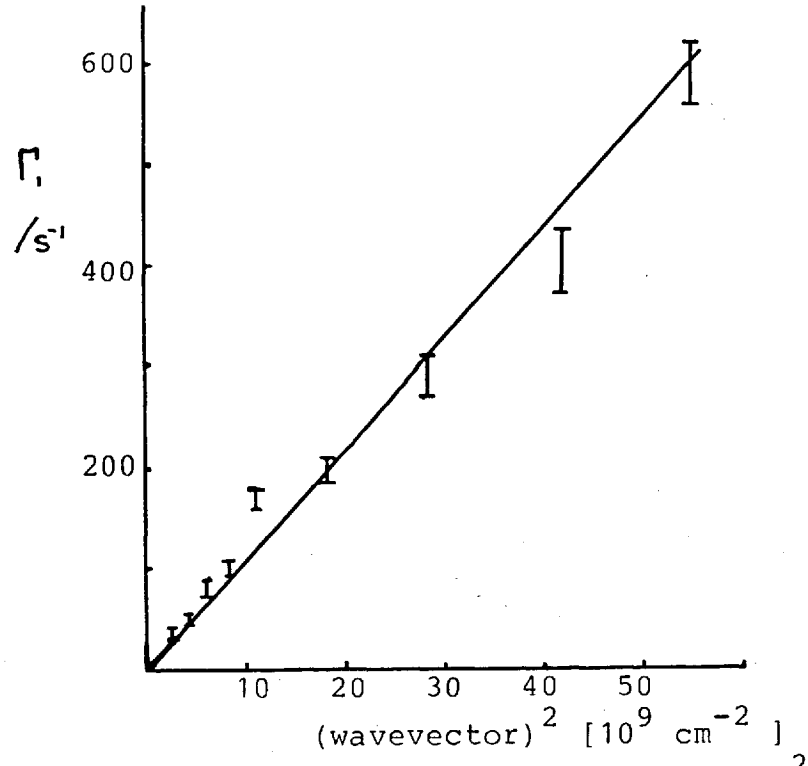


Figure 5.33 b First cumulant versus (wavevector)^2 for a 0.06 wt% agarose solution (batch 6409620) at 53.8 °C.

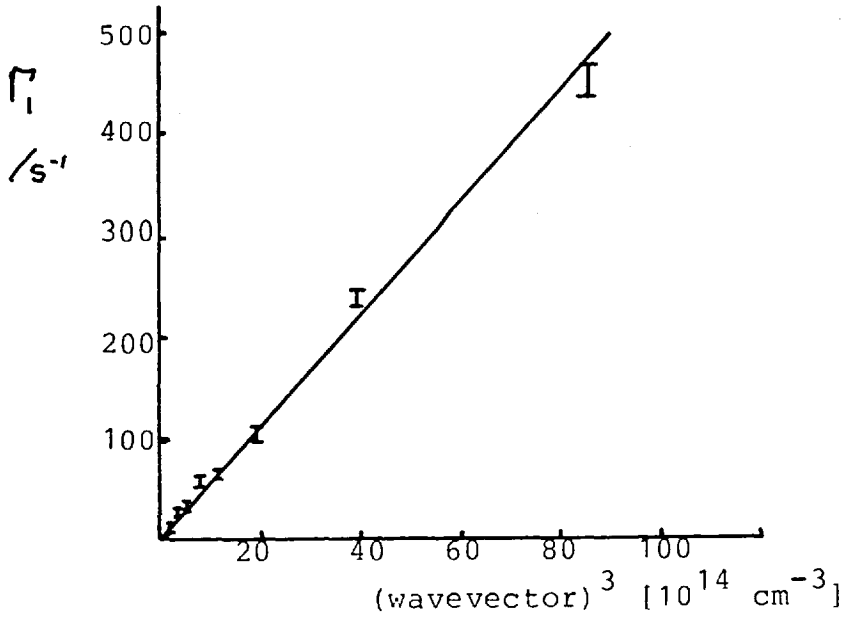


Figure 5.33 c First cumulant versus (wavevector)^3 for a 0.06 wt% agarose solution (batch 6409620) at 24 °C.

The characterisation plots show identical wavevector dependences as found for the main batch. Thus for a gelling solution a (wavevector)^3 dependence was obtained at 50°C with $\Phi \sim 0.9 \times 10^{-13}$. The non-gelling solution exhibited a (wavevector)^3 dependence at room temperature and (wavevector)^2 dependence at ~50°C in region I. The effective hydrodynamic radius evaluated from studies of the non-gelling solution was found to be ~0.8μm, in excellent agreement with data obtained for the main batch.

Precipitation

4g of agarose (batch 6409620) was placed in a round-bottomed flask. 100 cm^3 of distilled, deionised, filtered water was added and the solution heated to ~100°C under reflux for twenty minutes and then allowed to cool. A rigid, turbid gel was formed. The gel was reheated, melted and then held at 80°C with stirring. 100 cm^3 of a 40wt.% solution of polyethylene glycol (M.Wt. 6000; from B.D.H. Chemicals Ltd.) which was also at 80°C was then added. The solution was left for seven - ten minutes to flocculate. It was then filtered in a Buchner filter funnel. The precipitate was washed with warm distilled water (~40°C) and then cold distilled water, collected and then placed in a beaker of distilled water with stirring for ~10hrs.. It was then filtered, washed and collected, placed in another beaker of distilled water and stirred overnight. Finally the precipitate was filtered, washed with distilled water and acetone and dried.

The precipitate was then used to make gelling and non-gelling solutions of agarose to recheck the above properties.

Figure 5.34a shows the wavevector dependence of the first cumulant for a gelling sample (0.5wt.%) at 50°C. Figures 5.34b,c show the data obtained for the non-gelling solution at 55°C and 24°C respectively.

The wavevector dependences of the precipitate are of the same functional form as the native agarose; also the parameters Φ and r are in good agreement, showing that batch to batch variations of these parameters are not so great as to cause doubt about their reliability. The results clearly show that the precipitation technique with polyethylene glycol does not cause a significant variation in these parameters.

5.2b Hydrolysis and Elemental Analysis

Agarose from batch 6409620 was used throughout this experiment.

4.1g of agarose was weighed into a round-bottomed flask and 200 cm^3 of distilled, deionised filtered water added. The solution was heated and kept under reflux at 100°C. 25 cm^3 aliquots were removed at intervals and allowed to cool. Whilst still in the sol state at ~50°C the pH of the sample was measured using an E.I.L. model 3030 pH meter. The *pH* of a sample of solvent and two standard buffer solutions was also rechecked at each measurement. Table 5.5

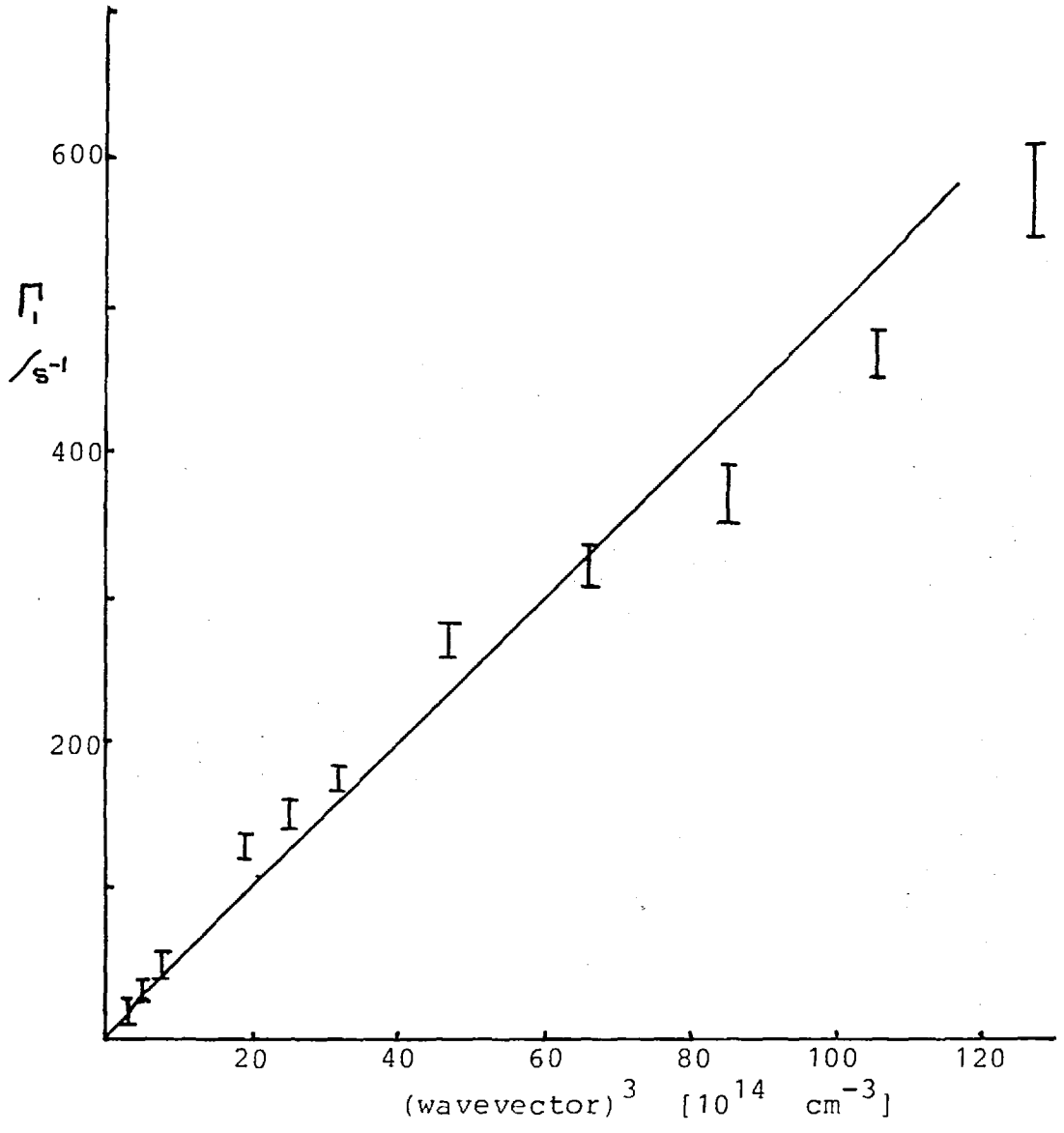


Figure 5.34 Pretreatment dependence.

Figure 5.34 a First cumulant versus (wavevector)^3 for a 0.5 wt% solution of agarose precipitate at 50°C.

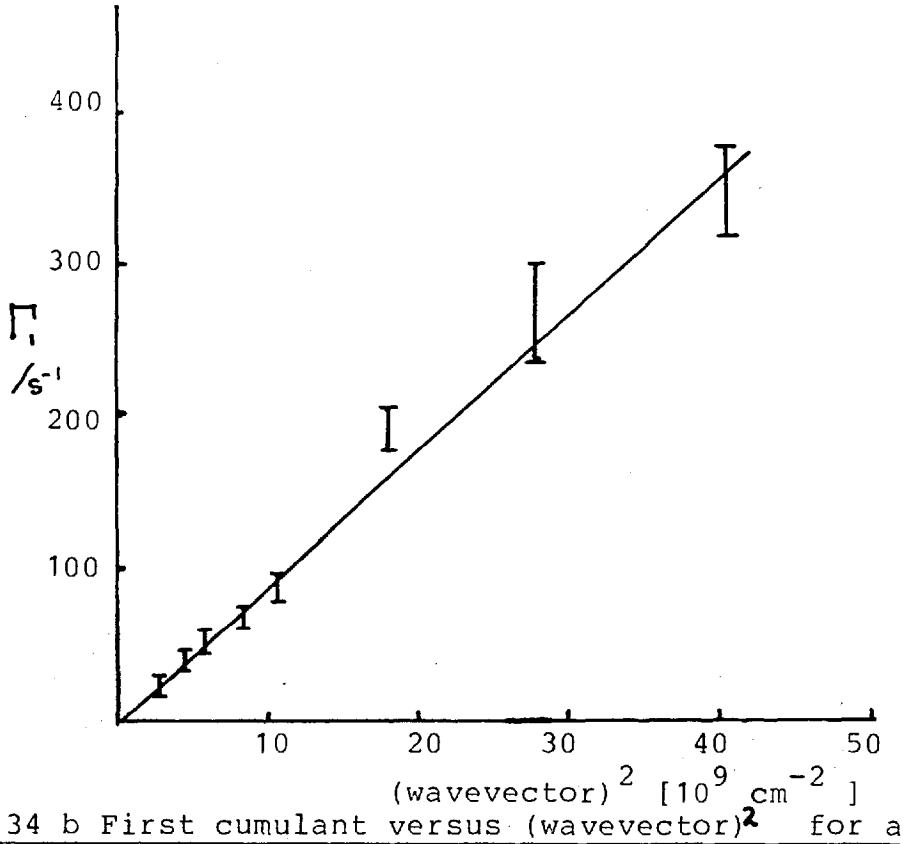


Figure 5.34 b First cumulant versus (wavevector)^2 for a 0.045 wt% solution of agarose precipitate at 55°C.

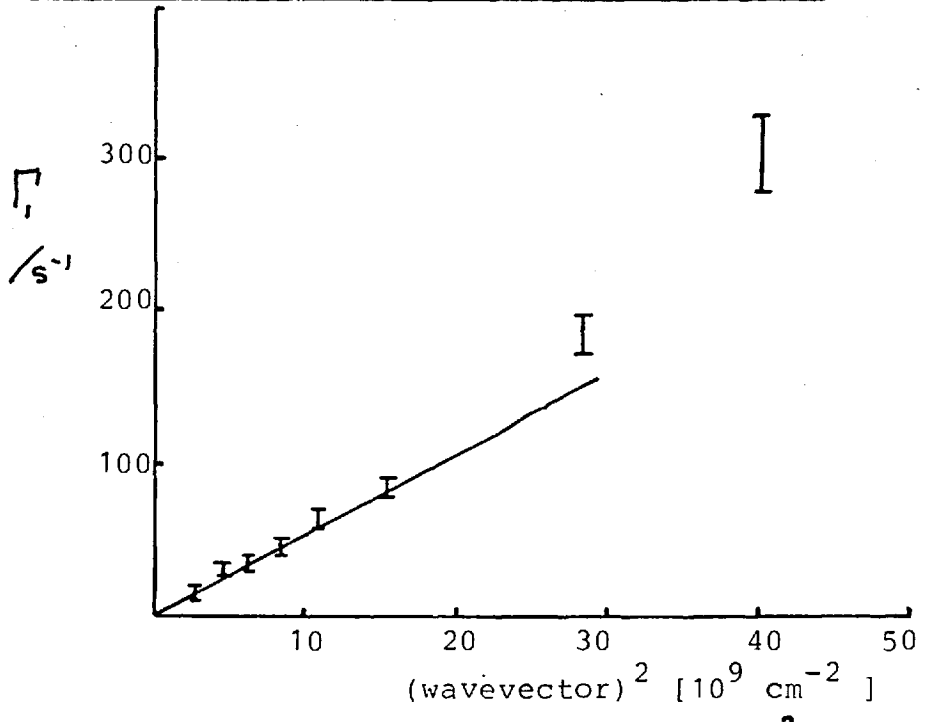


Figure 5.34 c First cumulant versus (wavevector)^2 for a 0.045 wt% solution of agarose precipitate at 24°C.

presents the variation of pH with time of reflux and also observations of the sample as cooling proceeded.

Table 5.5 Hydrolysis of Agarose

Time of reflux	pH measurements				Remarks
	pH 4 buffer	pH 9 buffer	solvent	sample	
20 mins.	4.5	9.7	6.6	6.5	Formed a stiff, turbid gel when cold.
3 hrs.	4.5	9.6	6.6	6.2	Formed a stiff, turbid gel when cold.
6 hrs.	4.5	9.75	6.4	5.9	Formed a stiff, turbid gel when cold.
25 hrs.	4.5	9.7	6.4	5.15	Formed a soft, turbid gel when cold. Slight yellow discoloration.
30 hrs.	4.5	9.75	6.4	4.9	Formed only small particles of gel (1-2 mm).
50 hrs.	4.6	9.7	6.5	4.6	Clear yellow liquid when warm, became cloudy on cooling and separated out.
54.5hrs.	4.7	9.9	6.4	4.52	Clear yellow liquid when warm, became cloudy on cooling and separated out.

The variation of pH with time of reflux at 100°C is shown in figure 5.35

The decrease in pH with time of reflux is in agreement with that found by Hickson and Polson [24]. The

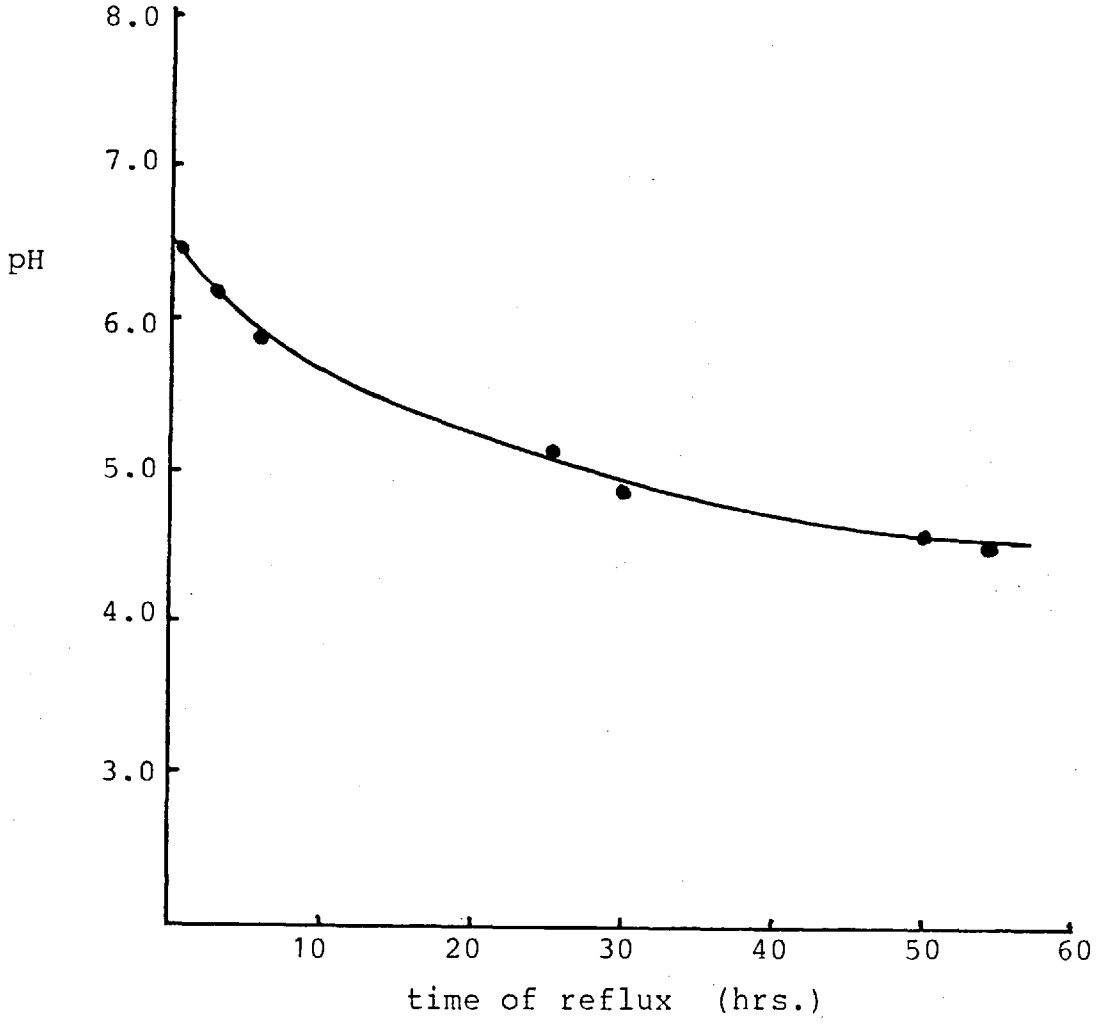


Figure 5.35 Variation of pH of an agarose solution with time of reflux at 100 °C.

results show that the preparation of samples (heating for fifteen - twenty minutes at 122°C) does not cause decomposition of the agarose molecule.

The Hydrolysate

It appeared that after reflux for more than ~20 hrs. the agarose was no longer capable of forming a rigid, three-dimensional gel. A 1wt.% solution of fresh agarose was prepared in a pH 4 buffer solution and when cold formed a rigid, turbid gel as normal. Thus the pH change upon refluxing was not responsible for the failure of the gel formation reaction.

The 54.5 hr. hydrolysate,when hot,was a clear pale yellow liquid. Upon cooling, however, a cloudiness developed which could be dispersed by heating. Obviously some elements of the hysteresis loop remained. The cold hydrolysate, when left to stand overnight, separated into a clear yellow supernatant liquid and a cloudy segregate.

A sample of the 54.5 hr. hydrolysate was then centrifuged at 20,000 r.p.m. for two hours. This produced a clear pale yellow supernatant liquid and a soft pale yellow gel segregate. Upon dehydration the segregate was found to contain ~50wt.% of water. The supernatant liquid when boiled to dryness produced a shiny yellow plastic film which was soluble in cold water. Obviously the agarose had been decomposed in some manner. In order to ascertain the type of decomposition an elemental analysis was carried out on:

1) the native agarose
2) the dehydrated segregate
3) the polymer film obtained from the supernatant liquid.

The results of the elemental analyses are presented in table 5.6. The hydrolysate was also examined in an optical microscope and results are presented in section 5.2d.

Table 5.6 Elemental Analysis

	Native agarose	Dehydrated segregate	Polymer film from supernatant	Calculated for pure agarose
% C	40.71	40.45	43.03	47.06
% H	5.83	4.88	5.93	5.88
% S	nil	nil	nil	nil
% N	nil	nil	nil	nil

5.2c Pyrolysis and Filtration

A sample from the main agarose batch (2091970) was pyrolysed in air at 475°C overnight. The product was a voluminous light brown powder constituting 0.44wt.% of the whole. The ash produced was investigated by optical and electron microscopy, the results of which appear in the next section. The ash was found to be insoluble in cold water.

Having ascertained the fraction of ash present in native agarose a 0.5wt.% gelling solution of agarose was prepared and filtered three times through a 0.2 μm. millipore filter. It was hoped that this procedure would remove

much of the ash content. However, pyrolysis of the filtrate showed virtually no decrease in ash content.

Photon correlation studies of the filtrate also gave wavevector dependences in agreement with unfiltered solution behaviour, (figures 5.63a,b) i.e. a K^3 dependence for a gelling agarose solution in the sol state (region I). Interpretation of the parameters Φ and r is not possible in this instance as filtration may well cause large changes in the actual solution concentration and hence solution viscosity.

5.2d Microscopy and X-ray Diffraction Studies

Optical Microscopy

A Carl Zeiss optical microscope was employed to investigate:

1) dried agarose films
2) dried films produced by the hydrolysed agarose
3) the ash obtained from the pyrolysis of agarose.

Agarose films were prepared by smearing agarose solutions onto a microscope slide and dehydrating in a desiccator cabinet for one - two days. The films were formed either from agarose solutions that had previously been heated to 122°C or from cold solutions. Figures 5.37a,b,c,d, show micrographs obtained from a hot smear of a 0.016wt.% agarose solution.

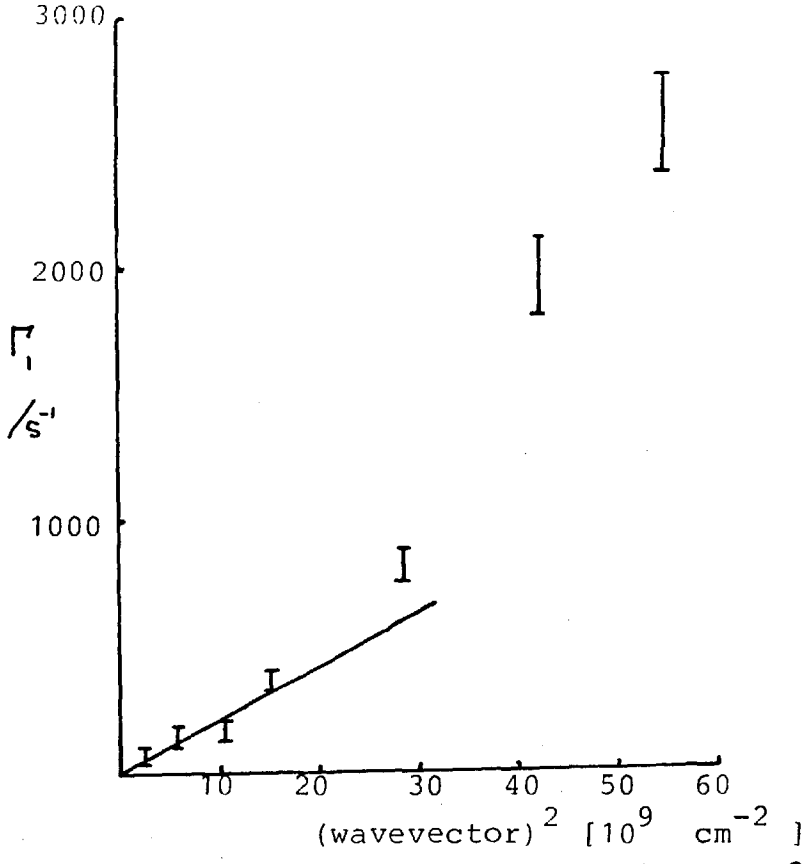


Figure 5.36 a First cumulant versus (wavevector)^2 for a filtered (0.2 μm) 0.5 wt% agarose solution at 52 °C.

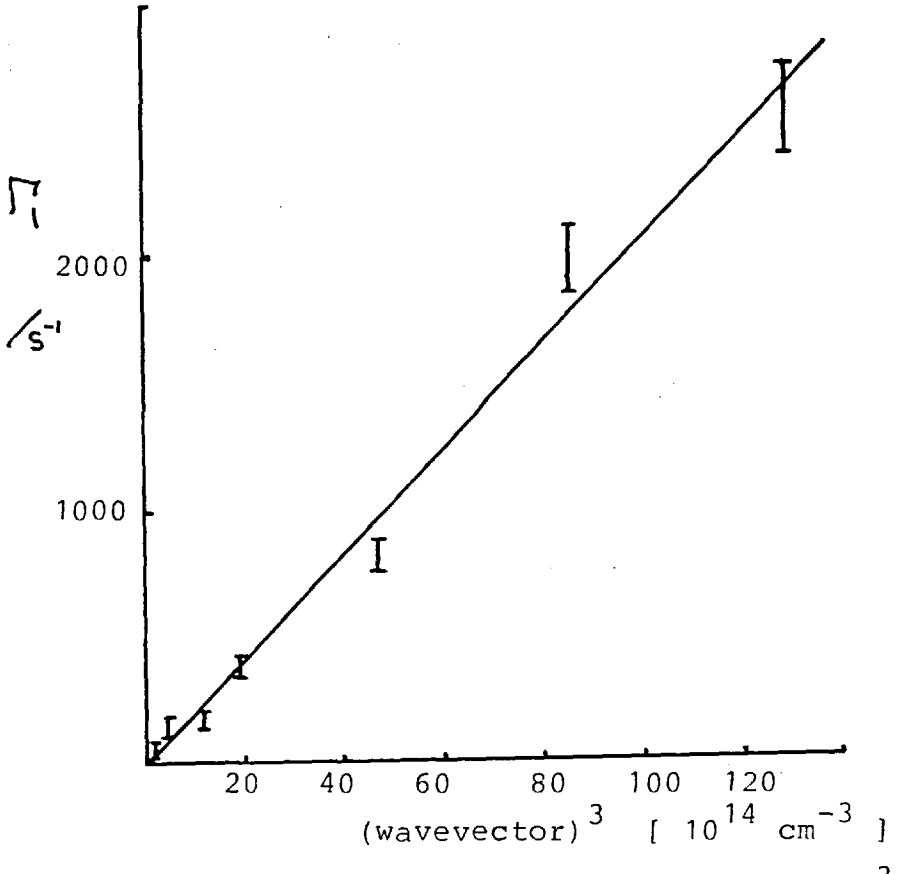


Figure 5.36 Above data plotted against (wavevector)^3.

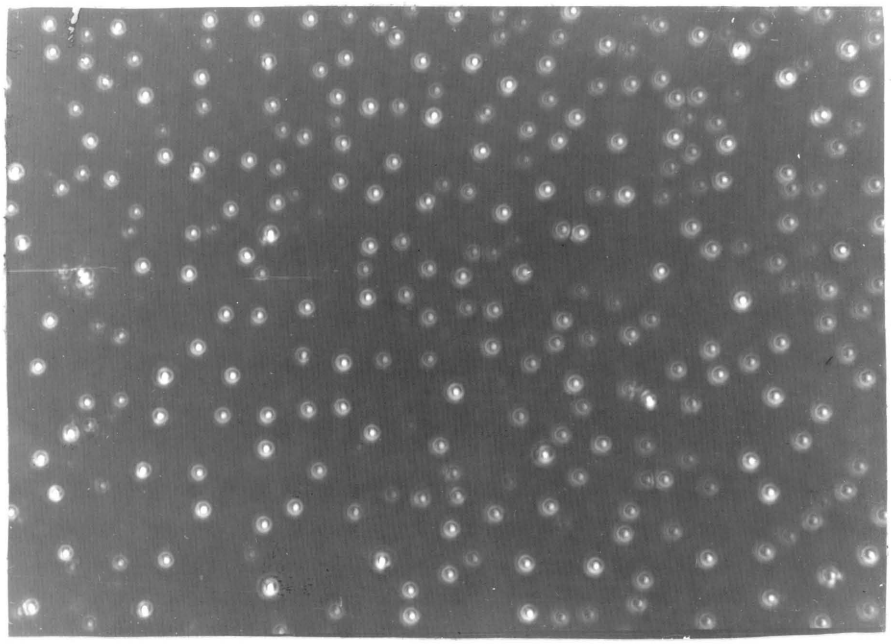


Figure 5.37a

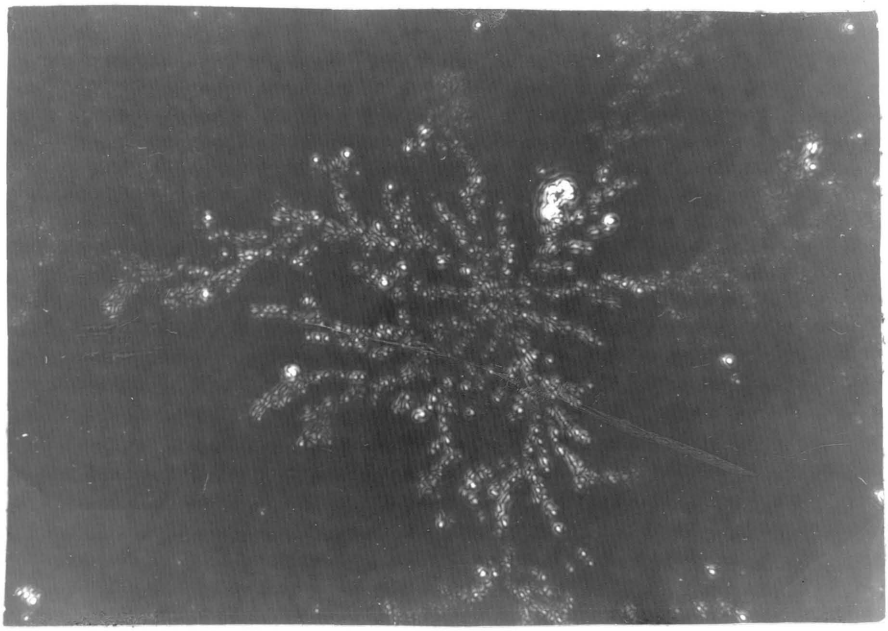


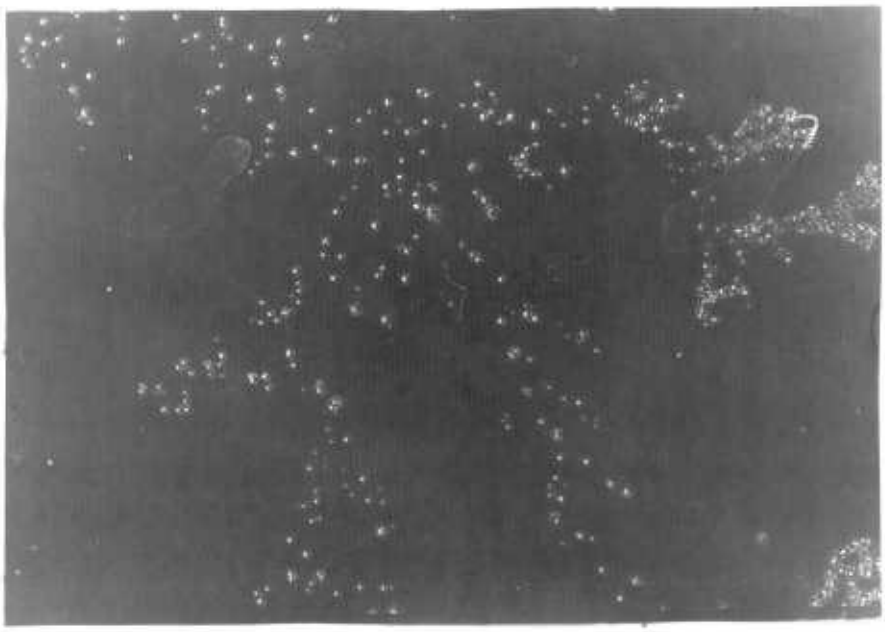
Figure 5.37b

Figure 5.37 Optical micrographs.

Figures 5.37a,b,c,d. The basic structure found in optical microscopy studies is shown in these photographs. The particulate matter observed is well represented in figure 5.37a, and typical dendrite formation is shown in figures 5.37b,c,d. All these photographs were obtained from hot smears of a 0.016wt.% agarose solution.

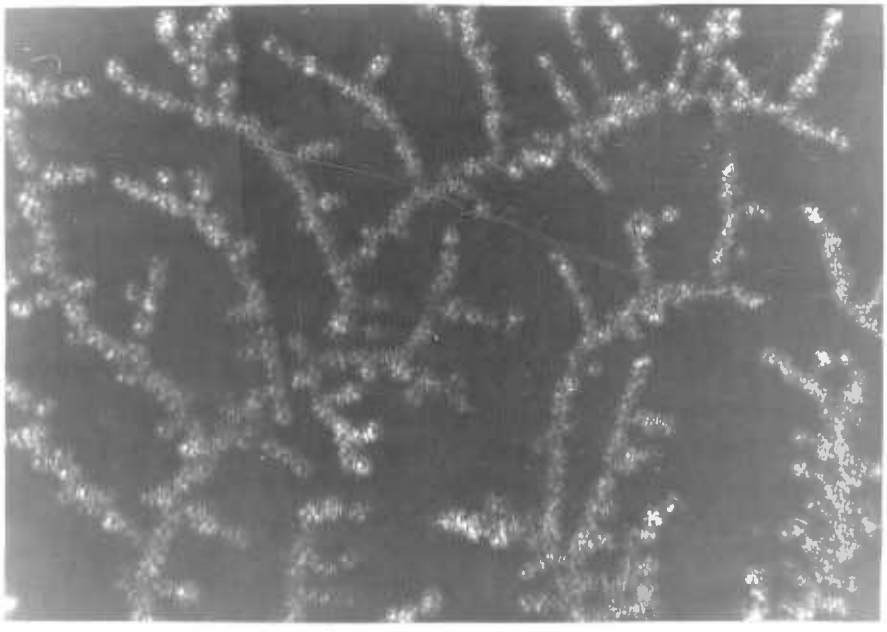
Scale for all optical micrographs (figures 5.37,38,39,40,41)

0.6 mm = 1.0 μm.



10 µm.

Figure 5.37c.



10 µm.

Figure 5.37d.

Similar structuring was also observed in cold smears of a 0.016wt.% agarose solution (figure 5.38) and a dehydrated film obtained from a 0.49wt.% agarose gel (figure 5.39). The hydrolysed sample (54.5 hrs.) also showed the same basic structuring (figure 5.40).

Optical microscopy of the ash content of the native agarose also revealed identical types of structure formation (figures 5.41a,b). It thus appears that this ash is responsible for the observed formations shown in all cases.

A study of agarose solutions revealed that no structuring or particulate matter could be observed within the resolving power of the microscope (0.4 μm.).

Electron Microscopy

Following the use of the optical microscope to give a qualitative examination of the agarose films, it was hoped that electron microscopy would provide more quantitative details, at higher magnifications.

Three facilities of the electron microscope were employed:

1) transmission electron microscopy
2) scanning electron microscopy
3) x-ray fluorescence for elemental analysis.

Because of electron beam damage to the specimen it was not possible to obtain transmission electron micrographs of agarose films. However, using the scanning facility it was possible to obtain pictures of the surface

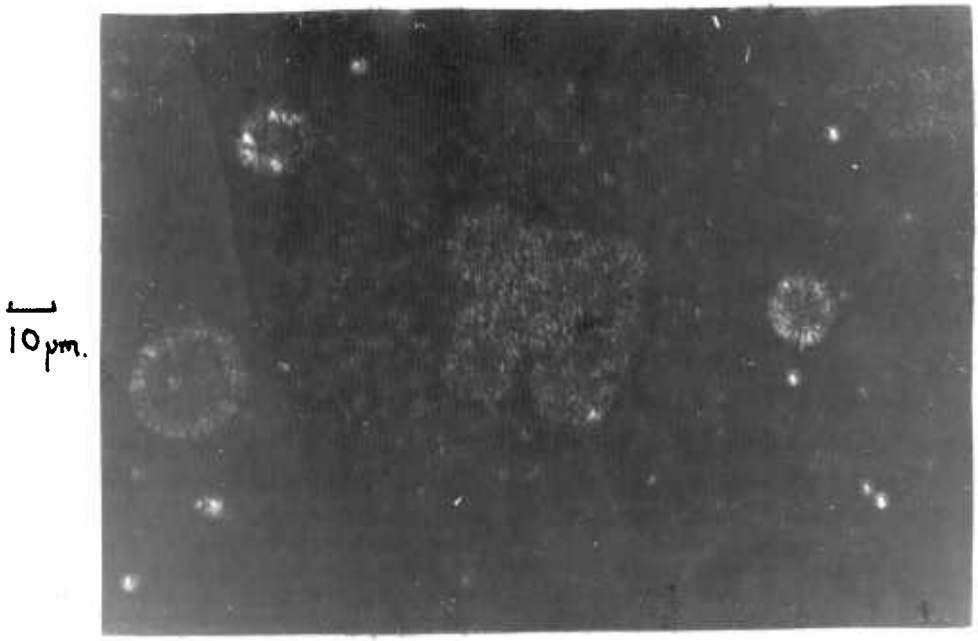


Figure 5.38. Optical micrograph from a cold smear of 0.016wt.% agarose solution showing particulate matter aggregated at the surface of bubbles.

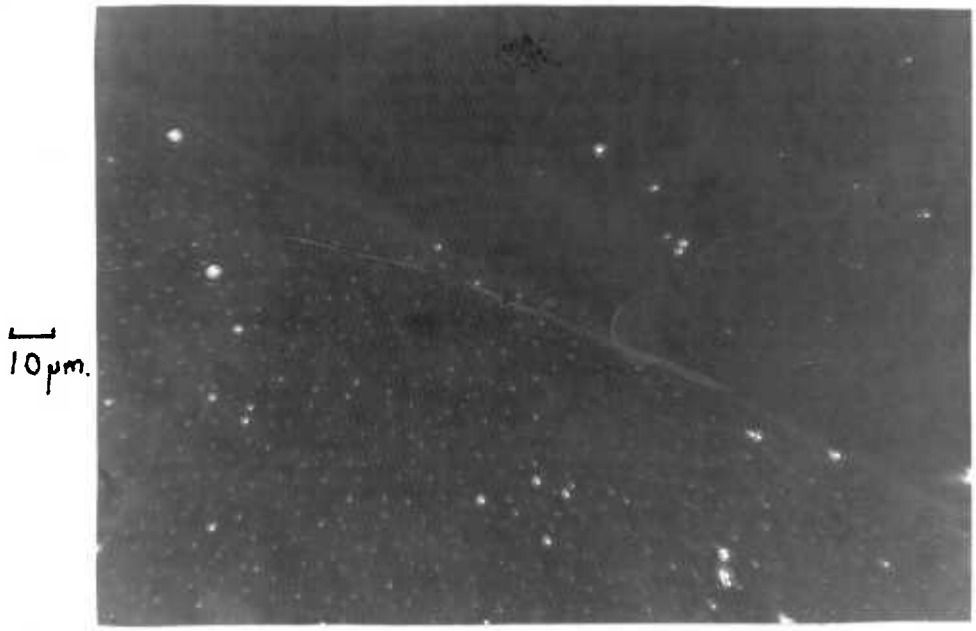


Figure 5.39. Optical micrograph obtained from a dehydrated agarose film (0.49wt.%) showing particulate matter identical to that observed whilst studying very dilute solutions.

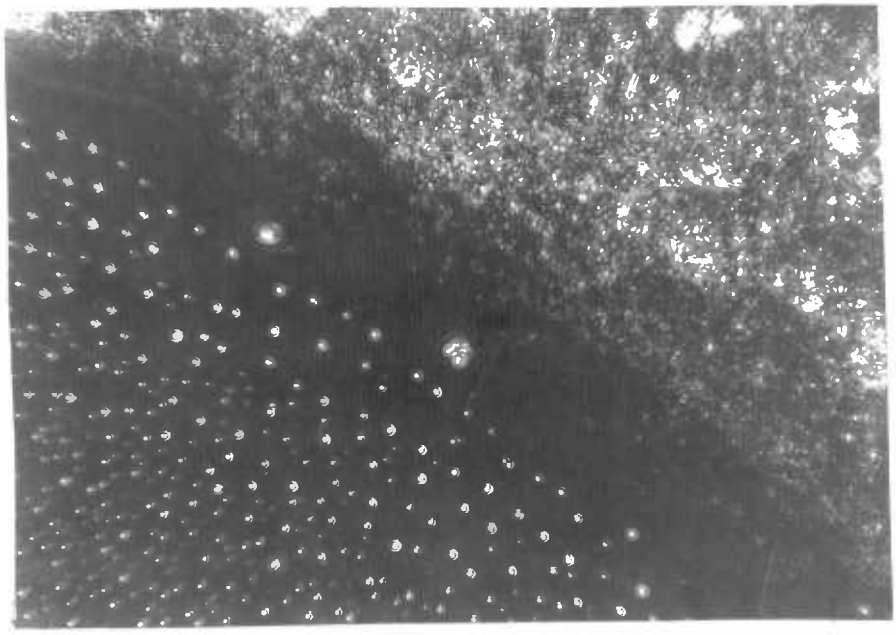


Figure 5.40 Optical micrograph obtained from a hydrolysed agarose solution (54.5 hrs.) showing a "gel" region (top right) and particulate matter.

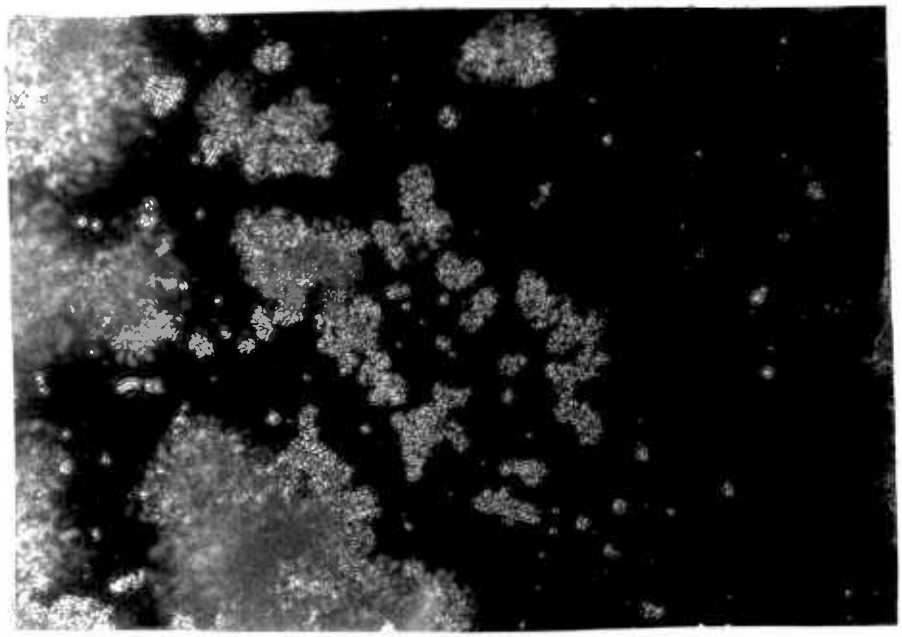


Figure 5.41a.

10 μm.

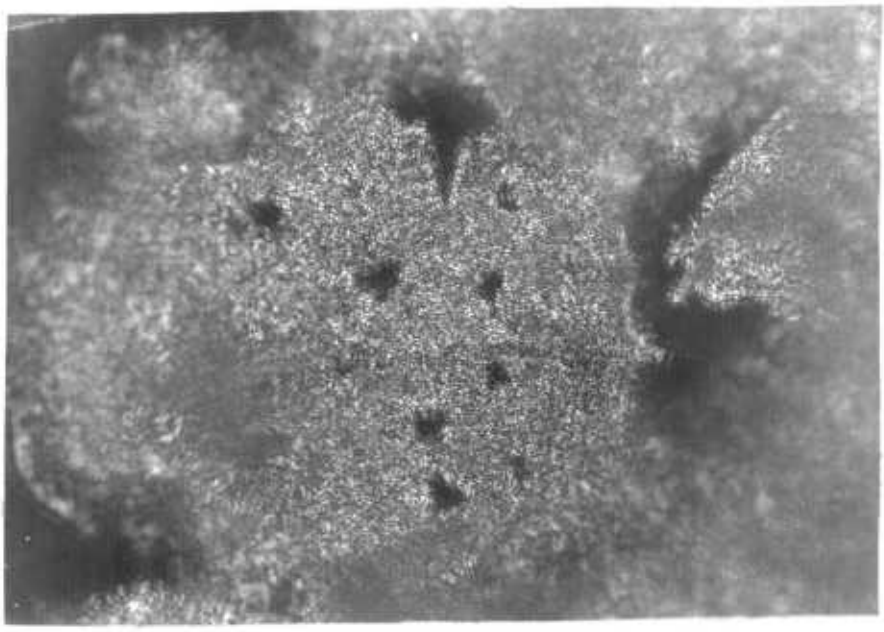


Figure 5.41b.

10 μm.

Figure 5.41a,b. Optical micrographs obtained from agarose ash.

topography (figures 5.42a,b). Damage to the specimen is also evident in these micrographs.

Analysis of the ash content of the native agarose proved to be much more successful when these techniques were applied. Figures 5.43a,b,c show transmission electron micrographs of the ash residue mounted on formvar-coated copper grids. These micrographs show the ash particles to be elliptical and rather monodisperse in nature with average particle dimensions of (0.08 × 0.13) μm.

An elemental analysis of the ash was performed using the X-ray analysis facility of the electron microscope. This analysis showed the ash to consist mainly of calcium and sulphur, but with varying, although much smaller, amounts of sodium, magnesium, aluminium, silicon and phosphorus (figure 5.44). In these analyses the copper peak comes from the copper mountings used and the iron peak is thought to come from an impurity in the "graphite dag" used to mount the specimens. Elements of atomic number less than 23(Na) cannot be detected by this technique.

Powder X-ray Diffraction

Agarose ash was mounted in a 0.3 mm. diameter glass capillary and the powder diffraction pattern obtained using a Phillips powder camera with Straumanis type film mounting. The sample was exposed to copper radiation (40kV;25mA) for 3 hrs..

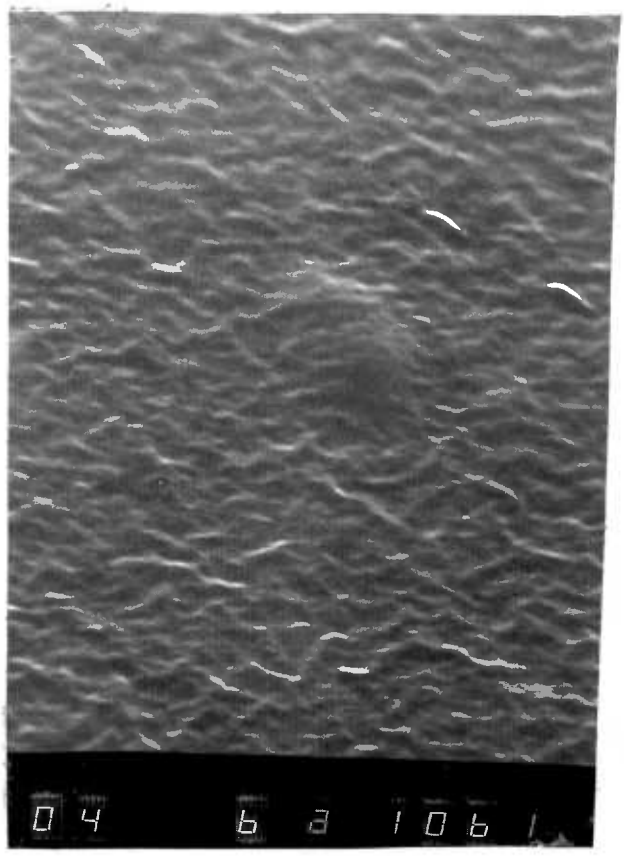


Figure 5.42a

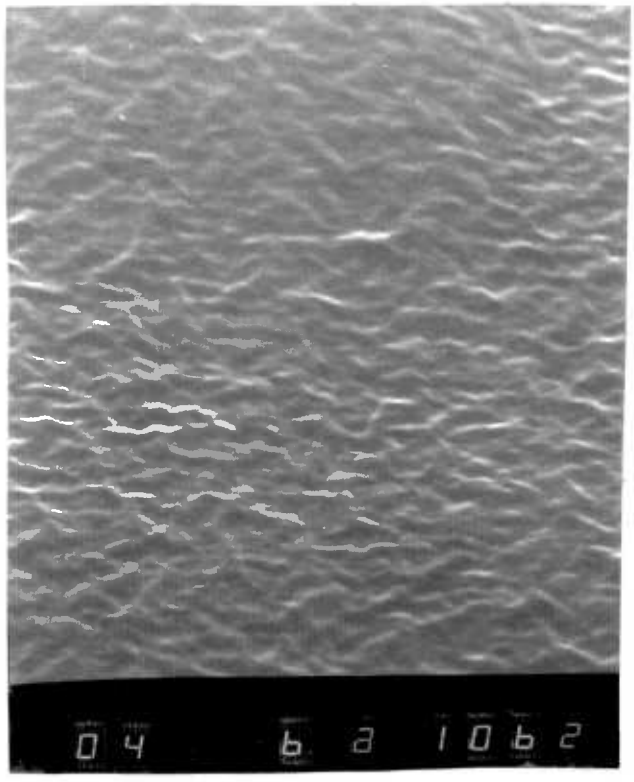


Figure 5.42b

Figures 5.42a,b. Scanning electron micrographs of a 0.49wt.% agarose film (dehydrated and sputtered with gold). The central blister in figure 5.42a is an indication of beam damage to the specimen. [Scale: 6.48 mm = 1.0 μm.]

Figure 5.43 Transmission electron micrographs of agarose ash.

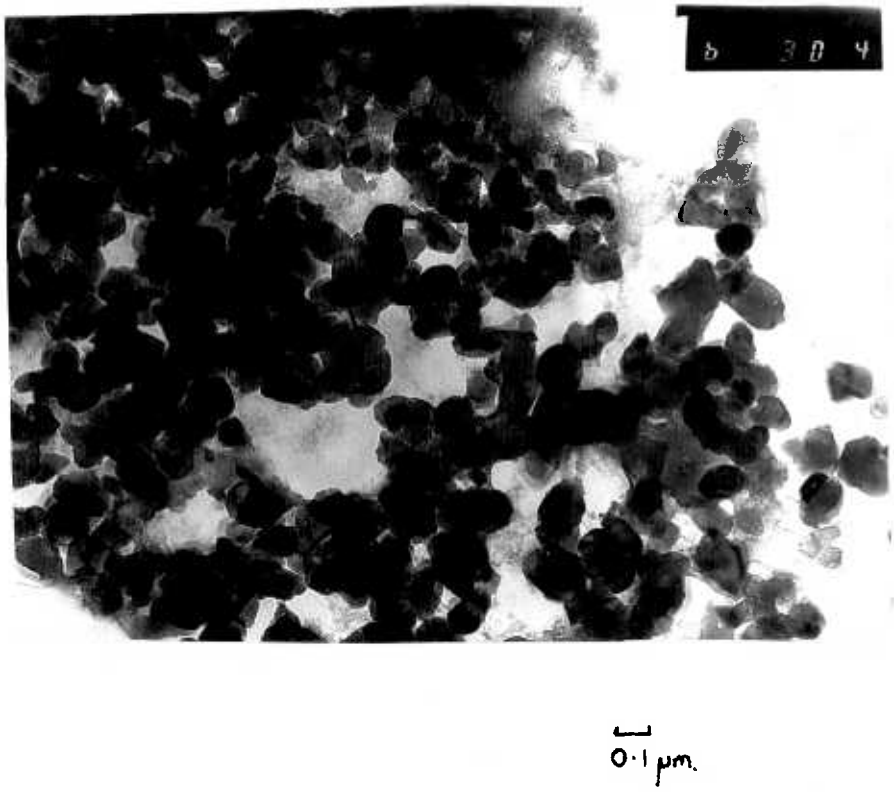


Figure 5.43a. Scale: 4.8 mm = 0.1 μm.

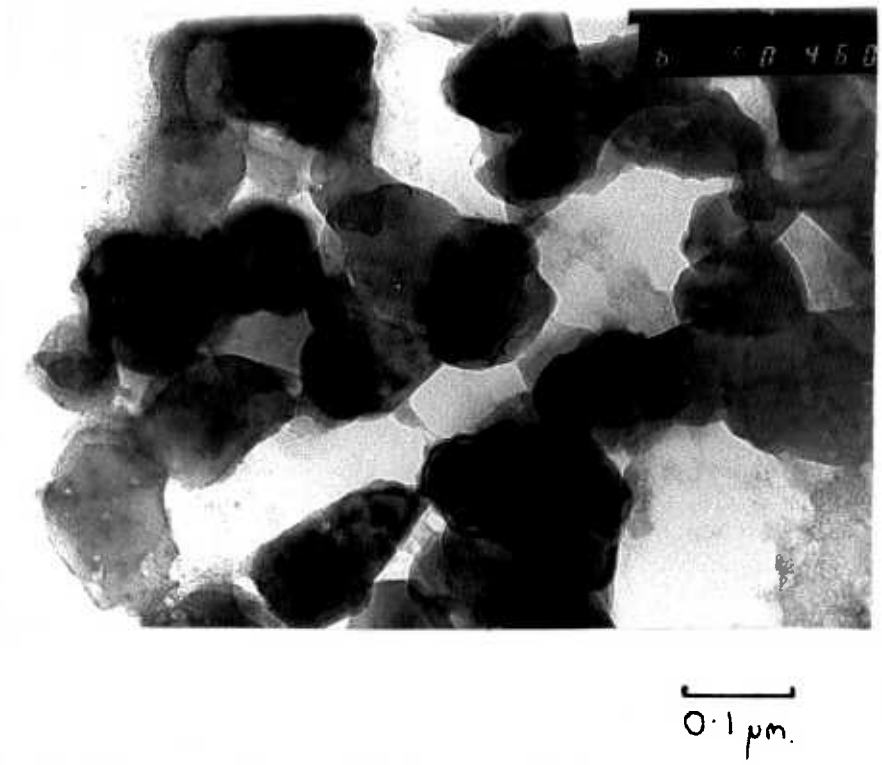


Figure 5.43b. Scale: 14.4 mm = 0.1 μm.

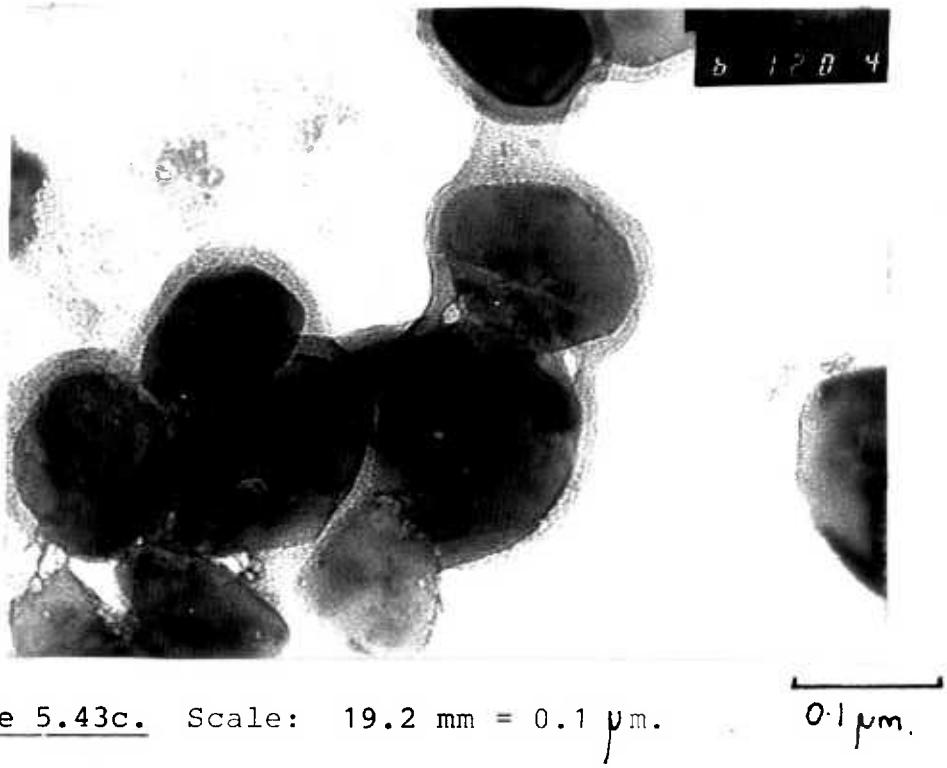
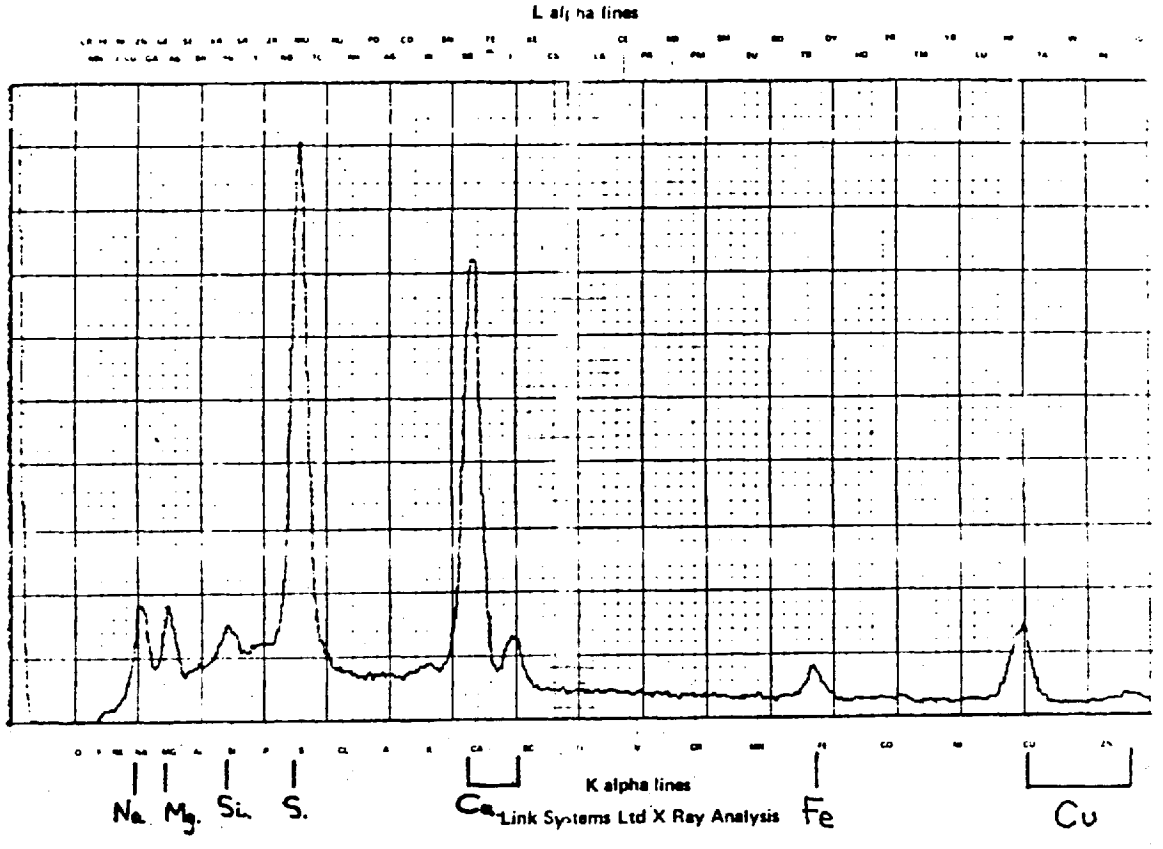


Figure 5.43c. Scale: 19.2 mm = 0.1 μm.

Laboratory ..... Researcher..... Date 20/2/80

Sample Agarose ASH

KeV 40 Seconds 100 Take off Angle 40°



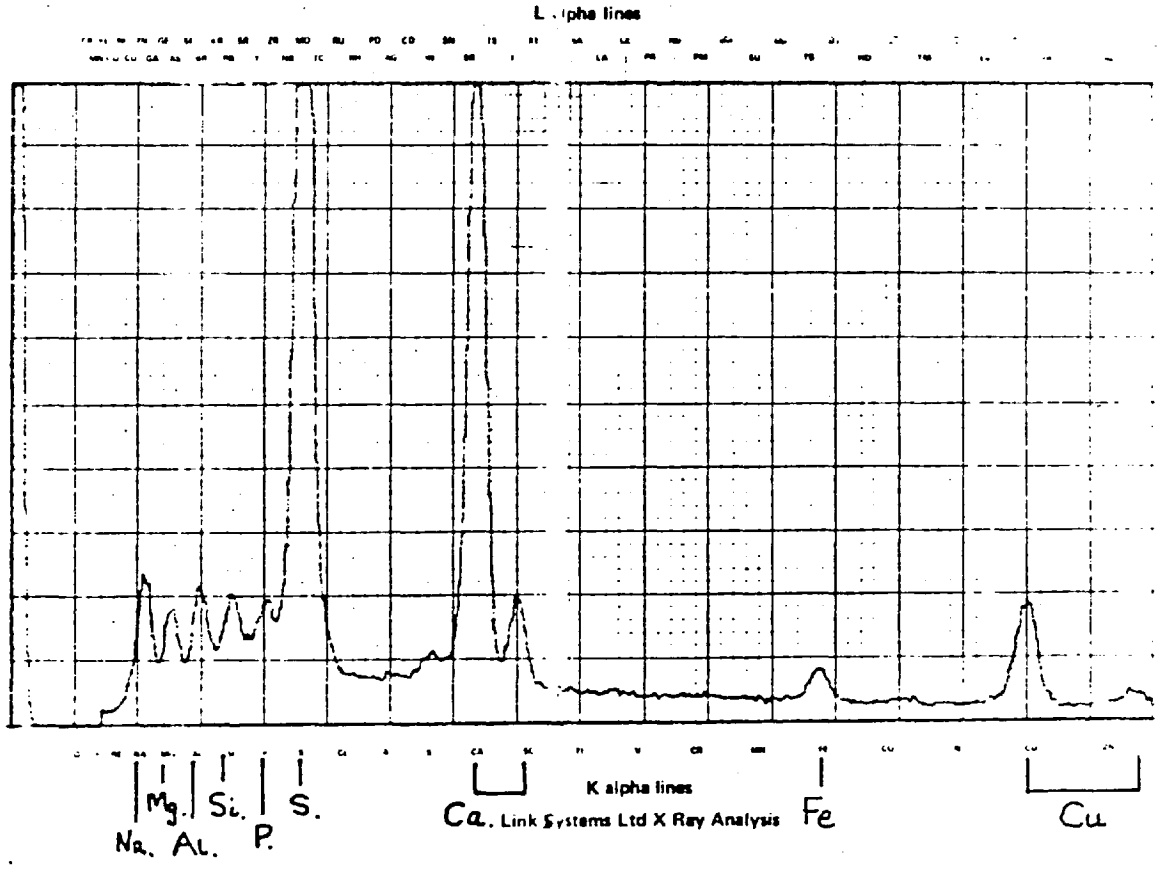


Figure 5.44 X-ray fluorescence studies of agarose ash.

No high angle reflections were observed and hence the nominal camera diameter (11.46 cm.) was used in order to calculate the scattering angles. Some sixteen reflections were easily visible and the d-spacings are shown in table 5.7.

Table 5.7 d-spacings from Powder X-ray Diffraction

Experimental results		
angle of reflection 2θ /°	d-spacing /Å	d-spacings for $CaSO_4$ anhydrite [80] /Å
2.28	3.90	3.87
2.47	3.61	nil
2.54	3.50	3.49
2.94	3.04	nil
3.13	2.85	2.85
3.36	2.67	nil
3.63	2.47	2.47
3.87	2.32	2.32
4.08	2.21	2.21
4.32	2.09	2.09
4.68	1.94	1.94
4.87	1.87	1.87
5.22	1.75	1.75
5.57	1.65	1.65
5.89	1.57	1.56
6.24	1.49	1.49

Of the sixteen observed reflections thirteen are in excellent agreement with the d-spacing of $CaSO_4$ anhydrite [80].

This finding is consistent with the X-ray fluorescence analyses which showed calcium and sulphur to be the main constituents of the ash. Impurities such as phosphorus and silicon may easily be incorporated in the ash since SiO_4^{4-}, PO_4^{3-},SO_4^{2-} are isomorphous [81]. The inclusion of such impurities would render the ash more insoluble. The three remaining d-spacings could not easily be identified with the impurities thought to be present.

5.2e Ion Interactions

Following the report of Hickson and Polson [24] that agarose would not form gels when dissolved in 2M potassium iodide, a study of the effects of addition of such ions was undertaken. It was found that no gelation or phase separation occurred for a 0.9wt.% agarose solution in 2M potassium iodide even when cooled to 3°C in an ice bath. However, when dialysed against distilled water to remove the ions, the normal rigid,turbid agarose gel was regenerated. Thus the potassium iodide was acting as a "gel inhibitor" and did not affect the structure of the agarose units.

The effects on gelation of a number of ionic compounds were briefly studied:

$KI;KI_3$

KNCS

NaCl

NaN_3

CsI

It was found that, at about 2M concentration, all these compounds except NaCl inhibited gelation; in each case the normal gel could be regenerated by dialysis. Since NaCl did not prevent gelation an ionic strength argument is clearly inappropriate and more detailed experiments were carried out.

Swelling of Dried Films and Fibres.

Dried agarose films were swelled in distilled water, KI solution and KNCS solution. The ionic solutions produced much greater swelling of the films (~3.5× for 2M KI) and it was noted that in the ionic solutions the swollen gels were far less turbid. Also with sufficiently concentrated ionic solutions it was possible to disperse preformed gels completely.

An extruded fibre of agarose was placed in KI solution and a crystal of iodine added. The fibre quickly took up the yellow/brown discoloration indicating selective adsorption of the I_3^- ion in the gel network.

Critical Concentration of Ions and Centrifugation

A 1.0wt.% agarose gel was made up in varying concentrations of potassium thiocyanate solution. Upon cooling the gels formed were carefully observed. The results are shown in table 5.8.

Table 5.8 Critical Concentration of KNCS

concentration of KNCS /M	0.244	0.495	0.828	1.014	2.13
remarks	gelled (turbid)	gelled (turbid)	gelled (clear)	small gel particles	non-gelling

Thus there is a critical concentration of KNCS required to prevent gelation.

A 2.54wt.% solution of agarose in 2M KNCS was centrifuged for five hours at 23,000 r.p.m.. No signs of segregation could be observed. Similar results were found with KI solutions. This is in marked contrast to the observed sedimentation of agarose gels in pure water; which leads to a segregate of overall concentration ~7wt.%.

Photon Correlation Measurements

Measurements of the diffusion coefficient of the agarose particles in KI and KNCS solutions were made using the photon correlation apparatus. Typical plots of the first cumulant versus $(\text{wavevector})^2$ are shown in figures 5.45,5.46. Unlike the corresponding aqueous solutions these plots show a linear dependence symptomatic of Brownian motion. The diffusion coefficient was investigated at 54°C for several agarose concentrations in the range 0.1-1.5wt.% in both 2M KI and 2M KNCS. The variation of the diffusion coefficient with agarose concentration is shown in figure 5.47.

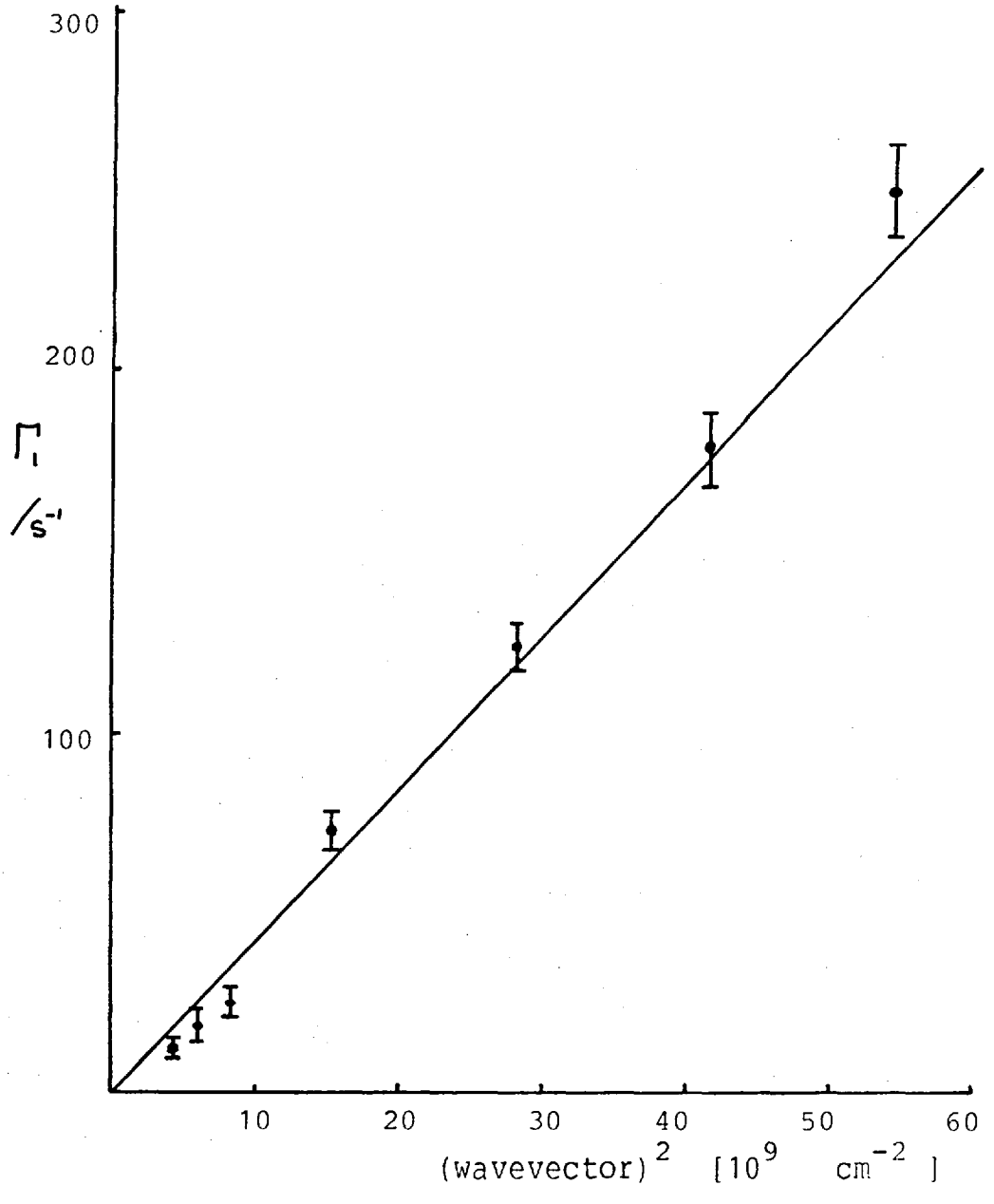


Figure 5.45 First cumulant versus (wavevector)^2 for a 1.04 wt% agarose solution in 2M potassium thiocyanate at 54 °C.

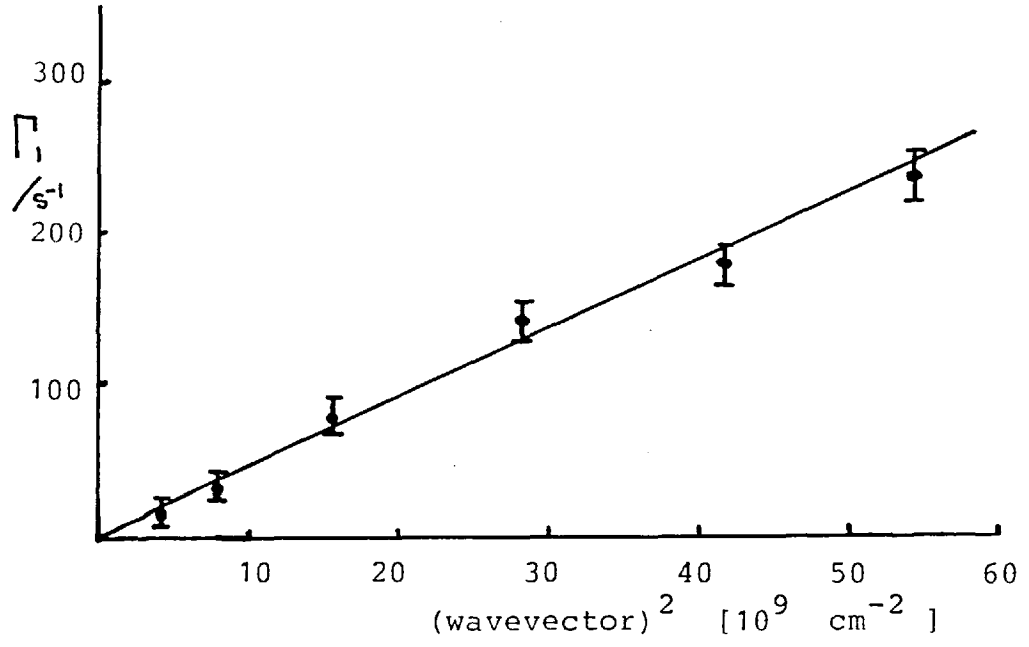


Figure 5.46 First cumulant versus (wavevector)^2 for a 1.00 wt% agarose solution in 2M potassium iodide at 54 °C.

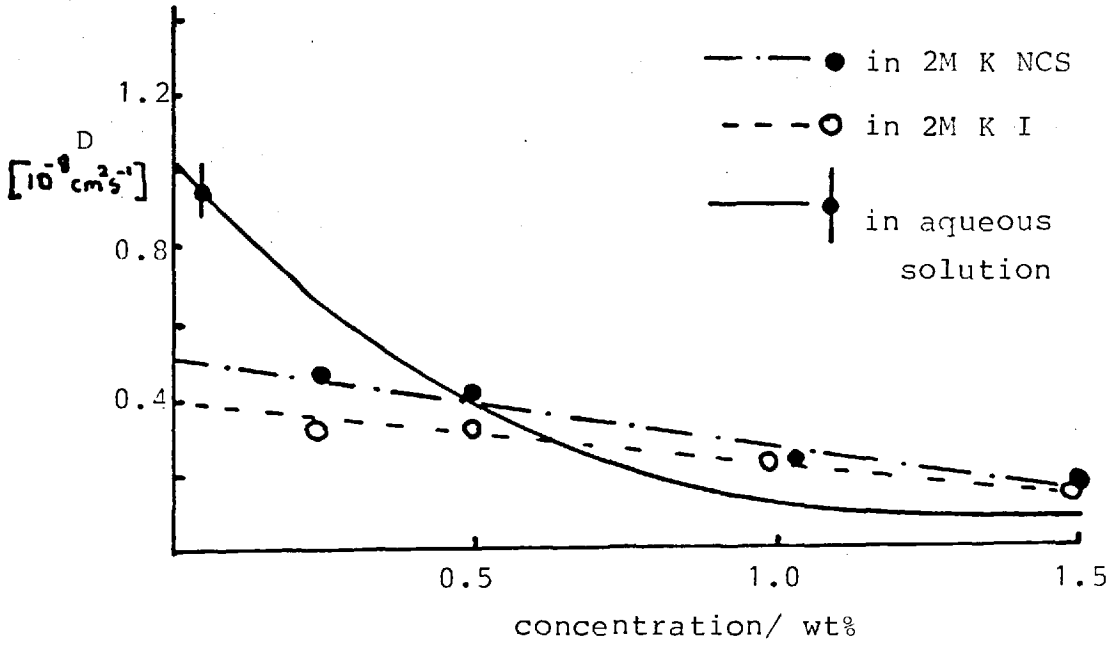


Figure 5.47 Concentration dependence of the effective diffusion coefficient in ionic solutions at 54 °C.

Figure 5.48 shows the temperature dependence of the intensity of scattered light for a 0.5wt.% agarose solution in 2M potassium thiocyanate. As can be seen there is no evidence of hysteresis occurring in this system between 20-100°C or of any gelation process whatsoever.

Further measurements on potassium iodide solutions by both light scattering and optical rotation similarly showed no evidence of a hysteresis cycle.

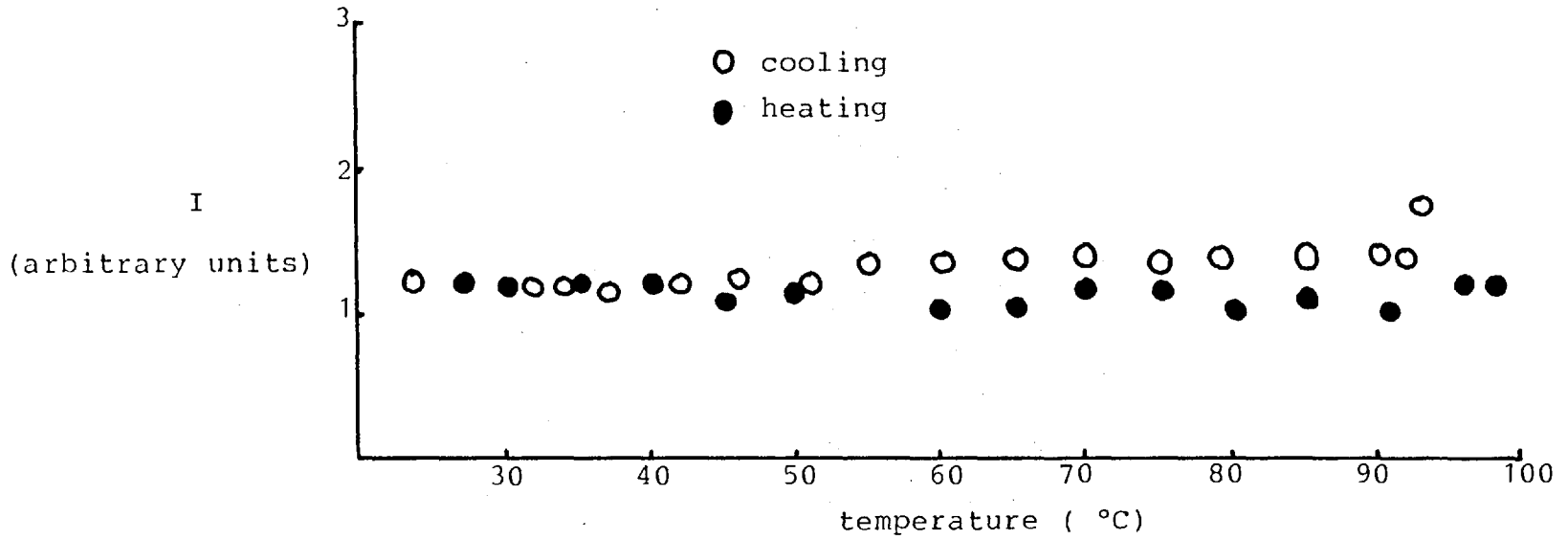


Figure 5.48 Scattered intensity versus temperature for a 0.5 wt% agarose solution in 2M potassium thiocyanate.

CHAPTER 6

Discussion and Interpretation

6.1 The Hysteresis Cycle

The existence of hysteresis phenomena in the agarose/water system has been confirmed by measurements of the scattered intensity and optical rotation as a function of temperature. A typical hysteresis loop is shown schematically in figure 6.1.

We may define four regions of special interest:

1) Region (I). This region pertains to the fluid, non-turbid solution as it is cooled from 100→40 °C, and is termed the "sol state". It is characterised by a constant and reproducible value of the parameter under study and exhibits complete reversibility when temperature cycled (100↔40 °C).

2) A sharp increase in the turbidity of the sample accompanied by a reproducible change in optical rotation is observed at some concentration-dependent temperature, T^* (region (II). This corresponds to the onset of gelation as indicated by the development of elastic properties.

3) A gradual decrease in turbidity as the fully formed gel (region III) is heated from, say, 20→90 °C (region IV). The decrease in turbidity is accompanied by a similar variation in optical rotation towards the sol state value.

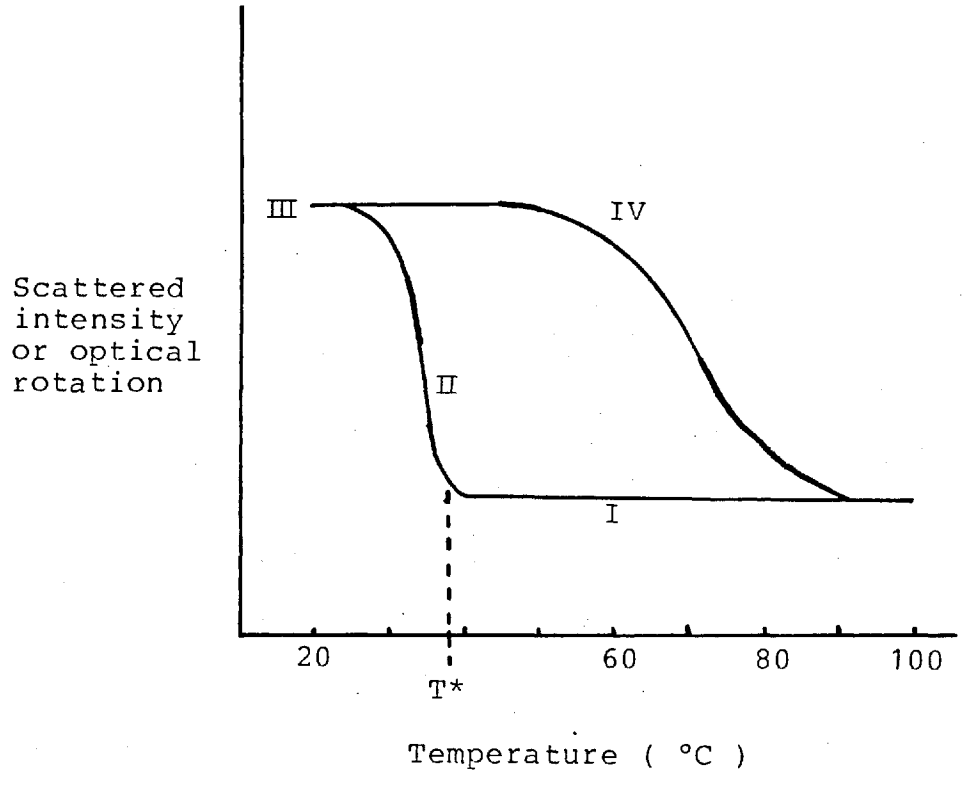


Figure 6.1 Schematic representation of the hysteresis cycle

Turbidity measurements have shown region IV (the dispersing gel) to be thermally irreversible when temperature cycled. The parameters in this region do not exhibit the high degree of reproducibility found in region I.

4) As the system is heated to 90-95 °C, the parameter (turbidity or optical rotation) re-establishes a value characteristic of the "sol state" when complete dispersion of the gel has been effected and the system regains its fluidity.

The existence of such a hysteresis cycle has been shown for both gelling and non-gelling solutions; thus it arises, not solely as a consequence of three-dimensional gel formation , but because of a change in some intrinsic property of the system.

Hysteresis is also evident from the variation of the effective hydrodynamic radius of the agarose units in non-gelling solutions as determined by photon correlation spectroscopy. This is shown in figure 6.2 together with values of the effective hydrodynamic radii for gelling agarose solutions as determined from the asymptotic behaviour of the first cumulant as wavevector, $K \rightarrow 0$.

Two major conclusions may be drawn from these data:

1) In non-gelling solutions the dramatic increase in turbidity is accompanied by a two-fold increase in the effective hydrodynamic radius.

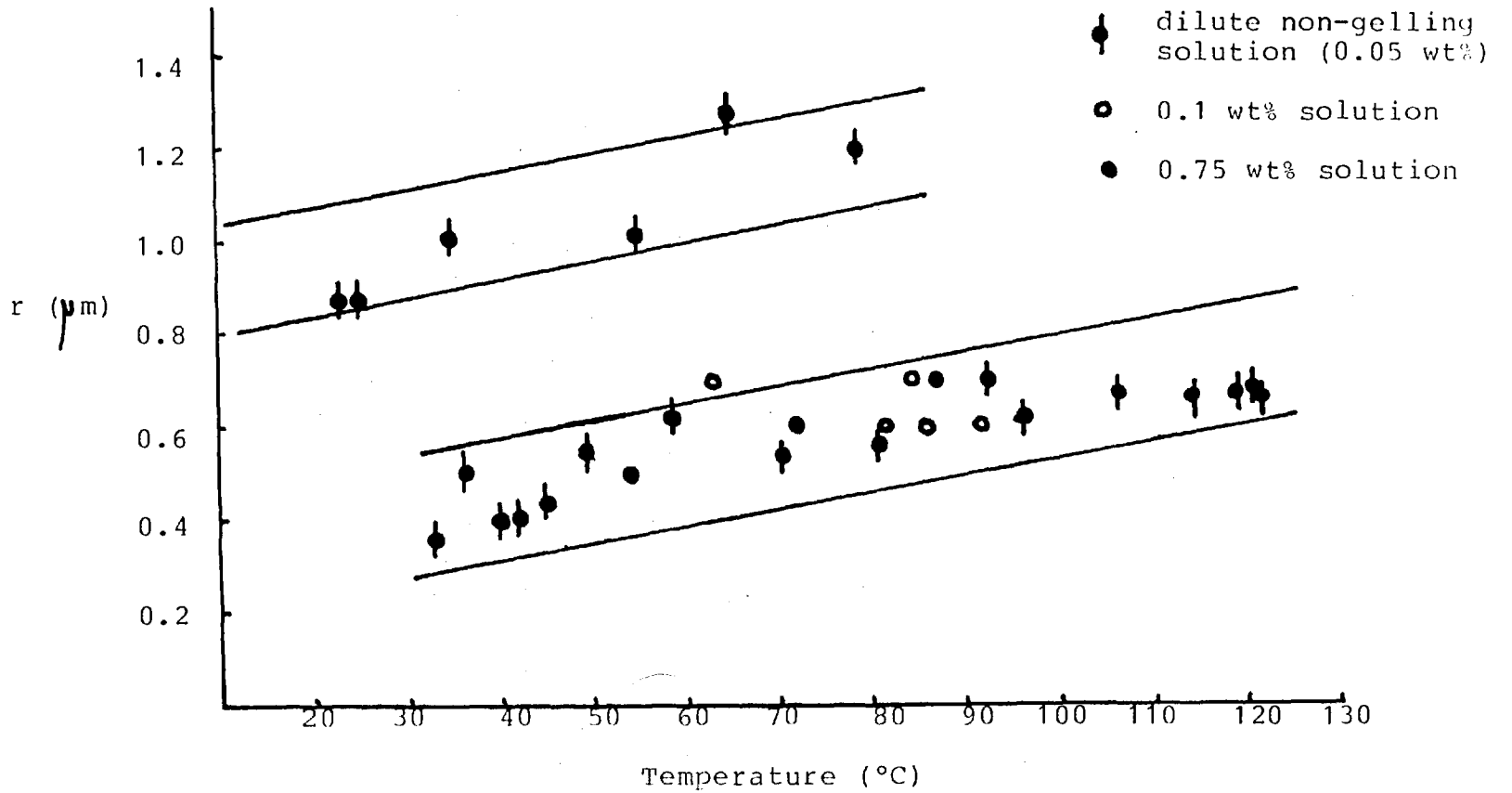


Figure 6.2 Variation of effective hydrodynamic radius (r) with temperature

Thus , although gelation does not occur in these dilute solutions, there is aggregation of the agarose units into larger domains.

2) The excellent agreement shown in values of the effective hydrodynamic radius for gelling and non-gelling solutions suggests that a common agarose unit is involved irrespective of whether gelation or aggregation occurs as the solution is cooled below T*.

Thus the concentration-dependent temperature, T*, may be identified as an aggregation temperature for the agarose system; noting that for concentrations $>\sim 0.1$ wt% there are sufficient agarose units to provide a connected three-dimensional aggregate structure throughout the solution. This finding is also supported by observations of very dilute non-gelling agarose solutions (~ 0.02 wt%) which, when left to stand for several months, were found to form a ring of turbid gel at the bottom of the vessel.

The hysteresis cycle for agarose is thus based upon what is essentially a two state system; viz:

1) The sol state - which will be defined as the fluid state of low turbidity existing in the temperature range 40-100 °C providing that the sample has not been allowed to cool below this lower limit during the period of observation.

2) The aggregated state - which exists in the temperature range 20-90 °C and is characterised by high turbidity, but which may be fluid or an elastic solid (gel) depending on concentration.

These two states are well defined by parameters obtained from photon correlation experiments. For dilute, non-gelling agarose solutions the wavevector dependence of the initial slope of the autocorrelation function provides a suitable characterisation. In the sol state a (wavevector)^2 dependence is observed, whilst in the aggregated state a (wavevector)^3 dependence is found. Similarly, for gelling agarose solutions different functional behaviour of the autocorrelation function is found depending on the state of the system:

1) In the sol state an exponential autocorrelation function is obtained; the initial slope of which is found to have a (wavevector)^3 dependence.

2) In the gel state exponential autocorrelation functions could not be obtained; only cosusoidal oscillatory functions were observed. Analysis of these functions showed them to be in excellent agreement with the predictions and observations of Nossal.

The various wavevector dependences observed provide a valuable insight, and will be discussed in the following sections.

6.1a (Wavevector)^2 Dependence

This behaviour is symptomatic of simple Brownian diffusion of the scattering species and was analysed accordingly; i.e.

$g^{(1)}(K,t) \propto \exp\ [-K^2 D_T t]$

where D_T is the translational diffusion coefficient.

The applicability of the above equation depends upon the relative magnitude of the experimental wavevector,K, and the effective radius,r, of the scattering species as discussed in section 3.4c . In order to monitor an overall translational motion, the experimental wavevector must probe distances greater than the radius of the scattering species. Thus the above equation is only valid provided that the product Kr is less than unity. When the magnitude of the wavevector is such that shorter distances are probed (i.e. Kr>1) internal motions within the scattering species, where they exist, will be able to contribute to the scattered spectrum and thus destroy the simple (wavevector)^2 dependence.

Considering typical experimental values for these parameters for dilute non-gelling agarose solutions in the sol state we obtain:

$r \sim 0.5 \times 10^{-4}$ cm; $K\ (90°) \sim 1.9 \times 10^{5}$ cm^{-1}

Hence $Kr \sim 9$

Since the product Kr is greater than unity, internal motions ought to contribute to the scattered spectrum, when a simple (wavevector)^2 dependence should not be observed. The experimental data thus seem to be in conflict with the basic principles of light scattering. This paradox may be solved by considering the following approach:

When studying polymer motions using scattering techniques it is generally assumed that the optical radius and

hydrodynamic radius both derive from the segmental distribution in the same manner and are thus equal. However, this need not be the case if the scattering unit consists of two species of different refractive index. For such a system the species of higher refractive index will contribute more per unit volume to the scattered spectrum and thus, save in the special case that the high refractive index component forms the outermost layer of the scattering particle, the hydrodynamic radius will be greater than the optical radius.

In order for the experimental data to be made consistent with this model approach, the optical radius must have a value $\sim 0.05\ \mu m$ or less. This implies that for the above data to be interpreted in a rational manner a "hard-core" within the particle must be responsible for the scattering phenomena over the relevant wavevector range, when a more diffuse sheath which scatters light more weakly will dominate the rheological properties (figure 6.3).

This structure for the agarose unit has been proposed solely from a consideration of photon correlation studies of non-gelling agarose solutions. It is conditioned by arguments on the value of the product Kr, and depends not at all on chemical analyses or microscopy, which can therefore be used to confirm or disprove this hypothesis. A major part of this work has been concerned with the verification or otherwise of this proposed structure and the rationalisation of the gelation process in the light of new experimental data.

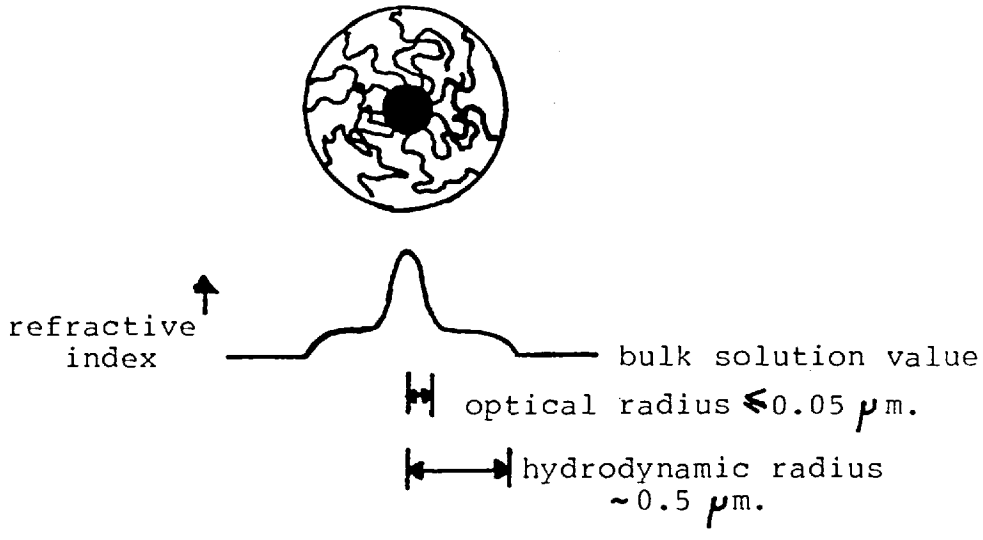


Figure 6.3 Postulated "hard-core" particle

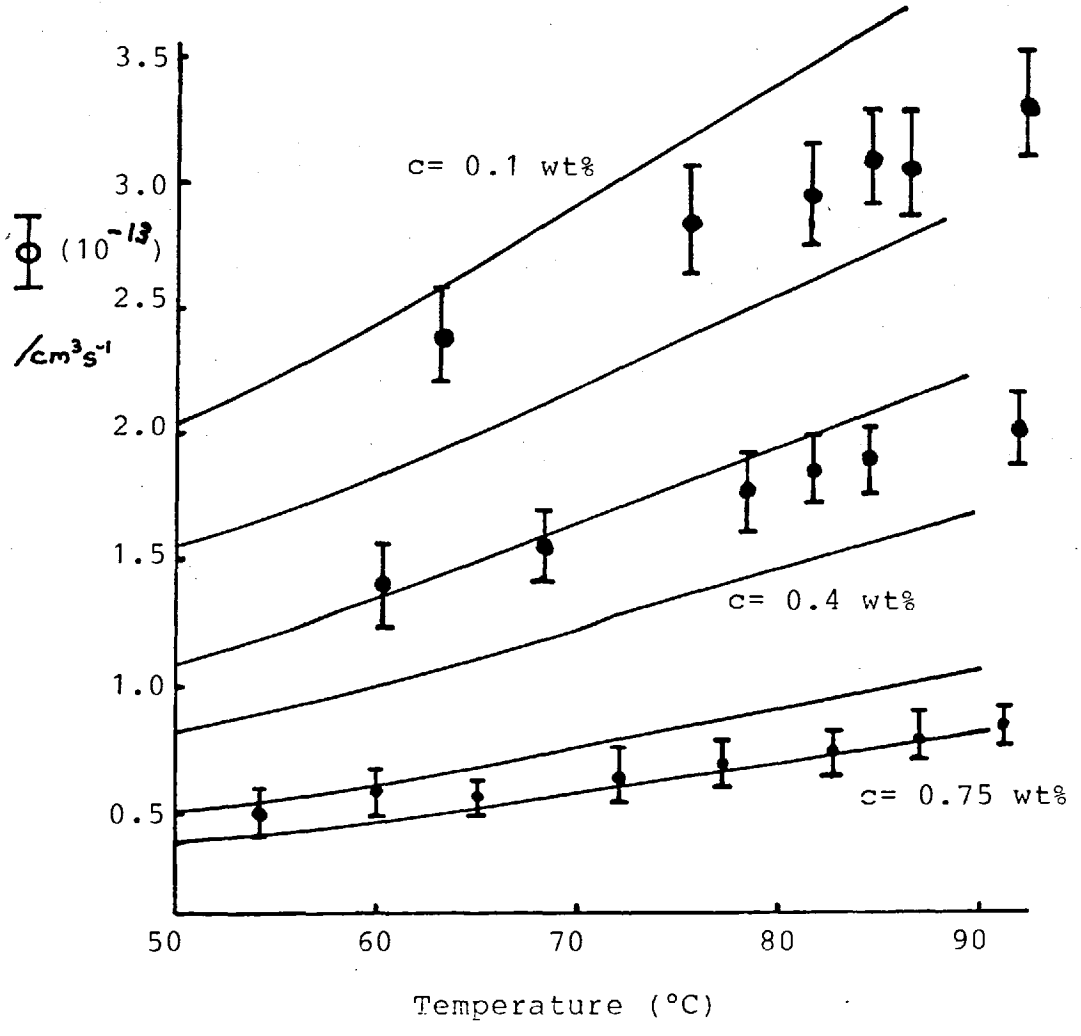


Figure 6.4 Variation of parameter Φ with temperature for various agarose solutions. [full line shows the function $(3.5 \pm 0.5) \times 10^{-18}\ T/\eta_{SOLN.}$]

6.1b (Wavevector)^3 Dependence

A (wavevector)^3 dependence of the initial slope of the autocorrelation function was observed both for non-gelling solutions in the aggregated state and gelling solutions in the sol state. From the dramatic appearance of the (wavevector)^3 dependence in non-gelling solutions as aggregation occurs it is reasonable to conclude that the origin of such a dependence lies quite generally in the virial and hydrodynamic interactions between agarose units. Similarly the proximity of agarose units as the concentration increases will favour interparticle interactions and thus a similar dependence would be expected in the sol state at gelling concentrations (region I).

Thus for gelling agarose solutions we find:

$$\Gamma_1 = \Phi K^3$$

where the constant Φ must have dimensions $[L]^3\ [T]^{-1}$ since for Brownian diffusion $\Gamma_1 = -2\ K^2\ D$ and

$$D = \frac{k_B T}{6\pi \eta_o r_o} \quad ; \quad [L]^2\ [T]^{-1}$$

Thus $\Phi\ (\ [L]^3\ [T]^{-1}\ ) \cong \frac{k_B T}{\eta^*}$

Experimentally Φ is found to be concentration-dependent. It then follows that in this dimensional argument η^* must also be concentration dependent and cannot simply be identified with the solvent viscosity, η_o.

The function CT/η_{SOLN} (where C is a constant) has been evaluated from solution viscosity measurements and compared with the experimentally determined Φ (figure 6.4). The excellent agreement obtained by such a comparison suggests

an empirical relationship of the form:

$$\Phi = 3.5\times10^{-18} \frac{T}{\eta_{SOLN}}$$

and thus

$$\Gamma' = 3.5\times10^{-18} \frac{T}{\eta_{SOLN}} K^3$$

The origins and meaning of this empirical relationship will be discussed in greater detail in section 6.3.

6.1c Viscosity

The relative viscosity of a suspension of spherical particles is usually quoted in terms of a power series in volume fraction:

$$\eta_{REL} = \frac{\eta_{SOLN}}{\eta_0} = 1 + k_1\Phi + k_2\Phi^2 + \ldots\ldots\ldots$$

where k_1 is taken to have a value of 2.5 so that the above relationship reduces to the Einstein equation as the volume fraction approaches zero. The coefficient k_2 is the two-body interaction coefficient calculated for collision doublets.

There are many theoretical treatments of the effect of increasing volume fraction on the relative viscosity of a suspension, and several excellent review articles are available [82,83,84]. The analysis and interpretation of viscosity data is hindered by the large variation in the parameters k_1 and k_2 produced by non-ideal suspensions. The Einstein coefficient, although defined as 2.5 for a system of monodisperse spheres is found experimentally to be in the range 1.9-4.0. Theoretically, the parameter k_2 has been found to have values in the range 5.1-14.1.

From the various theories available we have considered

two derivations which show close agreement. The approaches considered are due to Kynch [85], who solved the equations of motion for a concentrated suspension, and Vand [86] who considered the coefficient k_2 as arising from the formation of collision doublets. Vand's treatment has been further extended by Roscoe [87] , who considered the effect of polydispersity. As can be seen (figure 6.5) these two approaches show excellent agreement in the magnitude of the relative viscosity for a given volume fraction.

The experimental data were compared with these two approaches and a relationship between volume fraction and concentration derived (figure 6.6). Thus for $\phi \lesssim 0.2$

$$\phi = 0.50\ c$$

where c is wt% agarose.

The deviations at higher concentrations may stem from entanglement effects since we are actually dealing with a polymer solution rather than a suspension of hard spheres. The temperature variation of ϕ for a given concentration may also be explained in terms of entanglement effects since it has been shown in this work that the effective hydrodynamic radius of the particles increases with temperature.

6.2 The Agarose Unit

Using the foregoing derived data we are now in a position to discuss the structure of the agarose units. The main points of information arising from the experimental data are as follows:

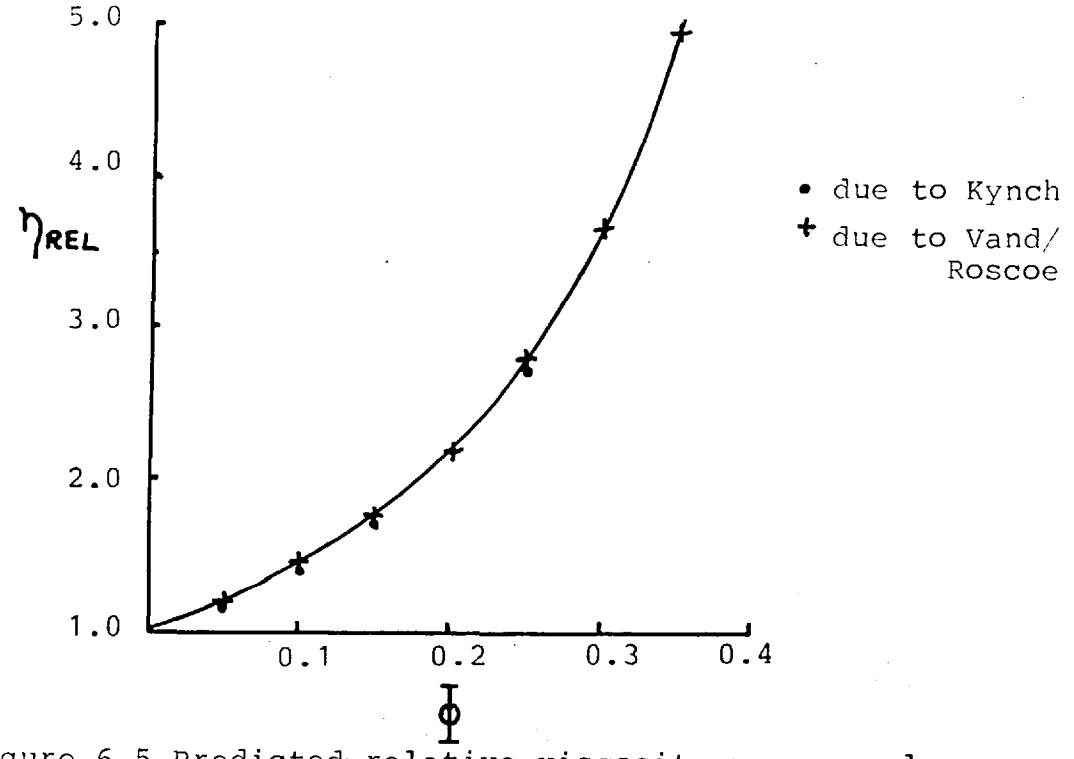


Figure 6.5 Predicted relative viscosity versus volume fraction for moderately concentrated solutions

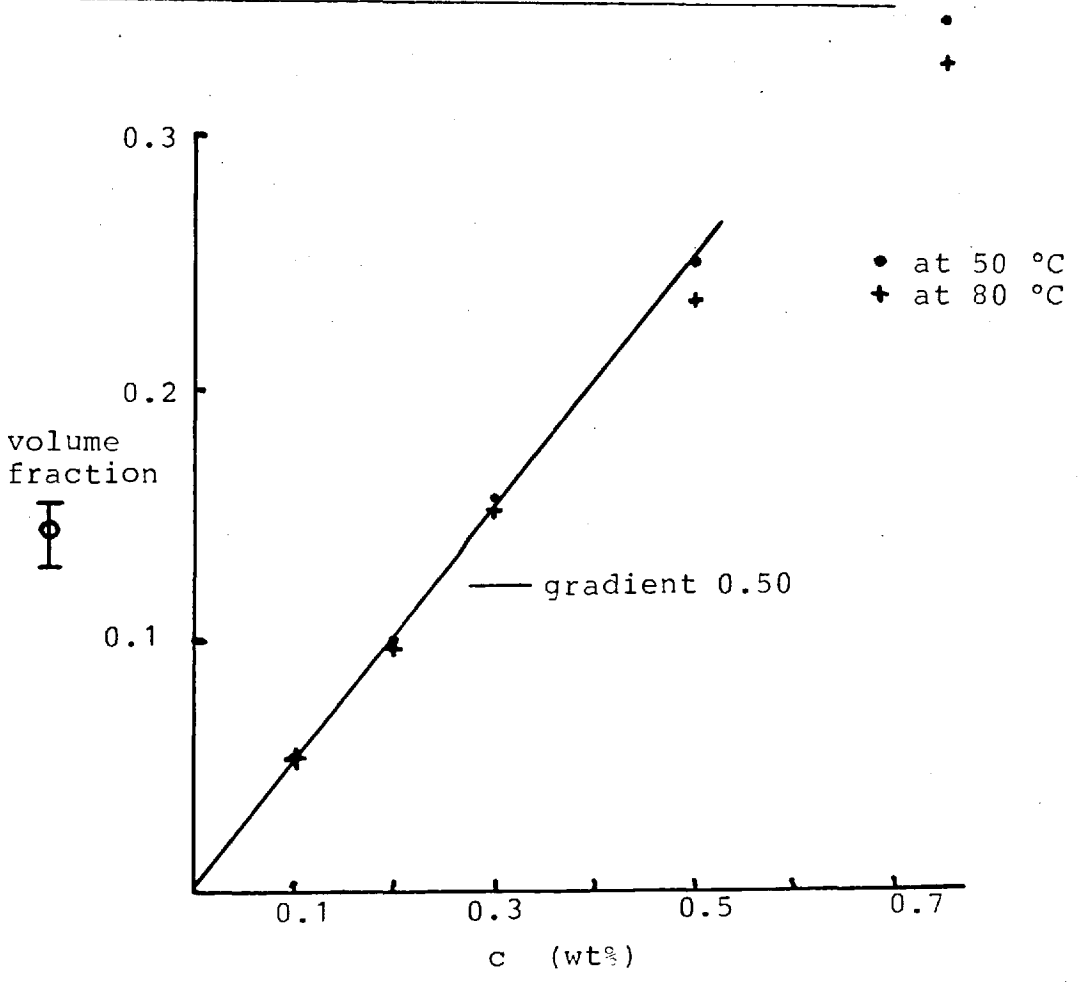


Figure 6.6 Volume fraction (from Kynch/Vand) versus concentration (wt%) for agarose solutions

1) From photon correlation studies of dilute non-gelling agarose solutions the effective hydrodynamic radii of the particles has been found to be large ($\sim 0.5\mu m$). In order to rationalise these data a "hard core" model has been proposed with a central core of refractive index n_{core} surrounded by a second component of refractive index n_{sheath}. The necessary condition being that the core is responsible for the bulk of the scattered spectrum in the wavevector range studied.

2) Optical microscopy revealed particulate matter of the correct dimensions to exist in dried agarose films. However, these particles could not be observed in solution. The fact that they could not be observed is consistent with $n_{core} > n_{sheath} \approx n_{solution}$; when the hydrated sheath contributes little to the scattered spectrum. The value of dn/dc for polysaccharides in water, at $0.14\ mlg^{-1}$, is small.

3) Pyrolysis of agarose revealed it to contain 0.44% by weight of insoluble "ash". Subsequent studies by X-ray fluorescence and X-ray diffraction confirmed the ash to be composed mainly of crystalline calcium sulphate. Electron microscopy revealed the ash particles to be elliptical, crystalline bodies exhibiting a high degree of monodispersity

and with average dimensions (0.08×0.13)μm.

3) Comparison of viscosity data with the theoretical models of Kynch and Roscoe led to the relationship:

$\Phi = 0.50c$ (for $c < \sim 0.4$wt.%)

The above data now enable a qualitative model of the agarose unit to be constructed. If we assume the cores to be roughly spherical of radius 0.05μm and to be composed of calcium sulphate (density 2.32g/cm^3) then 10^{-3}g of agarose contains 4.4×10^{-6}g of cores. Thus the number of cores present is given by:

$$n = \frac{4.4\times10^{-6}}{4/3\ \pi\ (5\times10^{-6})^3\ 2.32} = 3.62\times10^{9}$$

and the volume of the cores is 1.90×10^{-6}cm^3.

Thus the cores are only a very small fraction of the total weight and volume of the solute.

If one considers a 0.1wt.% agarose solution, i.e. 10^{-3}g of agarose/cm^3 then for such a system the volume fraction is (0.50×0.1) 0.05 and thus:

volume of cores/cm^3 - 1.90×10^{-6}cm^3

volume of polymer/cm^3 - 4.998×10^{-2}cm^3

weight of cores/cm^3 - 4.4×10^{-6}g

weight of polymer/cm^3 - 9.956×10^{-4}g.

The number of agarose chains/cm^3 is given by:

$$\frac{9.956\times10^{-4}\times6.023\times10^{23}}{\text{Molecular Weight } (\sim120{,}000)} = 4.997\times10^{15}$$

and the volume per chain, v_f is $\frac{4.998\times10^{-2}}{4.997\times10^{15}} \approx 10^{-17}$cm^3

Equating volumes:

$$0.05 = 3.622 \times 10^{9} \times \frac{4}{3} \times \pi \ (0.4 \times 10^{-4})^{3} + n_f v_f$$

where n_f is the number of free chains. The radius of the agarose unit has been taken to be 0.4μm i.e. the smallest value observed in photon correlation studies. Thus $n_f \approx 4.90 \times 10^{15}$.

Therefore the number of chains adsorbed on cores, n_{ads}, is $(4.997-4.903) \times 10^{15} = 9.4 \times 10^{13} \approx 10^{14}$ and there are therefore $\sim 2.6 \times 10^{4}$ chains adsorbed per core.

We conclude that for a 0.1wt.% agarose solution the mean separation of hard core particles is ~6.5μm and there are some 56,000 free chains present in the cylinder of solution between these particles (figure 6.7).

Thus these observations and calculations suggest that there could exist a "hard-core" particle with $\sim 2.6 \times 10^{4}$ agarose chains adsorbed per core. However, the bulk of the solution consists of free agarose chains which dominate the rheological behaviour of the system.

6.3 Properties of the Agarose Unit

In the previous section a model was proposed for the agarose system on the basis of experimental data. In this section the model is further scrutinised by comparison with other data.

The proposed model consists of a "hard-core" particle surrounded by adsorbed polysaccharide chains, which is immersed in a polysaccharide solution. The bulk of the

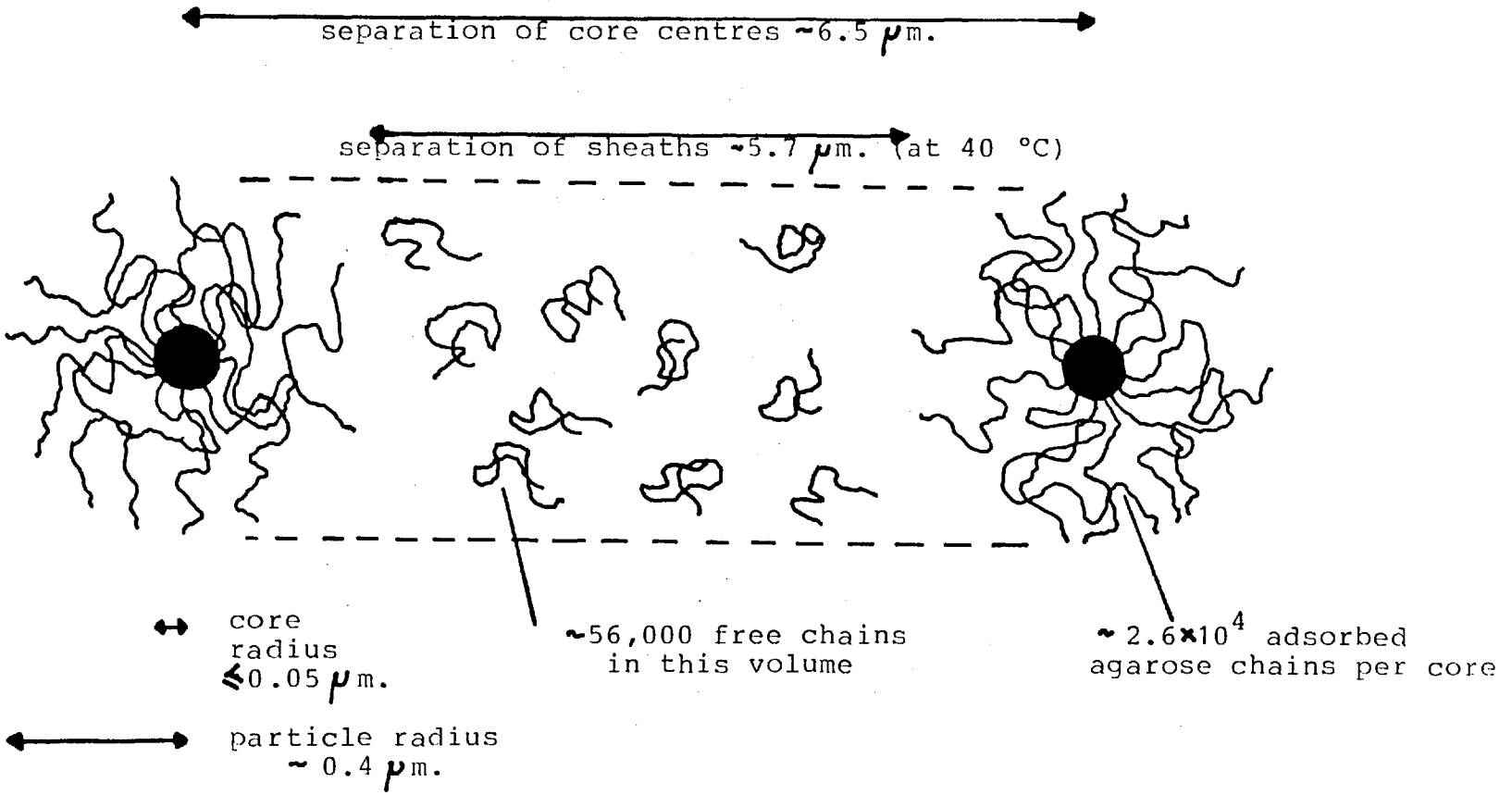


Figure 6.7 Model of a 0.1 wt% agarose solution

weight and volume of the solute is present in the form of free chains. The "hard-core" is thought to be mainly responsible for the scattering of light, but the rheological properties of the solution, for instance viscosity, will, however, be dominated by free chain behaviour.

Considering the hysteresis loop we find that in the "sol state" the effective hydrodynamic radius decreases with decreasing temperature, although the scattered intensity remains constant. Similarly the volume fraction is unaffected by the change in effective hydrodynamic radius for concentrations less than ~0.4wt.%. Both these observations are in complete agreement with the proposed model.

Perhaps the most striking experimental finding is the (wavevector)^3 behaviour exhibited by aggregated non-gelling solutions and sol state gelling solutions. This behaviour had tentatively been considered to arise from interactions between agarose units. This proposal may now be examined in greater detail.

The experimental results satisfy a relationship of the form:

$$\Gamma_1 = c \frac{T}{\eta_{SOLN}} K^3 \text{ where } c \sim 3.5 \times 10^{-18}$$

Considering the findings of Brown et. al. (see section 3.5) for a system of interacting particles:

$$\Gamma_1 = \frac{D_o K^2}{S(K)}$$

Then $$\frac{D_o K^2}{S(K)} \approx c \frac{T}{\eta_{SOLN}} K^3$$

or $$\frac{D_o}{S(K)} \approx c \frac{T}{\eta_{SOLN}} K$$

D_o is given by the Stokes-Einstein equation and thus:

$$\frac{K_B T}{6\pi \eta_o r_o} \cdot \frac{1}{S(K)} \approx \frac{c}{\eta_{SOLN}} \frac{T}{K}$$

i.e. $$\frac{c'}{\eta_o S(K)} \approx \frac{c}{\eta_{SOLN}} \frac{K}{T}$$

In order to complete this derivation we must replace η_o by η_{SOLN} The proposed model tells us we must do exactly this, since viscosity is governed by free chain behaviour. We then obtain the condition:

$$S(K) \propto \frac{1}{K}$$

S(K) has been discussed in section 3.1; it is the fourier transform of the pair correlation function (figure 6.8).

The form of the pair correlation function consistent with the postulated S(K) is consistent with temporary aggregation of the "hard-core" particles in the sol state because the mean separation between "hard-cores" at these solution concentrations is many times the separations shown above, in figure 6.8. The form of the dependence $S(K) \propto \frac{1}{[K]}$, $g(r) \propto \frac{1}{r^2}$; has not so far been justified theoretically, however, studies of the linear aggregation of polystyrene spheres have also shown similar behaviour [88].

The present finding that S(K) shall depend linearly on the inverse of K has also been investigated experimentally via the scattered intensity, for it is known that: $I(K) \propto P(K) . S(K)$.

The model for the core units which has been

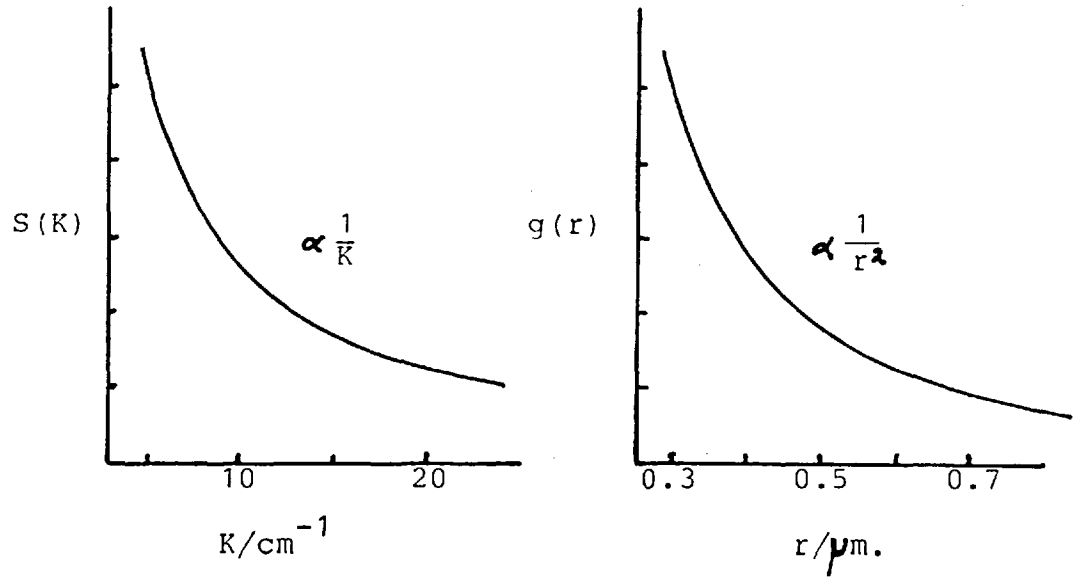


Figure 6.8 Static structure factor and pair correlation function

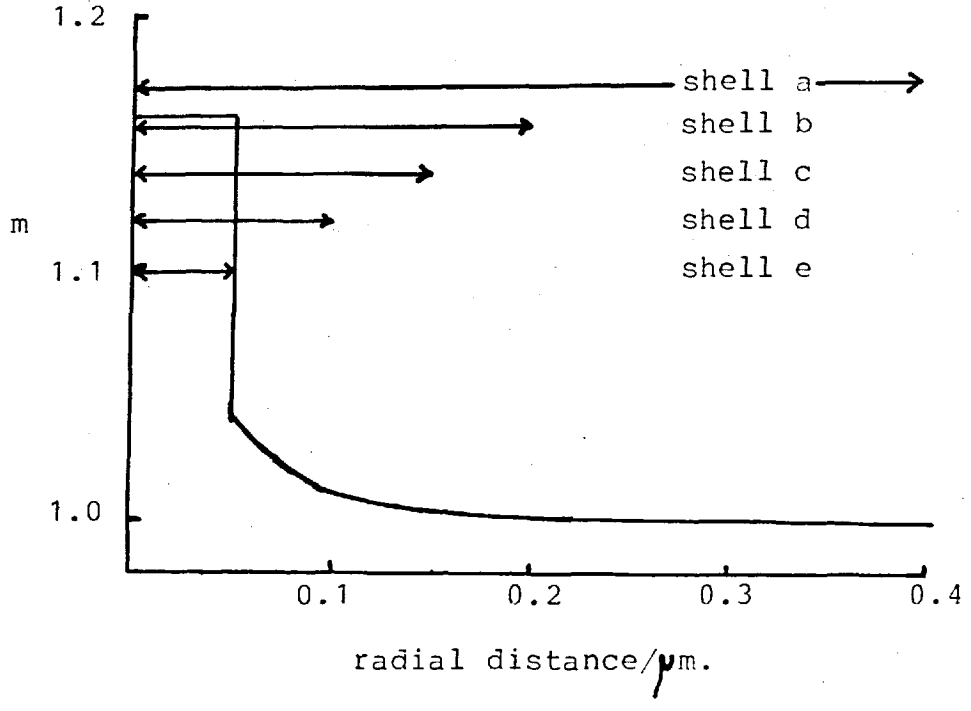


Figure 6.9 Relative refractive index (m) versus radial distance for proposed "hard-core" particles.

described in our hypothesis enables P(K) to be estimated, when a second qualitative study of S(K) can be made.

From the proposed model the variation of polymer concentration with radial distance from the core centre may be calculated, and hence the variation of refractive index may be obtained (figure6.9).

By considering the "hard-core" units to consist of i shells of relative refractive index m_i the contribution of each shell to P(K) may be estimated[89]:

$$P(K) = \frac{1}{V_a^2} \quad \frac{1}{(m_a-1)^2} \quad [(m_a-1)V_aG_a(K) + (m_b-m_a)V_bG_b(K)+..]^2$$

where V_i is the volume of shell i and $G_i(K)^2$ is the structure factor for that shell [32] (figure 6.10).

The particle scattering factor may then be evaluated (figure 6.11) and compared with intensity data (figure 6.12). Excellent agreement is found between the scattered intensity and the form of [P(K).S(K)] as predicted by the proposed model.

We conclude at this stage that the proposed model is in excellent agreement with experimental data. We now turn to the gelation process. In dilute non-gelling solutions the "hard-core" particles are isolated entities, free to undergo translational diffusion. When the solution is cooled the hydrodynamic radius of the particles gradually decreases as the polymer-polymer interactions begin to outweigh the polymer-solvent interactions. At some concentration-dependent temperature,T*, these units then flocculate to form larger aggregates.

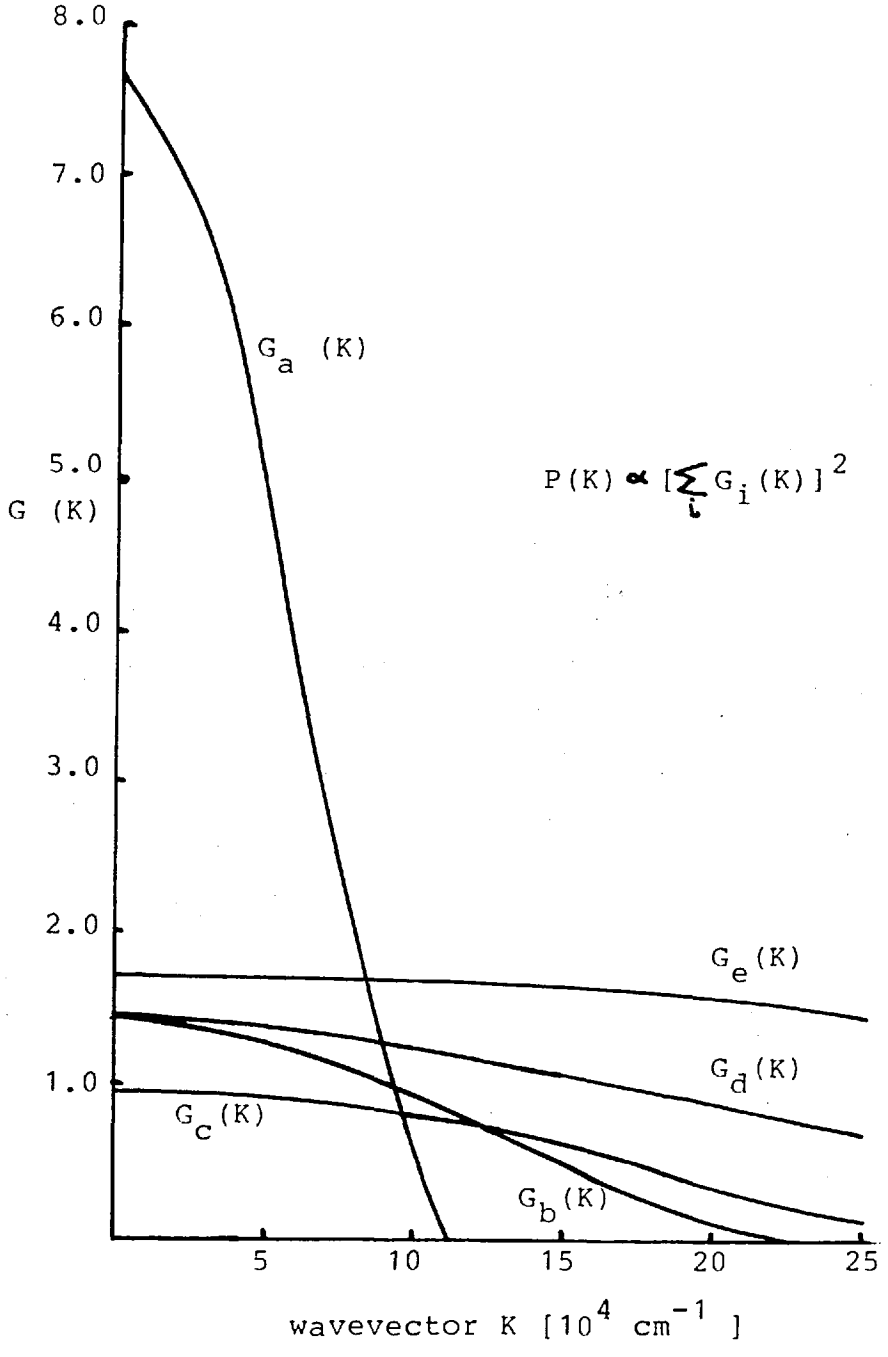
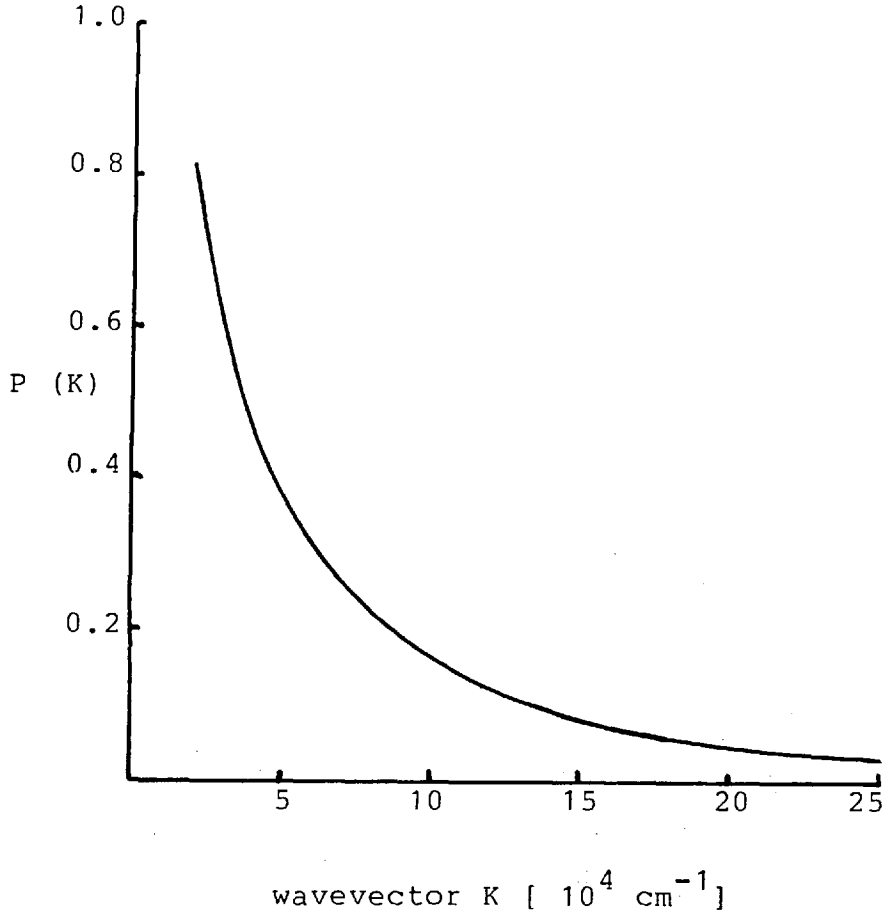


Figure 6.10 Contribution of each shell of the proposed "hard-core" to the particle scattering factor P(K)



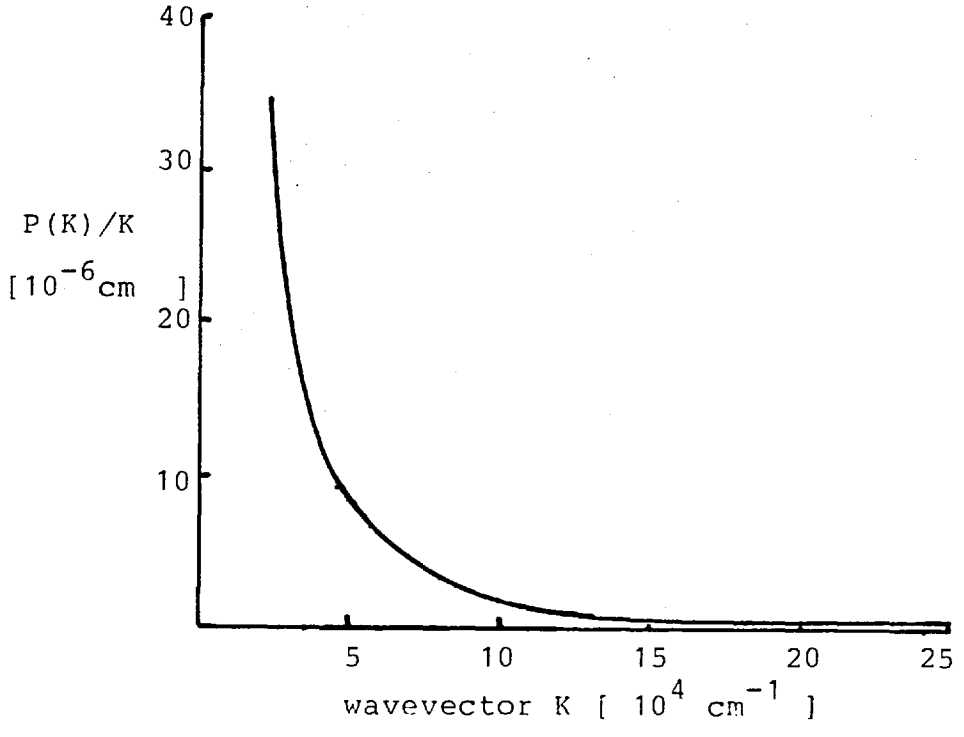


Figure 6.11 Particle scattering factor P(K) and P(K)/K for the proposed "hard-core" model.

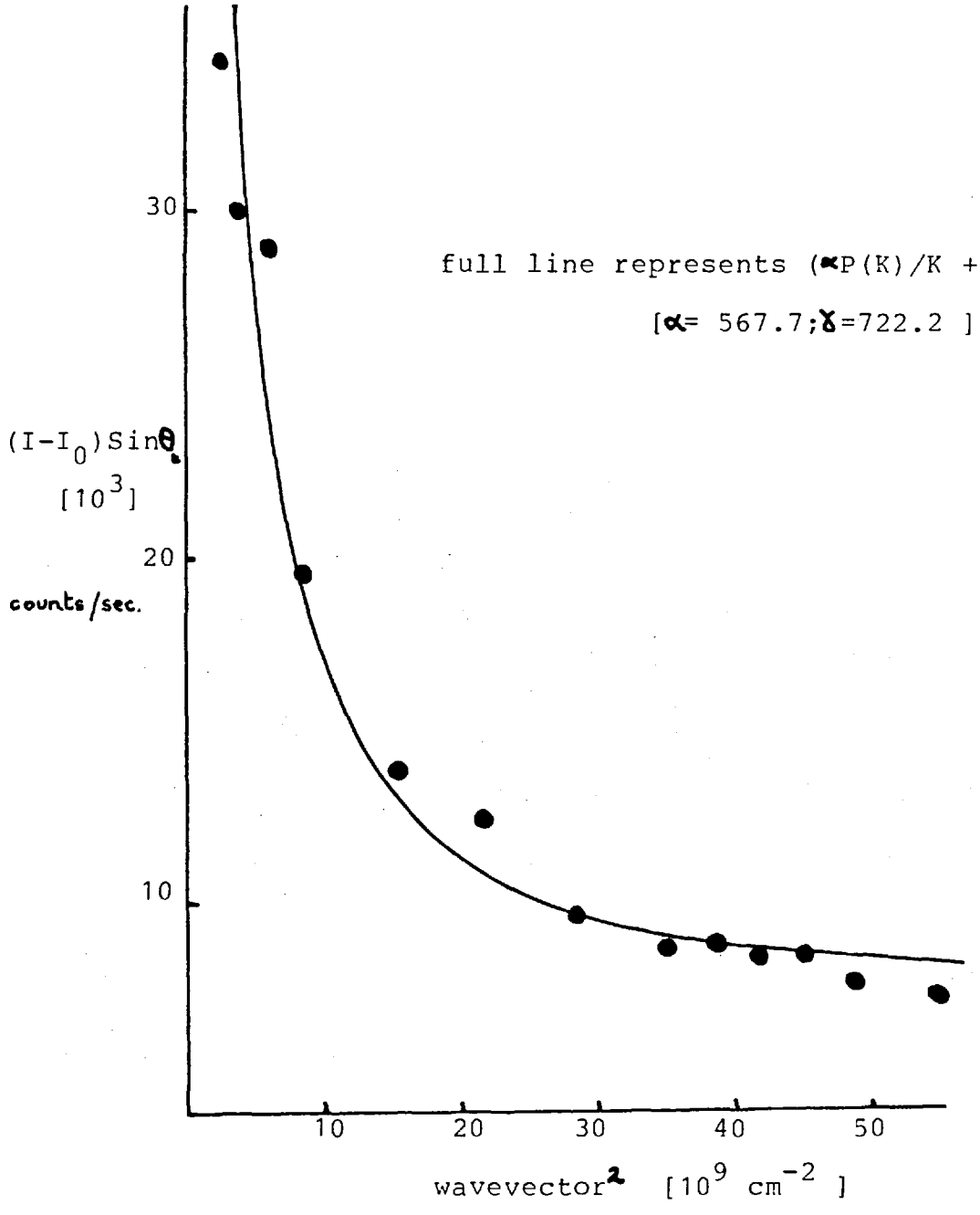


Figure 6.12 Comparison of scattered intensity with prediction based on the "hard-core" model.

The above experimental data were kindly supplied by Dr. J. Davis.

In more concentrated solutions the interactions between particles are such that dimers are formed in the sol state and this is reflected in both light scattering and viscosity measurements. Again as the solution is cooled a temperature is reached at which permanent aggregation of these particles occurs: because of the increased number density a three-dimensional aggregated structure or gel is formed. This phenomenon may be compared to the θ-point for an ordinary polymer solution. The free chains will also become "insoluble" at this point and will adsorb onto each other and onto the aggregated structure, thus strengthening the gel fibres. In many of the optical micrographs dendritic type growths were observed (figures 5.37b,c,d). Since van der Waals interactions between colloidal particles favour the formation of linear chain aggregates it seems reasonable to propose that the "hard-core" particles aggregate in this manner to form the backbone structure of the incipient gel. Several other observations give added support to a mechanism of this form:

1) The extrinsic fluctuations in scattered intensity observed in most samples a few degrees above the aggregation temperature, T^*, may be explained in terms of a heterogeneous gelation phenomena involving the aggregation of impurities which are most likely to be adventitious clusters of "hard-core" particles.
2) It has been shown [20] that, at temperatures slightly above the normal aggregation

temperature, a gelation process occurs but with very slow kinetics as found in this study by the formation of a soft gel after 3 - 6 days. Both this finding and the fact that the addition of colloidal material designed to simulate the naturally occurring ash markedly increased the aggregation temperature are in keeping with the concepts of heterogeneous gelation.

A useful interpretation of the variation of the intrinsic aggregation temperature with concentration may be obtained by considering a qualitative argument put forward by Everett [90].

Assuming that:

1) the chemical potential of an agarose unit in an aggregate can be taken to be constant, $\mu_{agg}(T)$, and
2) that the chemical potential of the dispersed agarose units is of the form:

$$\mu_{disp} = \mu^{\ominus}_{disp}(T) + RT \ln c$$

Then if the dispersed units are in equilibrium with those in the aggregate at T*:

$$\mu_{disp} = \mu_{agg}(T^*)$$

and:

$$\mu_{agg}(T^*) - \mu^{\ominus}_{disp}(T^*) = \Delta_{agg}\mu^{\ominus} = RT^* \ln c$$

where $\Delta_{agg}\mu^{\ominus}$ is the standard free energy change upon addition of a particle to the aggregate. Thus one obtains:

$$\frac{\partial T^*}{\partial \ln c} = R\left[\frac{\partial}{\partial T}\left(\frac{\Delta_{agg}\mu^{\ominus}}{T}\right)\right]^{-1}$$

This qualitative argument suggests that a plot of T* versus ℓn c should be linear with the gradient governed by the magnitude of $\Delta_{agg}\mu^{\ominus}$.

Figure 6.13 shows such a plot. There are three linear regions distinguishable in this figure; these correspond well with the following concentration regimes:

1) Dilute non-gelling agarose solutions ($c < 0.1$wt.%) (region I)
2) Gelling agarose solutions (0.1wt.%$< c <$ 1.0wt.%) which form elastic gels (region II)
3) Gelling agarose solutions ($c >$ 1.0wt.%) which form rigid gels (region III).

Although the assumptions made in the derivation may not strictly hold for agarose solutions, the approach does provide a consistent interpretation of the data in terms of the interactions between "hard-core" units in the sol state.

Thus:

1) For very dilute solutions (region I) the particles are non-interacting in the sol state giving a simple (wavevector)^2 dependence of the initial slope of the autocorrelation function.
2) In region II the particles interact to form temporary dimers in the sol state and hence give a (wavevector)^3 dependence.
3) Region III no doubt arises from the close proximity of the agarose units at higher

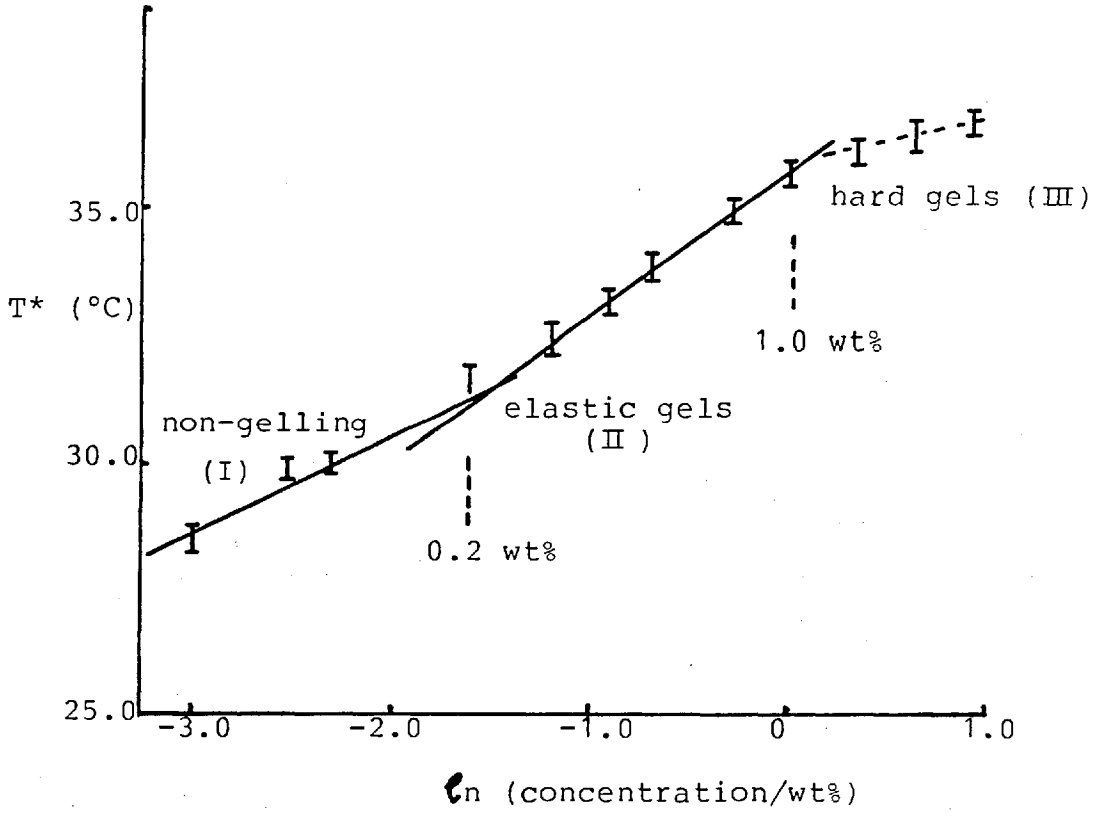


Figure 6.13 Temperature of aggregation (T*) versus ℓn (concentration/wt%)

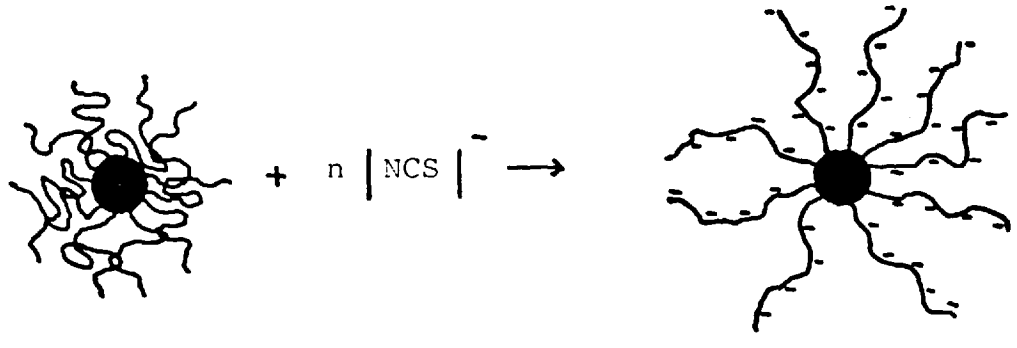


Figure 6.14 Effect of intramolecular repulsion

concentrations and the onset of permanent interaction/entanglement effects. This is in agreement with the interpretation of viscosity data in this concentration range.

Finally, we must consider the effect of addition of various ions; NCS^-, I_3^- etc. It has been shown that these ions prevent gelation when present in sufficient quantity. Since the inhibition of gelation is not a consequence of pH or ionic strength, reversible adsorption of these ions onto the polysaccharide chain must be responsible. Thus they act as gel inhibitors through the intra- and intermolecular repulsion that they produce. Considering the proposed model for the agarose coated "hard-core" particles, two major effects should be observable upon addition of such ions;

1) Intramolecular repulsion between adsorbed ions of the same sign will cause an extension of the polysaccharide chain and result in an increased hydrodynamic radius (figure 6.14).
2) Intermolecular repulsion will prevent the association of agarose units.

Both these effects have been observed experimentally. The increase in effective hydrodynamic radius is reflected in the magnitude of the diffusion coefficients obtained in potassium thiocyanate and potassium iodide solutions (figure 5.47). Perhaps the most striking feature is the loss of the $(\text{wavevector})^3$ dependence and its replacement by the simple $(\text{wavevector})^2$ dependence. The

(wavevector)^3 dependence has been shown to arise from an association of the agarose units which causes the static structure factor to become wavevector dependent over the wavevector range studied. The loss of this dependence can only be explained by the prevention of association of these particles. The now-charged agarose units are screened by the solution and hence undergo a largely independent Brownian type diffusion resulting in a (wavevector)^2 dependence.

Thus, as a result of light scattering studies and microscopy a model has been proposed for the agarose system which has enabled us to suggest a mechanism for the gelation process. The model is consistent with numerous other experimental findings such as intensity light scattering, ion interactions and hydrolysis. It can also rationalise the experimental findings of other research groups.

Unfortunately the mode of association of the polysaccharide chains cannot be ascertained from this work. However, the coil-helix transition as proposed by Rees seems very unlikely in the light of aggregation temperature results and seeding experiments. The more elongated model for chain association as proposed by Atkins, however, would be totally consistent with the results presented here.

6.4 The "hard-core"

The proposed model relies on the "hard-core" that has been postulated from the light scattering data on non-gelling agarose solutions. Subsequent microscopy of both

agarose solutions and the ash obtained by pyrolysis support the existence of these cores. They have been found to be mainly composed of calcium and sulphur with numerous other elements (Mg, SiO_4^{4-}, PO_4^{3-}) present in smaller amounts. The presence of "ash" in agarose samples is not a new finding, however; to date the nature and the role of the ash in the gelation process had not been investigated.

X-ray diffraction studies have shown the ash to contain calcium sulphate which itself is sparingly soluble. The inclusion of silicate, phosphate, sodium and magnesium ions into the matrix will reduce the solubility still further.

It has been shown that the ash content may be an important parameter in determining the gel-forming properties of the solute and thus a detailed study of the role of the ash may yield important information about the gelation mechanism. Preliminary filtration experiments to remove the "hard-core" particles have not been successful.

The monodisperse, crystalline nature of the ash indicates that these particles are intrinsic to the system. They are selectively replicated by nature in the seaweed itself. It then follows that other natural products may contain similar colloidal inclusions, which must therefore be taken into account in corresponding dynamic and structural studies. Previously reported properties of natural polymers could well be those of their inorganic inclusions!

References

1. P.J. Flory, Disc. Faraday Soc.,1974,N° 57,8.
2. D.A. Rees, Adv. Carbo. Chem.,1969,24,267.
3. See B.J. Berne and R. Pecora, Dynamic Light Scattering (Wiley-interscience,1976).
4. K.V. Thimann, The Life of Bacteria (Macmillan,N.Y., 1955),p. 146
5. C. Araki, Bull. Chem. Soc. Jap.,1956,29,543.
6. C. Araki, Sci. Technol., 1956,N°5,21.
7. C. Araki and S. Hirase, Bull. Chem. Soc. Jap.,1960, 33,597,291.
8. C. Araki, J. Chem. Soc. Jap. (Pure Chem. Sect.),1937, 58,1338.
9. S. Hjerten, Biochim. Biophys. Acta,1962,62,445.
10. B. Russell, T.H. Mead and A. Polson,Biochim. Biophys. Acta, 1964,86,169.
11. S. Arnott,A. Fulmer,W.E. Scott,I.C.M. Dea,R. Moorhouse and D.A. Rees,J. Mol. Biol.,1974,90,269.
12. K.L. Wun,G.T. Feke and W. Prins,Disc. Faraday Soc., 1974,N°57,146.
13. E. Pines and W. Prins, Macromolecules,1973,6,888.
14. T.F. Child and N.G. Pryce,Biopolymer,1972,11,409.
15. I.C.M. Dea,A.A. MacKinnon and D.A. Rees,J. Mol. Biol., 1972,68,153.
16. P.L. Indovina,E. Tettamanti,M.S. Micciancio-Giammarinaro, M.U. Palma,J. Chem. Phys.,1979,70,2841.
17. J. Andrasko,Biophys. J.,1975,15,1235.
18. W. Derbyshire and I.D. Duff,Disc. Faraday Soc.,1974, N°57,243.

19. S. Ablett,P.J. Lillford,S.M.A. Baghdadi and W. Derbyshire,A.C.S. Symp. Ser.,1974,36,344.

20. S. Ablett and P.J. Lillford,Chem. Phys. Lett.,1977, 50,97.

21. N.S. Anderson,J.W. Campbell,M.M. Harding,D.A. Rees and J.W.B. Samuel,J. Mol. Biol.,1969,45,85.

22. D.A. Rees,I.W. Steele and F.B. Williamson,J. Polym. Sci. C,1969,28,261.

23. E.D.T. Atkins, private communication:to be published.

24. T.G.L. Hickson and A. Polson,Biochim. Biophys. Acta, 1968,165,43.

25. T.C. Laurent,Biochim. Biophys. Acta,1967,136,199.

26. M. Duckworth,K.C. Hong and W. Yaphe,Carbo. Res.,1971, 16,189.

27. K.B. Guiseley,Carbo. Res.,1970,13,247.

28. W. Prins,L. Rimai and A.J. Chompff,Macromolecules, 1972,5,104.

29. A. Hayashi,K. Kinoshita and M. Kuwano,Polym. J.,1977, 9 (2),219.

30. See for instance B. Chu, Laser Light Scattering (Academic Press,1974).

31. See for instance D. MacIntyre and F. Gornick,Light Scattering from Dilute Polymer Solutions (Gordon and Breach,N.Y.,1964).

32. See for instance P. Kratochvil, Light Scattering from Polymer Solutions (Academic Press, 1972,Ed. M.B. Huglin), p. 333.

33. See for instance C.J. Oliver, Coherence and Quantum Optics (Plenum,N.Y.,1973,Eds. L. Mandel and E. Wolf) p.395.

34. S.H. Chen,W.B. Veldkamp and C.C. Lai,Rev. Sci. Instrum., 1975,46, N°10.

35. P.N. Pusey,D.E. Koppel,D.W. Schaefer,R.D. Camerini-Otero and S.H. Koenig, Biochem.,1974,13,952.

36. E. Jakeman,C.J. Oliver and E.R. Pike,J. Phys. A (Gen. Phys.),1971,4,827.

37. E. Jakeman and E.R. Pike,J. Phys. A (Gen. Phys.), 1969,2,115.

38. See B.J. Berne and R. Pecora,Dynamic Light Scattering (Wiley-interscience,1976),Chapters 5,7,8.

39. D.E. Koppel,J. Chem. Phys.,1972,57,4814.

40. P.N. Pusey,D.E. Koppel,D.W. Schaefer,R.D. Camerini-Otero and R.M. Franklin,J. Phys. (Paris),1972,33,C1-163.

41. R. Pecora,J. Chem. Phys., 1964,40,1604.

42. R. Pecora,J. Chem. Phys.,1968,49,1032.

43. R. Pecora,Annu. Rev. Biophys. Bioeng.,1972,1,257.

44. T. Maedo and N. Saito,J. Phys. Soc. Jap.,1969,27,984.

45. J.D.G. MacAdam and T.A. King,Chem. Phys.,1974,6,109.

46. M. Adam and M. Delsanti,J. Phys. Lettres,1977,38,L-271.

47. Z. Akcasu and J.S. Higgins, J. Poly. Sci. Pol. Phys. Ed.,1977,15,1745.

48. R. Kapral,D. Ng and S.G. Whittington,J. Chem. Phys., 1976,64,539.

49. P.G. de Gennes,Physics,1967,3,37.

50. E. Dubois-Violette and P.G. de Gennes,Physics,1967,3,181.

51. P.G. de Gennes,Macromolecules,1976,9,594.

52. Z. Akcasu and H. Gurol,J. Pol. Sci. Pol. Phys. Ed., 1976,14,1.

53. G.D.J. Phillies,J. Chem. Phys.,1975,62,3925.

54. T.J. Murphy and J.L. Aguirre,J. Chem. Phys.,1972,57, 2098.

55. J.L. Aguirre and T.J. Murphy,J. Chem. Phys.,1973,59, 1833.

56. A.R. Altenberger and J.M. Deutch,J. Chem. Phys.,1973, 59,894.

57. G.D.J. Phillies,J. Chem. Phys.,1974,60,976.

58. J.C. Brown,P.N. Pusey,J.W. Goodwin and R.H. Ottewill, J. Phys. A:Math. Gen.,1975,8,664.

59. D.W. Schaefer and B.J. Berne,Phys. Rev. Lett.,1974, 32,1110.

60. P.N. Pusey,J. Phys. A:Math. Gen.,1975,8,1433.

61. B.J. Ackerson,J. Chem. Phys.,1976,64,242.

62. B.J. Ackerson,J. Chem. Phys.,1978,69,684.

63. P.G. de Gennes,Macromolecules,1976,9,587.

64. T. Tanaka,L.O. Hocker and G.B. Benedek,J. Chem. Phys., 1973,59,5151.

65. J.P. Munch,S. Candau,R. Duplessix,C. Picot and H. Benoit,J. Phys. Lettres,1974,35,L-239.

66. J.P. Munch,S. Candau,R. Duplessix,C. Picot,J. Herz and H. Benoit,J. Pol. Sci. Pol. Phys. Ed.,1976,19,1097.

67. K.L. Wun and F.D. Carlson,Macromolecules,1975,8,190.

68. S.L. Brenner,R.A. Gelman and R. Nossal,Macromolecules, 1978,11,202.

69. R. Nossal and S.L. Brenner,Macromolecules,1978,11,207.

70. R.A. Gelman and R. Nossal,Macromolecules,1979,12,311.

71. R. Nossal,J. Appl. Phys.,1979,50,3105.

72. A.M. Hecht and E. Geissler , J.Chem. Phys.,1977,66,1416.

73. M. Daoud and G. Jannink,J. Phys.,1976,37,973.

74. M. Daoud,J.P. Cotton,B. Farnoux,G. Jannink,G. Sarma, H. Benoit,R. Duplessix,C. Picot and P.G. de Gennes, Macromolecules,1975,8,804.

75. See B. Chu,Laser Light Scattering (Academic Press,1974), p. 132.

76. G.C. Maitland and S.A. Sayegh:unpublished data.

77. K.L. Wun,G.T. Feke and W. Prins,Disc. Faraday Soc., 1974,N°57,146.

78. Handbook of Chemistry and Physics,59th Ed. (CRC Press).

79. J. Kestin,M. Sokolov and W. Wakeham,Appl. Sci. Res., 1973,27,241.

80. J.C.P.D.S. powder data file.

81. R.C. Evans,An Introduction to Crystal Chemistry (Camb. U. Press,1964), p. 225.

82. J.W. Goodwin,Rheology of Dispersions,Chapter 7, Spec. Per. Rep. Coll. Sci. Vol. 2,1975.

83. H.L Frisch and R. Simha,Rheology-Theory and Application (Academic Press,1956,Ed. F.R. Eirich).

84. J. Happel and H. Brenner,Low Reynolds Number Hydrodynamics (Prentice-Hall,1965), Chapter 9.

85. G.J. Kynch,Proc. Roy. Soc. (London),1956,A 237,90.

86. V. Vand,Phys. Colloid Chem.,1948,52,277.

87. R. Roscoe,Brit. J. Appl. Phys.,1952,3,267.

88. W.A. House,J.C.S. Faraday I,1978,5,1112.

89. M. Kerker,The Scattering of Light and Other Electromagnetic Radiation (Academic Press,1969).

90. D. Everett,Disc. Faraday Soc.,1978,65,313.